Novel Self-Healable Thermosets and Their Carbon Fiber Reinforced Polymer (CFRP) Composites

by

Lisha Zhang

A dissertation submitted in partial fulfillment
of the requirements for the degree of
Doctor of Philosophy
(Macromolecular Science and Engineering)
in The University of Michigan
2020

Doctoral Committee:

Professor Henry Sodano, Chair
Professor Jay Guo
Professor Daniel Inman
Professor Brian Love

Lisha Zhang

zhalisha@umich.edu

ORCID iD: 0000-0001-9493-686X

ACKNOWLEDGEMENTS

I would like to thank my advisor Dr. Henry Sodano for his exceptional guidance and assistance throughout my PhD program. The support and suggestion he provided were very precious and important to me for completing this dissertation. I feel lucky to have the chance to explore the self-healing material field under his mentoring and my learning experiences from him not only help me get my dream job at 3M but also, they will benefit my entire career life in the future. I am sincerely grateful to my dissertation committee members: Prof. Guo, Prof. Inman and Prof. Love for their generous feedback and support.

I would also like to express my sincere gratitude to Dr. Jiajun Lin, who is not only my mentor but also my close friend and has given me a lot of valuable advice along my PhD life. I want to thank Dr. Mohammad Malakooti and Dr. Yunseon Heo for their training at the beginning of my PhD study which enabled me to quickly adapt to the group culture as an independent researcher. I want to thank all the present and graduated members of Dr. Sodano's research group, Dr. Christopher C Bowland, Dr. Brendan A Patterson, Dr. Hyun-Sik Hwang, Dr. Alireza Nafari, LoriAnne Groo, Kelsey Steinke, Jalal Nasser, Jaehyun Jung, Ruowen Tu, Tianyu Yuan, Herbert Tian and Florian Julé for their generous support and warm company. I absolutely learn a lot from each of them, and the time we spent together, both in and out of the lab is certainly unforgettable.

Last but not the least, I would like to thank my family, especially Molin Guo, who drove three hours from Cleveland to Ann Arbor every weekend during the past four and a half years to gather with me. His enormous support and love are always with me in whatever I pursue, and I feel like my half of my incoming Ph.D. degree belongs to him. The tremendous encouragement from my parents have been significantly important and it has kept up my spirits and let me step steadily toward the right direction.

TABLE OF CONTENTS

LIST OF FIGURES

LISTS OF TABLES

ABSTRACT

Intrinsically self-healing polymers allow repeatable damage repair of a fracture located within materials without the need for external additives. Self-healing polymers possess promising potential for numerous structural applications, such as the construction, automobile, and aerospace industries, due to their capability to reduce system maintenance requirements and increase the longevity and safety of the composite structures. The healing capacity of the polymers is derived from the formation of covalent bonds between reactive components at the fracture spot. These reactive components are typically varied in their chemical structures and are dependent on the employed healing chemistry, therefore a variety of new chemistries have been reported. However, current self-healing polymers either 1) undergo significant thermal degradation at elevated temperatures, or 2) lose their mechanical strength and stiffness above their typically low glass transition temperature and are thus limited by the healing chemistry. Developing a new healing chemistry which exhibits thermal stability and maintains mechanical properties and mechanical stability at a higher temperature range is of great importance for the development of high-performance self-healing materials for structural applications and has been a long lasting challenge in the composites research field.

This dissertation details the discovery of a novel healing chemistry with stability at high temperature, based on which new self-healing materials with significantly improved high-temperature performance and mechanical stability have been developed. Initially, this new healing chemistry of isocyanurate-to-oxazolidone transformation is studied both in model compounds and in the polymer network, where the instability of isocyanurate in the presence of epoxide is confirmed. The isocyanurate-to-oxazolidone transformation is then embedded in isocyanurate-oxazolidone (ISOX) polymers and the polymerization mechanism of the ISOX polymers, including the initiation, cross-linking, and network propagation is further investigated. Based on the understanding of the polymerization mechanism, a two-step

curing procedure is designed for the ISOX polymers to ensure the presence of a large amount of two reactive components, isocyanurate and epoxide, for the isocyanurate-to-oxazolidone transformation within the polymers. Combined chemical characterization through Fourier-transform infrared (FTIR) spectroscopy and carbon nuclear magnetic resonance (NMR) spectroscopy is performed in order to quantify the chemical composition of the ISOX polymers, including the isocyanurate fraction which can be controlled through both the nucleophilicity of the polymerization catalyst and the duration of the post-cure of the polymers. Secondly, the developed ISOX polymers are evaluated and shown to achieve damage repair in the presence of a macroscopic crack, yielding considerable recovery of polymer strength after thermal annealing which is repeatable over multiple damage-repair cycles. The study on structure-property relationship of the ISOX polymers shows that the material properties of the polymers are uncompromised with the addition of the self-healing functionality, as their excellent mechanical properties and high-temperature performance remain comparable to that of an engineering grade epoxy. Lastly, self-healing carbon fiber reinforced polymer (CFRP) composites are developed using the ISOX polymers as the matrix material. After multiple delamination events, repeatable strength recovery of the composites has been demonstrated with a first healing efficiency of up to 85% after thermal treatment. The strength and stiffness of the composites are comparable to those of engineering grade polymer matrix composites typically used in aerospace applications, while their thermal stability places them in the polybismaleimide performance region. This dissertation details the development of novel self-healing materials which have great potential for advanced structural applications in extreme environments.

CHAPTER 1

Introduction

1.1 Motivation

The motivation for this study lies in the damage management of fiber reinforced polymer (FRP) composites which use fibers such as glass, aramid, boron, and carbon fiber as reinforcement. While the polymer matrix is relatively weak compared to the fiber reinforcement, it is an important binder for the reinforcement which allows the support and transfer of mechanical loads within the composites (1). Recently, FRP composites have provided an excellent substitute for traditional materials, such as metals and ceramics, due to their superior chemical and corrosion resistance, along with their high strength and stiffness. These important factors have resulted in their rapidly increasing use in the automobile, naval and aerospace industries (2-4) , and as a result, industry analysts expect the global market for carbon FRP composites to grow to $37.2 billion by 2022 (5). While glass fiber reinforced polymer composites represent the largest class of polymer matrix composites, carbon fiber reinforced polymer (CFRP) composites are widely used as structural composites particularly in the aerospace field. The high specific strength and stiffness of the CFRP composites, derived from their light weight, is especially attractive in transportation where reduced weight results in significant energy savings. As a result, carbon fiber reinforced epoxy composites have been extensively used in the fabrication of commercial aircrafts such as Boeing 787 and Airbus A380. Specifically, the Boeing 787 Dreamliner is manufactured with about 50% CFRP composite materials in its airframe, which has allowed approximately 20% improvement in fuel efficiency compared to its predecessor, the Boeing 767 (6). CFRP composites offer a higher structural strength-to-weight ratio, among other

desirable properties, over many other structural materials, thus leading to their expanding use in applications ranging from defense and aerospace systems to industrial equipment and consumer goods.

For structural applications, micro/macroscopic damage including microcracks, transverse cracks, and delamination can form and propagate within the composites when they are subject to mechanical loading. For internal composite damage, in-situ material repair is difficult or sometimes impossible (7, 8), and its accumulation can lead to the ejection of plies and, ultimately, catastrophic failure of the composite materials. To manage the internal damage within the composites for longer service life and safer structures, two strategies have been adopted: 1) improved damage resistance and 2) improved damage tolerance of the materials (9). The concept of damage resistance emphasizes that the initiation of damage can be prevented by developing stronger and tougher materials, while the damage tolerance approach emphasizes that damage is bearable if it can be self-repaired in-place, similar to biological systems such as human bones. Strategies for improving the damage tolerance of the FRP composites focus on the polymer matrix, as all classes of polymers, from thermoplastics to thermosets, have the potential for healing microcracks or delamination under external stimuli (10). Despite the development of many self-healing polymers over the past several decades, the majority of the results are low modulus polymers where the chains exhibit a high degree of flexibility to overcome steric issues, and thus are not suitable for structural application. Another gap in this research field is the lack of high temperature self-healing polymers, as the current chemistry for self-healing polymers would undergo significant thermal degradation at elevated temperatures. For example, the widely explored urethane bonds in self-healing polyurethanes undergo four degradation pathways above 150 °C (11), causing poor thermal stability to be a limiting factor for their use in high temperature CFRP composite applications.

In this dissertation, both approaches of improving damage resistance and improving damage tolerance are utilized to develop advanced materials which possess high strength to prevent the formation of damage and are self-healable in order to repair the damage once it occurs and to stop the propagation and accumulation of the damage

modes within the materials. Novel self-healing polymers and CFRP composites, with comparable mechanical strength and stiffness to their commercial counterparts, are developed based on the discovered healing chemistry of isocyanurate-to-oxazolidone transformation which possesses stability at high temperatures. Using this healing chemistry, efficient strength recovery of the polymers can be repeatedly achieved below the glass transition temperature (Tg) of the polymers. In other words, a large portion of the mechanical strength and stiffness can be preserved at the healing temperature, which is an unachievable feature in most reported self-healing systems. The developed self-healing materials are thermally stable up to 360 °C, and have excellent mechanical stability derived from their high Tg (up to 270 °C), which is the highest Tg among currently reported self-healing materials.

1.2. Solutions to Internal Damage in Fiber Reinforced Polymer Composites

1.2.1. Internal damage in fiber reinforced polymer composites

Lightweight, high-strength, and high-stiffness fiber reinforced polymer (FRP) composites have been widely used as structural components and parts for improved energy efficiency and reliability in a large number of engineering applications such as luxury cars, wind turbines, and aircrafts. Typically, FRP composites consist of fibers that provide the primary structural reinforcement, and a polymer matrix which binds the reinforcement together. Moreover, the matrix also transfers the applied loads to the tougher fibers and protects them from environmental degradation due to chemical corrosion or moisture absorption which is more aggressive when combined with temperature rise. In addition to the light weight and durability of FRP composites, the design flexibility of these composite materials offers an opportunity to achieve most desired combinations of fiber reinforcement and polymer matrix, by using the proper fraction of each, to meet stiffness, strength, and other application requirements.

The fiber reinforcements used in FRP composites are classified into continuous fibers and short fibers/whiskers. The specific classification of composites, based on the form of the reinforcement and the reinforcement configuration, is shown in Figure 1.1 (4) . In addition to

long and short fibers, whiskers and particulates can also be combined with polymers to achieve composites with superior strength/stiffness to the neat polymers at reduced cost compared to longer fiber reinforcement. However, the improvement in mechanical properties with particulates is considerably less than that predicted by the rule of mixtures (12, 13). The incorporation of whiskers, which are single crystal short fibers, can significantly improve the strength of the composites, however, they present expensive manufacturing costs and are difficult to uniformly mix into the polymer matrix. Figure 1.2 shows the elastic modulus of composites as a function of reinforcement volume fraction for continuous fibers, whiskers, and particles. As can be clearly seen, for a fixed volume fraction, the highest reinforcement efficiency is obtained with the continuous fiber reinforcement. Therefore, given their superior structural performance, the following paragraphs will discuss and focus on continuous fiber reinforced polymer composites.

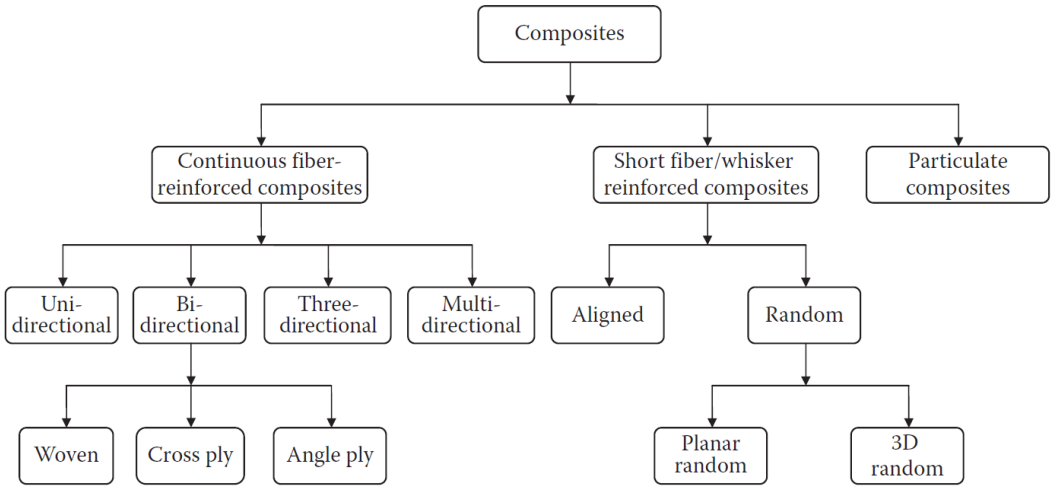

Figure 1.1. Classification of composites based on dispersed phase and adopted configuration (14).

Polymer matrices used for FRP composites can be categorized into thermoplastics and thermosets. Thermoplastics consist of long-chain molecules containing one or more repeating units of atoms, where the molecules are held together by weak, secondary bonds such as van der Waals forces or hydrogen bonds (15). At elevated temperatures, these secondary bonds break down, allowing for the softening and melting of the thermoplastics for reshaping. In contrast, the chains in thermosets are cross-linked through strong covalent bonds, resulting in

a permanent, three-dimensional networked structure that accounts for the highly restricted molecular motions in such polymers. These cross-links result in the high strength, stiffness, temperature stability, and chemical resistance of the thermosets (16). In FRP composites, thermosets are favored over thermoplastics mainly because of their processing advantage. Uncured thermosets are readily available as liquids which are low-viscosity at room temperature and are thus convenient for the fabrication of composites through a variety of processing techniques. In contrast, high melt and high solution viscosities of the thermoplastics are the major reasons why these polymers have limited applications in continuous FRP composites, as high pressure is required to fully wet the reinforcing fibers at high temperatures during processing. Typical examples of thermoplastics and thermosets used for FRP composites are listed in Table 1.1 (14). The majority of FRP composites use a thermosetting matrix; for example, epoxies and polyesters have been the principle polymer matrices for FRP composites for several decades.

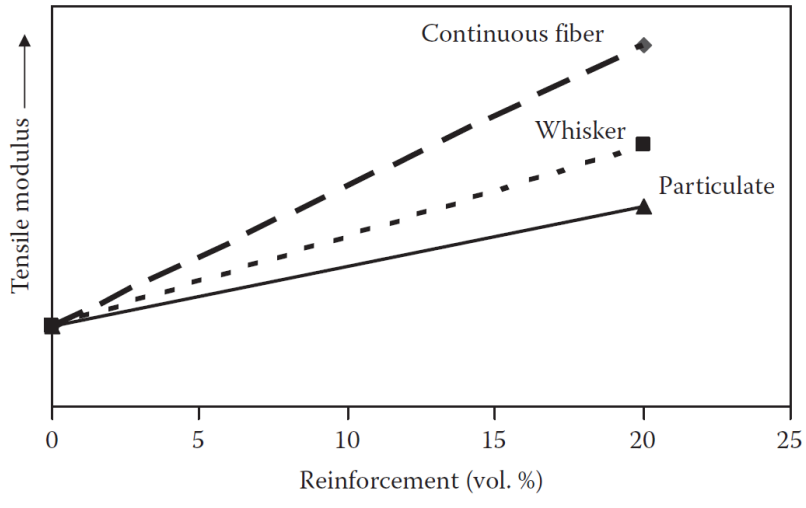

p

Figure 1.2. Tensile modulus as a function of reinforcement volume fraction for continuous fiber, whisker, and particulate-reinforced composites (14).

While polymer matrices play a minor role in the load-bearing capacity of FRP composites, they have a major effect on the interlaminar and in-plane shear properties. Both the interlaminar and in-plane shear strength are important considerations for the performance of composites subjected to bending and torsion loading conditions (17). Polymer matrices undergo physical (typically for thermoplastics) or chemical changes (mostly for thermosets)

during the manufacturing process, and the temperature at which the polymer matrices are processed usually determines the use temperature of the composites. Compared to fiber reinforced metal and ceramic matrix composites, current FRP composites have limited high temperature applications, as the polymer matrices are at risk of either melting or decomposing at elevated temperatures. While the choice of polymer matrix and fiber reinforcement is critical to the final properties of the FRP composites, other determining factors include the volume fraction of the constituents, the fiber orientation, and the fabrication process. For example, the fiber reinforcement can be oriented in any direction in order to directionally tailor the final mechanical properties of the FRP composites. Continuous fiber reinforced polymer composites, therefore, show strong anisotropic properties.

Table 1.1. Typical polymer matrix for FRP composites and their applications (14).

Categories	Examples	Applications
Thermosets	Epoxies	Principally used in aerospace applications
	Unsaturated polyesters	Commonly used in automobile, marine, chemical and electrical applications
	Vinyl esters	
	Phenolics	Used in bulk molding compounds
	Polybenzimidazoles	For high-temperature aerospace applications (250°C–400°C)
	Polyphenylquinoxaline	
	Cyanate ester	
Thermoplastics	Aliphatic polyamides, polyesters, polycarbonate, polyacetals	Used with discontinuous fibers in injection-molded articles
	Aromatic polyamide, PEEK, polysulfone, PPS, PEI	Suitable for moderately high-temperature applications with continuous fibers

Despite the exceptional structural performance of FRP composites, fabrication defects, which are left as structural defects within the materials, are inevitable despite great care during the fabrication process (18, 19). To some extent, the defects in a composite material depend strongly on the characteristic properties of the polymer matrix, such as viscosity, melting point (in the case of a thermoplastic polymer matrix) and curing temperature (in the case of a

thermoset polymer matrix). Debulking is the final stage of fabricating FRP composites, where a thick laminate is treated under simultaneous heat and pressure/vacuum to remove entrapped air within the composites (20, 21). The purpose of debulking is to reduce the number of internal defects to the largest extent, however, it is not possible to get a "perfect" composite without any defects even with debulking. Common manufacturing defects found within FRP composites include resin-rich regions, voids, microcracks formed due to stresses developed during curing, de-bonded and delaminated regions, and fiber misalignment. Among these defects, voids especially present a very serious problem, as high void extent can significantly degrade the structural performance of the composites.

Alternatively, structural defects also form and accumulate within the materials during service because of the heterogeneity in the microstructure of continuous FRP composites. Multiple damage modes can occur depending on the loading conditions and microstructure of the composites. Among them are matrix crazing, matrix cracking, fiber fracture, delamination, debonding, and multidirectional crack propagation, as can be seen in Figure 1.3 (22) . Delamination, a damage mode associated with the separation of plies and the fiber/matrix, is very critical for the performance of FRP composites employed in long term structural applications, for example, under fatigue conditions. Additionally, delamination is a major problem for continuous fiber reinforced polymer composites that show anisotropic characteristics (23, 24). In general, continuous fiber reinforced composites are strong and stiff along the fiber axis, however the properties are considerably weaker in the direction orthogonal to the fiber axis, leaving the polymer matrix vulnerable to damage under out-of-plane loading such as impact and compression. Accidental application of high-stresses in the transverse direction to the fibers may lead to the fracture of these composites as a mixture of intra-ply matrix cracks and inter-ply delamination. Generally, a mixture of these damage modes can form and accumulate within composites under thermo-mechanical loading (22), and these structural defects are difficult to visually detect and remove due to their location deep within the composites. The intra-ply matrix cracks and inter-ply delamination can also progressively reduce the stiffness and strength of the composite structure, which may ultimately lead to catastrophic failure.

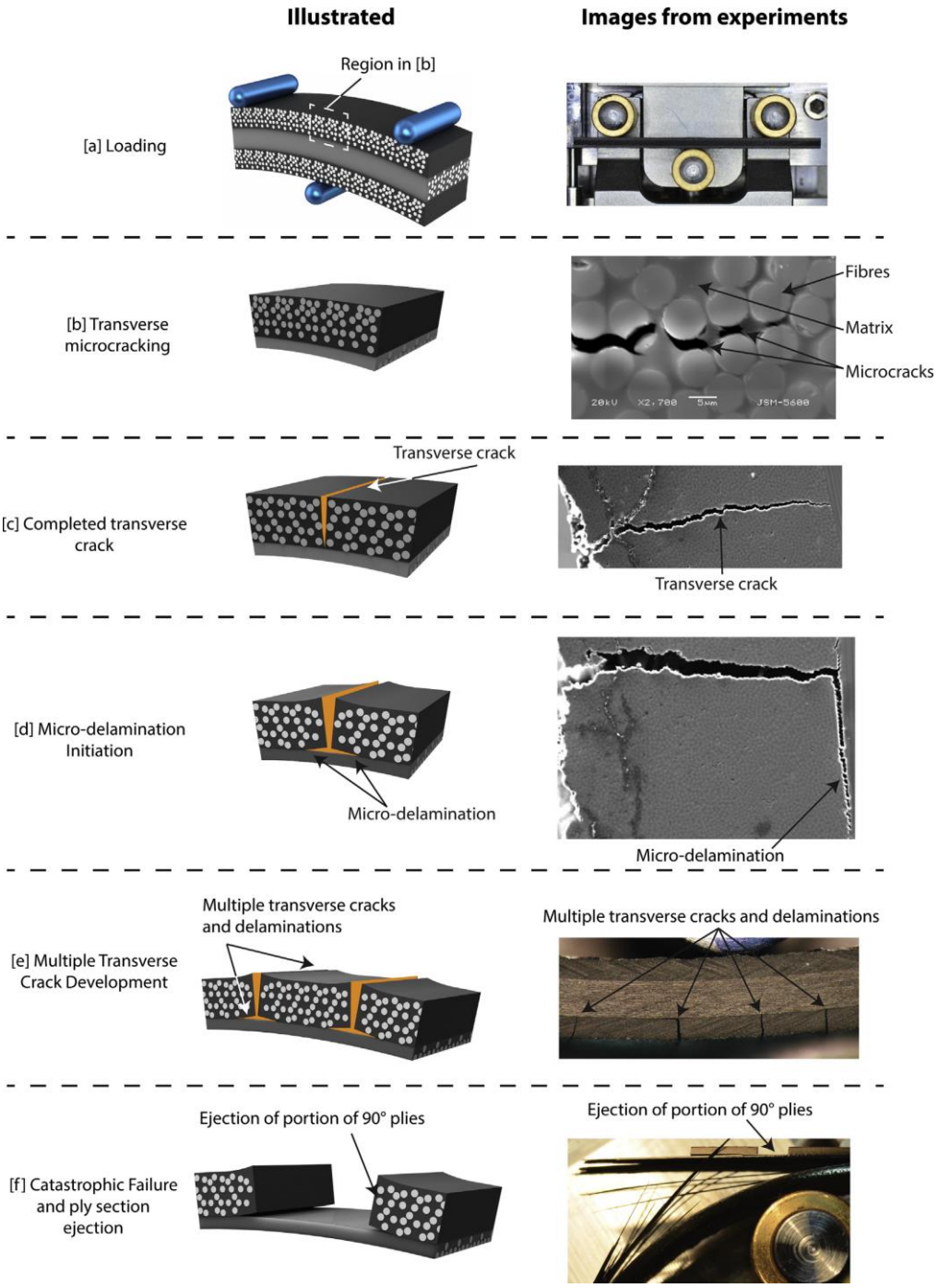

Figure 1.3. (a) Typical flexural loading specimen; (b) representative element taken from the tensile surface, actual transverse damage visible in electron micrograph; (c) transverse crack growth after microcracks have coalesced; (d) micro-delamination initiation at ply boundary; (e) multiple transverse cracks and micro-delaminations; (f) specimen after micro-delaminations coalesced and ejection of 90 °ply section (22).

The degradation of the properties of the FRP composites in the presence of accumulative structural defects is an important cause for mandatory and frequent inspection and maintenance of FRP structures during service, and heavily loaded primary structural FRPs have been

successfully repaired for many years (25). The visibility of the occurring damage is typically highly dependent on the impact energy, as low energy impact usually leads to more “hidden” damage, and high energy impact can lead to clear signs of damage, such as dents, delaminate, cracks, etc. The assessment of damage in FRP composite structures can be completed using a variety of non-destructive inspection techniques to determine the extent of damage including tap tests, C-scan, *etc.* (26-28). Once damage is detected, maintenance is mandatory to prevent further damage, and the concerned structures must be replaced or repaired. In the case where part replacement is unaffordable, repair must be an option in order to keep the structural function of the composites. The repair process for removing the damaged region of a composite includes firstly removing the paint/coating and then removing the damaged FRP skin through routing or grinding. All damaged materials are the cut out and removed, using a selected damage removal approach, until only sound laminate remains before initiating repair. The most commonly used repair method is patch repair, as shown in Figure 1.3 (25). The patch repair can be applied to all types of FRP composites, and it is a relatively low-cost repair technique that needs the least preparation.

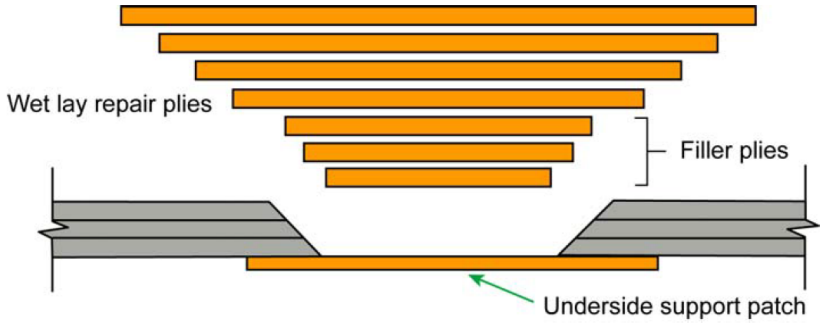

Figure 1.4. Schematic of laminated patch repair (25).

Other repair methods are scarf joint repair, pre-cured doubler, plug, bolted plates, and resin infusion or injection repair (29, 30). It is worthwhile to note that epoxy, polyester, and vinyl ester are the most widely used resins for the repair of FTP composites. Currently in the aerospace industry, secondary structures within wings and radomes are regularly refurbished following accidental impact damage or lightning strikes. This is carried out by approved personal using one or several of the repair methods which were discussed above. These

repairs require the addition of external fixtures, since the structure itself does not have an inherent self-repair capacity. Yet such structures would benefit from an embedded self-repairing functionality, which would eliminate the need for full replacement of the parts. Generally, current approaches to repairs of FRP composites tend to be difficult and costly to apply, as both the inspection and maintenance procedures are highly labor-intensive and time-consuming. Therefore, as discussed concretely in the next section, great effort has been devoted to improving the damage management of FRP composites in order to reduce cost and improve safety for a variety of structural applications.

1.2.2. Damage management in fiber reinforced polymer composites

Structural materials including metals, ceramics, polymers, and composites, are designed and developed to perform mechanical functions, therefore a large emphasis is on their ability to resist buckling and fracture to survive damage during use (9). Damage is defined here as the presence of micro/macroscopic cracks that are initially absent within the materials. Repair of damaged FRP composites used in structural applications is briefly discussed above; however, damage repair is a small part of damage management which is further reviewed here. The approach to damage management for FRP composites is of great importance as it can improve the reliability and stability and increase the longevity of critical engineering systems. Generally, there are two strategies for damage management of FRP composites to achieve longer-serving structures which are further reviewed in the following paragraphs: 1) improving damage resistance and 2) improving damage tolerance.

Improving damage resistance, a damage prevention philosophy, has been a major guideline for structural materials, including structural polymers and their fiber reinforced composites, for multiple decades. Significant efforts have been made to improve the strength and reliability of materials based on this paradigm, which emphasizes damage prevention by avoiding crack formation and extension with increased loading and service time to the greatest extent. To design stronger materials,

several strategies, including tuning structure-property relationships during the material production stage and optimizing material processing to avoid manufacturing defects, have been widely explored and utilized. Regardless of the material strength, once damage is initiated, it is usually irreversible. A schematic demonstration of this damage resistance concept is shown in Figure. 1.4 (a), where A represents a reference material which is exposed to an increasing load for a constant amount of time, or a constant load for an increasing amount of time (9). Below a certain threshold, there is no damage for A; however, after a damage initiation event, the damage level keeps rising until reaching Damage Level 1, which represents the catastrophic failure of A. Material B in Figure. 1.4 (a), which is a stronger version of material A, has a significantly improved damage threshold, although the damage propagates at a much faster rate than material A. This rapid increase in damage level is representative of "stronger" materials which are more brittle. Material C in Figure. 1.4 (a) is a more advanced version of material A, as both an increased damage threshold and a slower rate of damage propagation are achieved. However, regardless of the delayed damage initiation of material C, the damage level is either constant or increasing as a function of load or time, indicating that the formation of damage during use cannot be avoided. Therefore, in safety critical applications where FRP composites are used, the adoption of a "no growth" approach (damage propagation from a defect constitutes failure) has been widely exercised, and the structures to which this approach is applied require frequent inspection and maintenance (31, 32).

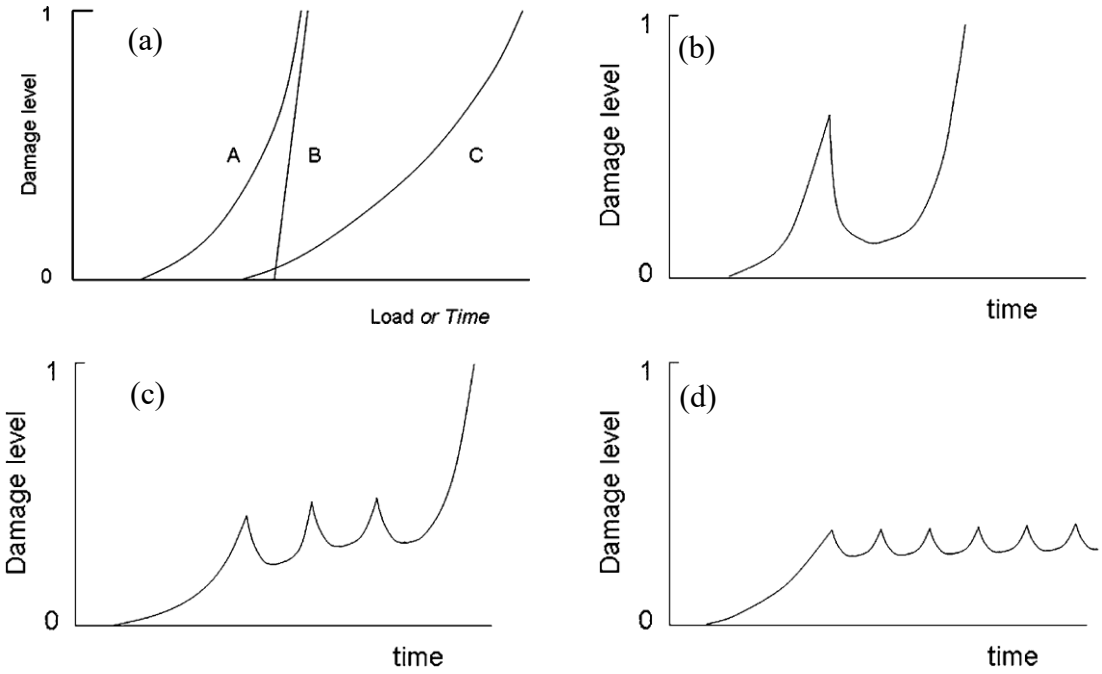

Figure 1.5. (a) Schematic diagram of the damage level in classical materials as a function of time or load. Material A sets the reference behavior. Materials B and C are improved material grades. (b)-(d) Schematic diagram of the damage development in three grades of self-healing materials (9).

Remedies for internal damage in FRP composites, derived from the improving damage resistance concept, have been found in both the fiber reinforcement and the polymer matrix. Toughened interlayers resulting from 3D fabrics, stitching, tufting, braiding, Z-pinning, and a tougher matrix achieved using woven/non-woven reinforcement have been widely researched (33-36). These solutions focus on the suppression of both matrix cracking and delamination by incorporating out-of-plane reinforcement that helps absorb a greater loading energy and arrest crack growth (37). However, the introduction of such features often has a negative effect on the integral mechanical properties of the host composites, as strength and toughness are typically mutually exclusive properties. Generally, a polymer matrix with higher toughness leads to greater resistance to crack propagation and delamination. Thermoplastic matrices usually possess higher impact strength than their thermoset counterpart because of their higher strain-to-failure and ductility. However, the viscosity of the high-performance thermoplastics is many orders of magnitude higher than that of the thermosets because of their high molecular weight. The viscosity of the polymer

matrix dictates the wetting of the fiber reinforcement and is thus a significantly important criteria for FRP composites to achieve good mechanical properties. Thermosetting polymer matrices typically have a lower viscosity, they have a processing advantage over thermoplastics and are therefore used for the majority of current FRP composites. Generally, thermosets also have higher strength and stiffness compared to those of thermoplastics, except for specialty thermoplastic polymers, like polyether ether ketone (PEEK), however their inherent brittleness has been a long-term issue. For this reason, tougher thermosets have been researched and developed for the improved damage resistance of composite materials. For commonly used epoxy, elastomers such as carboxyl-terminated butadiene acrylonitrile (CTBN), have been added into the polymer network as a toughener (38-42). The CTBN form a second phase in the polymer matrix that can effectively help prevent the formation of microcracks. Alternatively, a dispersion of rubber particles also results in an increase in toughness through the formation of microcavities ahead of the crack tip (43). The main drawback of the addition of such a second phase is a decreased modulus and reduced glass transition temperature of the host polymers, thus resulting in degraded performance at elevated temperature. Moreover, achieving a uniform distribution of the second phase within the polymer matrix remains a challenging task during both matrix modification and composite fabrication (44).

Improving damage tolerance, rather than improving damage resistance, is an alternative approach to damage management within structural materials. In the case of damage tolerance, microscopic or macroscopic cracks are acceptable when formed during use, on the condition that they are reparable using a built-in material capacity that restores the original functionality. This philosophy is derived from the regenerative abilities of skin tissues and bones which have “lifelong” structural performance, provided there are suitable healing conditions (45-48). Such self-healing abilities would provide considerable weight and cost savings for FRP composites by reducing inspection and maintenance requirements, while offering design engineers greater freedom to formulate innovative designs. Many self-healing mechanisms have been developed based on the described damage tolerant or “fail-safe”

concept which is further illustrated in Figure 1.4 (37). Figure 1.4 (b) – (d) are schematic examples of the concept of damage tolerance, where Figure 1.4 (b) shows the occurrence of a single healing event after which the damage level continues to increase with time/load until material failure. Multiple-time healing is achieved for the material represented in Figure 1.4 (c), however the damage level of the material continues to increase with time/load in the presence of weakening defects. Catastrophic failure occurs in this material when healing is no longer possible. The ideal revision of the materials represented in Figure 1.4 (b) and (c) is shown in Figure 1.4 (d), where healing is achieved multiple times, and the damage level remains constant as a result of the complete removal of damage after each healing cycle. Given the loading and healing conditions, the self-healing material in the case shown in Figure 1.4 (d) can have an infinite lifetime, although in real applications they also have a finite service time similar to the case of partially removed damage shown in Figure 1.4 (c). Ideally, self-healing materials should possess several important characteristics such as autonomous multiple-time healing capacity, effective damage repair to maintain low damage levels without limitations on the defect size, preservation of mechanical properties with the addition of self-healing functionality, and cost-efficiency for large-scale production and application. Although currently reported self-healing materials with experimental validation can meet one or several of these requirements, the development of the ideal self-healing materials for widespread and large-scale application will require further research in order to fully address all challenges presented above.

For FRP composites, the remedies for internal damage based on the strategy of improving damage tolerance have been found in novel multifunctional FRP composites. In this class of FRP composites, both the fiber reinforcement and the polymer matrix can retain their form and properties for introduction of additional functionality, allowing for the exploitation of the characteristic advantages of both components. The structure of the composites is an important reason for the described design flexibility of FRP composites. Most recently developed new materials and structures have combined structural functions with important nonstructural functions including

thermal stability, thermal conductivity, electromagnetic interference shielding, etc. within the materials (2). For example, in the case of automobile body parts, the desired thermal insulation can be achieved using the polymer matrix of the FRP composites, while the smooth surface of the same composite material can satisfy the strict aesthetics and aerodynamic requirements. The multifunctionality of the materials is obtained through both surface modification of the reinforcing fibers and modification of the versatile matrix material. It would be additionally beneficial for the development of more efficient and sustainable FRP composites if the reinforcing component, which provides the majority of the strength and stiffness to FRP composite materials, also possesses a self-healing capacity in order to reverse several fiber-related failure modes. However, the repair of fractured reinforcement in FRP composites is yet to be achieved in any engineering context (37). As typical impact damage, including matrix cracking and delamination, occurs within the polymer matrix, most FRP composites focus on modifying the polymer matrix in order to achieve effective healing performance.

Strategies for improving the damage tolerance of CFRP composites primarily focus on the polymer resins, as all classes of polymers, from thermoplastics to thermosets, have the potential for self-healing under external stimuli, for example heat stimulus (10). Self-healing polymers are mainly based on two different mechanisms: extrinsic healing or intrinsic healing, as shown in Figure 1.5 (10). Extrinsic healing works by adding healing agents to the polymers in the form of capsules (49) or vascular channels (50, 51). Examples of the healing agent systems include PDMS with tin-based catalysts (52), epoxy resin and amine-based curing agents, (53, 54) epoxy and mercaptan (55), and dicyclopentadiene (56, 57). When an initiated crack passes through a capsule or vascular channel, the healing agents are free to flow from the vesicle and encounters a dispersed particulate catalyst which initiates a polymerization process that can repair the crack. A key advantage of the microencapsulation approach is its ease of incorporation into any polymer matrix, however, despite the quick healing performance, empty capsules or vascular channels are left as defects inside the material. These induced defects can then negatively impact the mechanical

properties of the composite structure. Also, in the case of capsules, the material is not healable once the fractured location has exhausted its available healing agents. Finally, the healing agents are also prone to degradation under long storage periods, which would decrease the durability of the self-healing capacity of the composite. Degradation resulting from time-dependent diffusion of the monomers out of the microcapsules has been reported, and the subsequent initiation of chemical reactions originally designed for the healing process was observed without the occurrence of damage, despite careful preparation of the self-healing composites (58). In fiber reinforced polymer composites, the diameter of microcapsules is usually within the range of 10 to 100 μm, which can cause additional problems by disrupting the fiber architecture. Specifically, Kessler and White's work have indicated problems regarding the healing performance of self-healable fiber reinforced composites due to the clumping of microcapsules into woven-roving wells whilst cracks propagate along woven-roving peaks (59, 60). In addition, a good dispersion of the catalyst to provide uniform healing functionality is needed which could be challenging during the composite fabrication process.

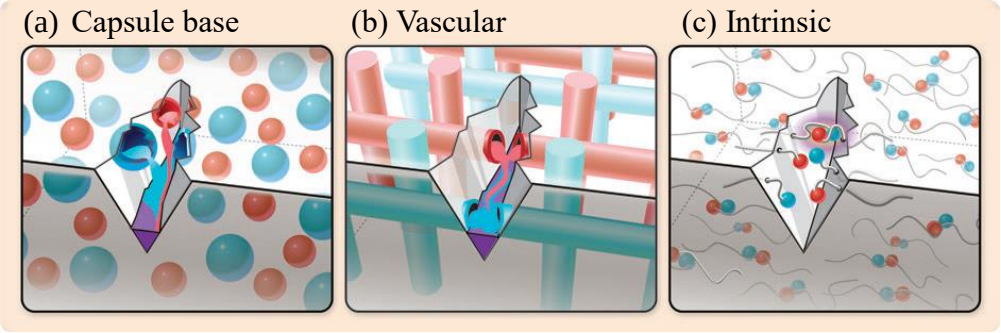

Figure 1.6. Schematic of extrinsic healing mechanism of (a) capsule-based and (b) vascular based. (c) Schematic of intrinsic healing (10).

In additional work investigating extrinsic healing mechanisms, liquid resin-filled hollow fibers were embedded in bulk epoxy, where the cracking of the resin-filled fibers and subsequent release of the repair chemical agents was observed under optical microscopy (61, 62). Motuku et al. incorporated millimeter length resin-filled fibers in addition to the reinforcing fibers into glass reinforced polymer composites and

investigated their performance when subjected to low velocity impact (63). In later work by Bleay, epoxy-filled commercial glass fibers with length on the scale of micrometers were developed (64). The glass fibers were consolidated into a lamina, and then fabricated into composite laminates where the self-healing material also undertook structural functionality. The key advantage of the hollow fiber concept is that the fibers can be aligned to match the orientation of the surrounding reinforcing fibers, thus addressing specific failure modes (65, 66). The disadvantages of the hollow-fibers based healing are also obvious, as the healing requires the fracture of the introduced healing fibers which possess a relatively larger diameter that than of the reinforcing fibers. Similar to the microcapsule-based healing, the additional processing stage required for the fiber infusion is also challenging.

The second main healing mechanism, referred to as intrinsic healing, is based on reversible molecular interactions within the polymer matrix under certain stimuli such as an external stimulus such as heat, light, or pressure (10). Intrinsic healing mechanisms can achieve multiple-time repair at the same location without the addition of any reactants or catalysts. Because of this attractive advantage, a great variety of intrinsically self-healing polymers based on different healing chemistries have been developed over the past few decades, and these systems are further reviewed in the next section.

1.3. Development of Self-Healable Polymers for Multiple-Time Repair

Thermoplastic resins are usually tougher than their thermosetting counterparts and can be melted and deformed as many times as required. Due to this characteristic, any microcracks within a thermoplastic matrix theoretically can be eliminated by melting the matrix under heat and reshaping it (58). However, some depolymerization or degradation can occur during the heating process, and the polymer quality can be significantly reduced with increased melting cycles (67). Additionally, thermoplastics have high melt or solution viscosities because of their high molecular weight and are typically in the range of 10^3 to 10^6 Pa·s for high-performance

thermoplastics which makes the processability of their CFRP composites challenging. For instance, polysulfone resins, which are suitable for high temperature applications up to 160 °C, must be melt manufactured at very high temperatures ranging from 310 °C to 410 °C (67). In contrast, for thermosets like epoxies, the viscosity of the resins is around 10-1000 cP at room temperature, and thus their CFRP composites can be fabricated without the need of high temperatures. This superior processing advantage of thermosets, plus their well-known high strength and high stiffness, excellent thermal stability, and chemical and creep resistance, are the important reasons why the development of self-healing thermosets rather than thermoplastics is more of a focus in the current literature.

Generally, the higher cross-link density of thermosets is the cause of their higher strength and modulus, improved chemical resistance, and thermal stability when compared to thermoplastics. However, thermosets with high cross-link density are also inherently brittle, and their composites are prone to excessive microcracking within the polymer matrix. To overcome this problem, the literature has reported modified thermosets that are self-repairable. Initial studies investigated thermosets with the addition of certain thermoplastics, including poly(bisphenol-A-coepichlorohydrin) and poly(caprolactone) (68-70), as the meltable thermoplastics can flow into the crack region and heal cracks under thermal stimulus. However, it was also reported that voids formed after the embedded thermoplastics flowed into the damaged location, negatively affecting the integrity of the material (71). Additionally, the maximum operating temperature of the blended CFRP composites was limited to the melting temperature of the added thermoplastic in the polymer matrix, which is 160 °C for poly(bisphenol-A-coepichlorohydrin) and 59 °C for poly(caprolactone). Without a compromise in the use temperatures of the resultant materials, currently developed self-healing composites with a thermosetting matrix for structural applications are classified into extrinsically self-healable composites and intrinsically self-healable composites. As briefly discussed in the last section, classic examples of extrinsically healable composites include capsules, hollow fibers, or tubes filled with a healing agent that are embedded in the polymer matrix (59, 60, 72-78) . Despite of its autonomous healing

behaviors, one of the biggest challenges with the extrinsic healing technique is that it is not repeatable without replenishing the healing agents.

Unlike extrinsically healable composites, the healing behavior of intrinsically healable materials exploits the healing chemistry within the polymers by using their inherit capacity to reform bonds. This allows for repeated healing after multiple occurrences of damage at the same fracture location. However, many intrinsic approaches require some form of external stimulus, for instance thermal energy in the case of sterically hindered polymers. The literature has reported a number of examples of intrinsically covalent self-healing polymers which demonstrated excellent matrix strength recovery under a thermal stimulus (10). For example, reversible Diels–Alder (DA) reactions between furan (F) and maleimide (M) (79, 80) or anthracene (A) and M (81-83) have been broadly studied and have demonstrated great potential for self-healing. Wudl et al. (79) first reported a novel self-healing polymer based on the DA mechanism, which showed a healing efficiency of 57% using the reversible F-M DA reaction. Additionally, Heo and Sodano (80) incorporated the F-M adducts into a polyurethane and obtained a healable polymer that utilized the shape memory effect of the polyurethane. The resultant polymer was shown to achieve repeatable healing with high recovery rate of fracture toughness at 86% without an externally applied load. In comparison to extrinsic self-healing polymers, intrinsic self-healing polymers based on the DA reaction are easier to prepare and repeatedly healable, however, the retro-DA reaction takes place at roughly 120 °C (79, 84) which results in the cleavage of F-M adducts. This cleavage leads to a significant drop in the mechanical performance of the polymer due to the loss of the F-M cross-links. This chemical instability at temperatures above 120 °C somewhat limits the potential of the self-healing polymers based on F-M DA adducts to applications where the operating temperatures typically fall below 100 °C (79). More recently, anthracene has been used as a substitute for furan in the DA reaction to achieve higher cleavage temperatures, thus expanding the application space of these polymer materials (81, 82). Due to the high cleaving temperature of >250 °C (85, 86), the use of thermal cleaving to assist in healing is limited when the cleaving temperature of the A-M DA adducts is

beyond the decomposition temperature of the polymers. For this reason, self-healing polymers based on the thermally induced retro-DA reaction between A and M have are yet to be reported. Existing healing concepts are based on the mechano-chemical cleavage of A-M DA adducts, followed by thermally initializing the forward DA reaction to reform the mechanically cleaved DA linkages (81, 82). For example, polyurethane-based polymers with thermally reversible DA linkages have previously been incorporated into FRP composites and were shown to yield up to a 96% recovery of the strength of the composite post-annealing (82, 87, 88). However, despite the successful demonstrations of intrinsically healable composites, their operating temperatures are often under 200 °C, as they are limited by either the predomination of undesirable chemical reactions at high temperatures or the relatively low Tg of the polymer matrix. Additionally, the use of polymers with a low Tg has limited their integration within structural applications because of the significant loss of strength at high temperatures (89). Thus, the development of self-healing polymers which exhibit a higher Tg is needed in order for them to be used at the elevated temperatures which are often required in high performance applications. Furthermore, polyurethane-based self-healing polymers also have limited thermal stability as polyurethanes undergo four degradation pathways above 150 °C (11), which results in limited use for composite applications (90).

Other alternative intrinsic self-healing mechanisms resulting in excellent healing performance have also been developed, however the resulting polymers exhibit low mechanical strength which limits their use in the field of structural materials. Matyjaszewski et al. (91) reported a self-healing gel which incorporated reshuffling trithiocarbonate units in a flexible poly (n-butyl acrylate) matrix where the high chain mobility of the gel played an important role in the 94% recovery of tensile modulus for the healed sample. Additionally, a self-healing rubber which was based on siloxane equilibration was reported to recover 87% of its initial fracture toughness after healing at 90 °C for 24 h following the crack initiation (92). In addition to covalent interactions, intrinsically self-healing supramolecular polymers have also been reported (93-103). Supramolecular polymers are materials where the monomers are associated

through noncovalent interactions. The reversibility of the noncovalent interactions imparts unique dynamic features that are useful for the self-repair of the materials. Meijer et al. have developed supramolecular polymers based on quadruple hydrogen bonds (94, 104). The 2-ureido-4-pyrimidone (UPy) end groups form dimers, and therefore their polymers are held together by the self-complementary hydrogen bonds. The three-binding sites led to the formation of cross-linked polymers with a high dimerization constant, and at temperatures above 90 °C, the polymer network would dissociate and melt because of the loss of hydrogen bonds. As a result, the polymer can undergo effective thermal healing, however, the dynamic feature also limits the operating temperature of these polymers to below 90 °C. As was discussed above, the challenges that still exist in the development of intrinsic healing strategies to broaden the applications of self-healing polymeric materials include: (1) chemical stability of the polymers under extreme environments; (2) a high Tg which would allow the polymers to maintain their high mechanical strength and stiffness under elevated temperatures; and (3) excellent mechanical properties of the polymers which would be comparable to engineering plastics. This dissertation therefore focuses on overcoming these limitations by developing a novel self-healable polymer that yields high Tg and onset decomposition temperature (Td), where both the tensile strength and Young's modulus of the polymer are within the range of those of composite grade epoxies (4).

1.4. Isocyanurate-Oxazolidone (ISOX) Polymers

Polyurethanes (PU) and polyureas, two of the most famous polymers in the "isocyanate family," are attained by step polyaddition of diisocyanates with diols or diamines (Figure 1.6). PU can be found in a variety of end-use applications such as coatings, adhesives, and sealants because of its versatile chemistry and unique properties (105). High performance PU coatings have been widely used in the automobile industry to provide high gloss exteriors, improved color retention, and improved scratch and corrosion resistance (106). Rigid PU foams prepared in the

presence of blowing agents have also been widely used in construction and industrial insulation in addition to marine equipment (107). The intrinsic features of the isocyanate moiety (-N=C=O) imply that mono- or poly-isocyanates can undergo a variety of reactions and polymerization processes following a step-growth mechanism. Step-polyadditions of isocyanates with diepoxides give poly(2-oxazolidone)s (108), and polyaddition of isocyanates results in either uretidiones from dimerization or isocyanurates from trimerization. Monomeric isocyanurates have been known for more than a century, (109, 110) and they have been primarily used to tune the cross-link density of PU (111-113), and improve the high-temperature resistance and flame retardancy of polyurethane foams (114-116). Isocyanates, especially aromatic ones, react with alkylene oxides, and a 1,3-cycloaddition with the alkylene oxides then yield 2-oxazolidones five member rings as mixtures of isomeric products. The monomers for polymerization of poly-2-(oxazolidone)s are diisocyanates and diepoxides (typically diglycidyl ethers of various bisphenols in conventional epoxy resins), and the typical reaction scheme can be found in Figure 1.7 (117). Successful polymerization of poly-2-oxazolidones from 2,4-toluene diisocyanate have been demonstrated in dimethylformamide (DMF) solvent at temperatures ranging between 120 and 160 °C in the presence of a variety of catalysts including tetramethylammonium iodide, pyridine, and $ZnBr_2$ (118, 119).

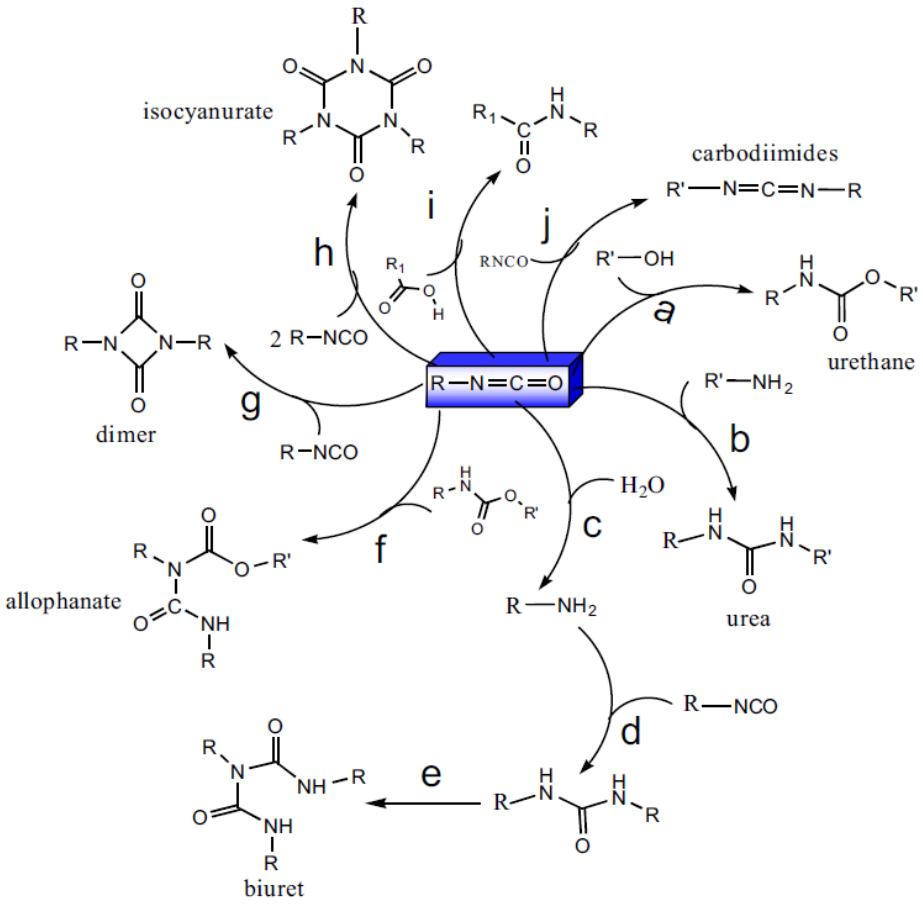

Figure 1.7. Basic reactions of isocyanate with different reactants (120).

Isocyanurate-oxazolidone (ISOX) polymers are prepared from the trimerization of isocyanates and their reaction with epoxides to produce two heat-resistant heterocyclic rings in the polymer backbones, specifically isocyanurates and oxazolidones, respectively. Their application of the ISOX polymers is well-known in high-performance thermoset, especially in high-temperature applications (121). The network structure of the ISOX polymers can be significantly altered by controlling the ratio and type of diisocyanate and diepoxide reactants, the employed catalyst, and the presence of solvents. The combination of these factors acts to control the fraction of the isocyanurate cross-links and oxazolidone chain extenders (121-123). While diisocyanates, which include methylene diphenyl diisocyanate (MDI), toluene diisocyanate (TDI), hexamethylene diisocyanate (HDI), and diepoxides such as bisphenol A diglycidyl ether (DGEBA), bisphenol F diglycidyl ether (DGEBF) (124), have been the most extensively used reactants for the ISOX polymers, a number of

catalysts have been explored for the same polymerization including tertiary amines (NR_3), pyridines (125), imidazoles (126-130), quaternary ammonium halides (131), Lewis acids (132) (133), and alkoxides and phenoxides of alkali earth metals (134, 135). Among these catalysts, tertiary amines have been the most commonly used for the bulk polymerization of ISOX polymers due to their excellent catalytic efficiency and good miscibility with the resins (136, 137). For bulk polymerization of the ISOX polymers with nucleophiles such as tertiary amines, previous studies have shown agreement on the order of the main reactions. Specifically, the reactions proceed in the order of increasing temperatures during the polymerization as follows: (1) trimerization of isocyanate to isocyanurate, (2) oxazolidone formation due to the isocyanate and epoxide reaction, and (3) transformation of isocyanurate to oxazolidone through reaction with excessive epoxide (126, 128, 138).

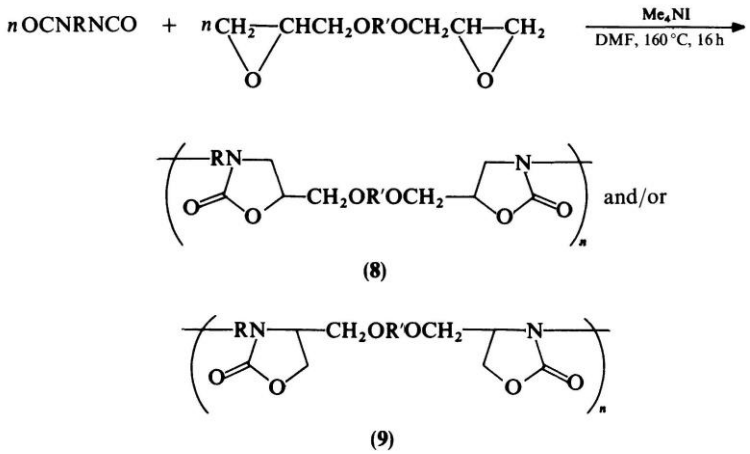

Figure 1.8. Reaction Scheme of synthesis of poly-2-(oxazolidone)s (117).

The high cross-link density of ISOX polymers endows them with high thermal stability and excellent physical and mechanical properties (139, 140). The aromatic isocyanurate can withstand high temperatures of up to 417 °C, while aromatic oxazolidone is stable up to 348 °C (141). In addition to their excellent thermal stability, ISOX polymers have been shown to have superior physical and mechanical properties which provide them with potential to be integrated into or utilized as structural adhesives, high strength foams, and composites in the automobile and

aerospace industries (134, 138). Given the mentioned advantages of ISOX polymers, there have been constant efforts in studying the polymerization of the ISOX polymers to achieve optimal material properties (137). However, there remains no agreement between researchers for the reaction mechanism when using catalytic nucleophiles in the bulk polymerization of ISOX polymers. During the initiation stage of the polymerization, the role of the nucleophile, epoxide, and isocyanate were not accurately assigned. Some reports suggest that two different initiation mechanisms, including zwitterions formed between the nucleophile and epoxide, and zwitterions formed between the nucleophile and isocyanate, which have temperature dependent reactivity, are both active during the polymerization (122). Others later reported that the zwitterions formed between the nucleophile and isocyanate were the catalytic species, as the nucleophile was able to polymerize diisocyanate into isocyanurate polymer at 80 °C (142, 143). Although the trimerization of phenylisocyanate at room temperature in the presence of a catalytic amount of epoxide and R_4NBr/R_3N was also reported (144), few studies in the literature have investigated and reported the nature of the catalytic species during the polymerization of ISOX polymers.

1.5. Dissertation Overview

In the following section, a detailed description of the research performed in each of the ensuing chapters is provided:

Chapter 2 investigates the bulk polymerization mechanism of the isocyanurate-oxazolidone (ISOX) polymers under the catalytic effect of nucleophiles, such as tertiary amines and pyridines. Polymerization of ISOX polymers begins with nucleophiles attacking the epoxide before the zwitterion of the nucleophile/epoxide/isocyanate initiates polymerization. Based on the understanding of the polymerization mechanism, three ISOX polymers 1TDI/1DGEBF, 1.5TDI/1DGEBF, and 2TDI/1DGEBF are developed using commodity reactants through the formation of an isocyanurate-oxazolidone network. Additionally, the isocyanurate-to-oxazolidone transformation within the ISOX polymers is further studied as a promising, novel, high-

temperature stable self-healing chemistry. The isocyanurate transformation is characterized through the chemical composition of the ISOX polymers catalyzed under nucleophiles with varied nucleophilicity and for different post-cure durations. The chemical composition of the ISOX polymers is characterized using Fourier-transform infrared spectroscopy (FTIR) with the assistance of a working curve which is developed using combined characterizations of several model compounds in solution through FT-IR and carbon nuclear magnetic resonance (NMR) spectroscopy. The results show that the isocyanurate fraction of the ISOX polymers can be tuned through monomer stoichiometry, the nucleophilicity of the polymerization catalyst, and post-cure time after an initial two-step curing. The two-step curing, where the ISOX resins are cured at 80 °C and then 200 °C, is designed to ensure the presence of a large amount of isocyanurate within the cured ISOX polymers for healing purposes. The study of the structure - thermal property relationship of the ISOX polymers shows excellent thermal stability of all three developed ISOX polymers in this chapter. The high service temperatures of the ISOX polymers are shown by their Tg which reaches up to 270 °C and the decomposition temperature (Td) which reaches up to 365 °C. The effect of the fraction of isocyanurate, characterized using the cross-link density of the ISOX polymers, on both the Tg and Td of the ISOX polymers is also demonstrated in this chapter.

Building on the great self-healing potential shown in Chapter 2, Chapter 3 focuses on the characterization and evaluation of the healing performance of the developed ISOX polymers. In this chapter, it is shown that this network polymer is repeatedly self-healable in the presence of a macroscopic crack, yielding considerable recovery of the original strength of the polymer after thermal annealing. This self-healing behavior is partialy derived from the high density of the mechano-responsive isocyanurate rings which are introduced as cross-links in the network. After mechanically initiating cycloreversion, the recovery of the isocyanurate rings in a solid state is thermally initiated. Another important factor in the self-healing behaviors of the ISOX polymers is the isocyanruate-to-oxazolidone transformation on the fracture surfaces of the ISOX polymers at elevated temperatures. This transformation is

restricted in the cured ISOX polymers because of the heavy steric effect given the high density of isocyanurate cross-linkers in the polymer network. However, the weakening of the steric effect on the crack surfaces at high temperatures in the presence of epoxide is an important reason for the occurrence of the isocyanurate-to-oxazolidone transformation during the healing and is therefore concluded to be important for the preparation of polymers with high healing efficiencies. By correlating the change in oxazolidone fraction in the polymers during the healing event with the corresponding healing performance of the polymers, the polymer healing efficiencies are evaluated and are shown to be proportional to the isocyanurate fraction in the ISOX polymers. These novel self-healable ISOX polymers exhibit stability at extreme temperatures and demonstrate mechanical properties and mechanical stability which are comparable to widely used engineering plastics. The high cross-link density of the ISOX matrix contributes to its retention of mechanical strength and stiffness at high temperatures, as demonstrated by the high Tg of the polymer. Thus, the addition of the self-healing functionality does not compromise the structural performance of the polymer and this combination of structural function and non-structural function of the polymer would greatly impact the application of thermosets in the fields of structural laminates and electronics packaging.

In extension to the results reported in in chapters 2 and3, novel self-healing, structural CFRP composites with high application temperatures of up to 285 °C, are developed in chapter 4 by using the ISOX thermosets as the polymer matrix. Since major impact and out-of-plane damage typically occur in the polymer matrix for CFRP composites, the repair of the delaminated composites is achieved by the healing of the ISOX polymer matrix under thermal stimulus. Three different self-healing CFRP composites are fabricated with unidirectional carbon fibers as the reinforcement and ISOX thermosets with varying cross-link density as the matrix. These three composites with increasing cross-link density in the polymer matrix are termed ISOX_C1, ISOX_C1.5 and ISOX_C2, respectively. The ISOX thermosets with increased cross-link density are developed by varying the molar ratio of tolylene diisocyanate (TDI) to DGEBF from 1 to 1, 1.5 to 1, and 2 to 1. Each composite sample

is delaminated multiple times under short beam shear (SBS) loading, after which it is treated according to a standard healing procedure after each damage event. Specifically, the standard healing procedure includes heating the composite sample at 200 °C for 12 h under approximately 100 psi. The average recovery of SBS strength for the delaminated ISOX_C2 is characterized by a first healing efficiency of up to 85% and a second healing efficiency above 70%. Both the microcracks and delamination initiated within the composite through shear loading are repeatedly eliminated under heat without the use of any additives by using the inherent self-healing capacity of the ISOX matrix. The mechanical properties of the developed self-healing CFRP composites are comparable to those of engineering grade CFRP composites with an epoxy matrix, as is demonstrated by their high strength and elastic modulus characterized using a tensile test. Without compromising the structural advantages of the CFRP composites, both at room temperatures and high temperatures, the self-healing capability is successfully introduced into the composites, thus demonstrating their great potential as advanced multifunctional structural materials.

The final chapter of this dissertation starts with a brief overview of the findings throughout the dissertation. After the overview, the contributions of this dissertation and their possible influence on future research investigating intrinsically self-healing polymers for structural applications is discussed. Additionally, the final section of this chapter describes potential future work.

CHAPTER 2

Study of Isocyanurate-to-Oxazolidone Transformation as a New Healing Chemistry in Isocyanurate-Oxazolidone (ISOX) Polymers

2.1 Chapter Introduction

This chapter focuses on the understanding of the polymerization mechanism of Isocyanurate-oxazolidone (ISOX) polymers under the catalytic effect of nucleophiles including tertiary amines and pyridines. A variety of nucleophiles are carefully evaluated in terms of the catalytic efficiencies, and the individual role of the nucleophiles, epoxides and isocyanates, during the initiation of the polymerization, is studied as forming nucleophile/epoxide/isocyanate zwitterions at room temperature. Stronger nucleophiles lead to faster formation of the zwitterion and stronger catalytic effect for the trimerization of the isocyanates at the early stage of the polymerization. At higher temperatures, as the chain mobility is improved, further conversion of isocyanates and epoxides leads to more oxazolidone and isocyanurate formation, and higher extent of polymerization. However, the maximum polymerization extent of the ISOX polymers is reached before the depletion of all reactants because of the heavy steric effect resulting from the distribution of dense isocyanurate cross-links in the polymer network.

Building on the study on the polymerization mechanism, isocyanurate-to-oxazolidone transformation within the ISOX polymers are thoroughly investigated because of its potential as a novel, high-temperature stable healing chemistry. The isocyanurate-to-oxazolidone transformation comes from the instability of the isocyanurate rings in the presence of epoxides at elevated temperatures, and each isocyanurate ring transforms into three oxazolidone rings through this transformation.

Combined characterizations of Fourier-transform infrared (FTIR) spectroscopy and carbon nuclear magnetic resonance (NMR) spectroscopy are used to measure the isocyanurate fraction in the ISOX polymers, which can be tuned through both the nucleophilicity of the polymerization catalysts and post-cure time of the ISOX polymers.

2.2 Investigation of Isocyanurate-to-Oxazolidone Transformation

Isocyanurate, as the trimer of isocyanates, is a thermally stable heterocyclic ring which can withstand temperatures up to 417 °C with aromatic pendants, and it has been widely utilized to improve high-temperature resistance and flame retardancy of polyurethanes (114-116). However, it is reported that isocyanurate is not stable in the presence of epoxides at elevated temperatures where it transforms into three oxazolidone rings (141). The product of this transformation, oxazolidone, by itself is also thermally stable up to 348 °C (141). Because of the outstanding thermal stability of the isocyanurate and oxazolidone, the isocyanurate-to-oxazolidone transformation (Figure 2.1) is first studied in this chapter because of its great potential as a new healing chemistry with high-temperature resistance. Under heat stimulus, isocyanurates react with epoxides to form oxazolidones right on the damage spot to serve the self-healing purposes.

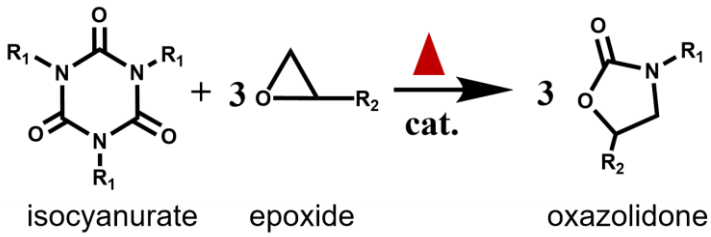

Figure 2. 1. Scheme of the isocyanurate-to-oxazolidone transformation.

This isocyanurate-to-oxazolidone transformation is first studied in solution using a model compound, which is consist of 1 mmol p-tolyl isocyanate (PTI), and 1 mmol 1.4-butanediol diglycideyl ether (BDE) in dimethyl sulfoxide (DMSO) solvent, with

0.1 wt% of benzyldimethylamine (BDMA) added as the reaction catalyst. The mixture is first kept at 80 °C for 1 h, and then at 150 °C for 3 h in an oven. Both Fourier-transform infrared (FTIR) spectroscopy and carbon nuclear magnetic resonance (NMR) spectroscopy are used to characterize the reaction products after the 80 °C and 150 °C reaction. FTIR is widely used as a chemical composition characterization technique, which can provide information about chemical structures such as chemical bonds, functional groups, and chain conformations. By measuring how much of infrared light with different frequencies is absorbed by the sample, the absorption at different wavelengths is then obtained. Absorption occurs when the frequency of infrared spectroscopy matches the characteristic vibrational frequency of a bond. FTIR is therefore a convenient and efficient method to validate the composition change of the model compound reaction at different reaction temperatures, as the carboxyl groups of isocyanates, isocyanurates, and oxazolidones have their characteristic absorptions under FTIR. FTIR measurements of the reaction products are performed by a Nicolet iS50 spectrometer (Thermo Scientific) with a diamond ATR in the wavenumber range of 600~4000 cm^{-1}. Each spectrum is collected with 16 scans and a resolution number of 4. The FTIR results of the products after 80 °C and 150 °C are shown in Figure 2.2, where completed conversion of isocyanate is detected after the 80 °C reaction while the strong absorption of isocyanurates is observed in the product, as there is no absorption of carboxyl of isocyanate at 2250 cm^{-1} and only the absorption at 1710 cm^{-1} from the carboxyl of isocyanurate can be seen. However, no isocycanurate is detected under FTIR after the 150 °C reaction as no peak presents at 1710 cm^{-1}. Instead, a new peak appears at 1750 cm^{-1}, indicating the oxazolidone formation under the raised reaction temperature.

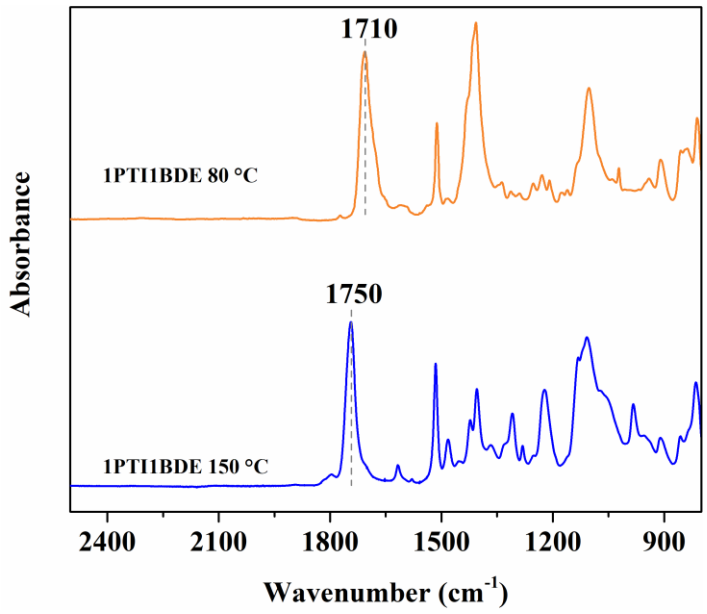

Figure 2.2. FTIR spectra of 1PTI/1BDE/BDMA reaction after 80 °C (dash line represents isocyanurate absorption band at 1710 cm^{-1}) and then 150 °C (dash line represents oxazolidone absorption band at 1750 cm^{-1}).

Although FTIR is a powerful qualitative characterization technique for detecting any change in chemical structures in the 1PTI/1BDE/BDMA model compound, it cannot quantify the compositional change with high accuracy. For quantitative characterization, nuclear magnetic resonance (NMR) spectroscopy is considered as a definitive method to identify organic compounds and measure the molar ratio between different components. NMR is a spectroscopic technique, which can produce nuclear magnetic resonance signals through the excitation of the nuclei with radio waves. For a specific atom in a molecule, its unique and characteristic intramolecular magnetic field determines its resonance frequency and NMR can therefore provide detailed electronic structures of the specific molecule (145). For proton NMR, the integration of the peaks is proportional to the number of the hydrogen atoms at specific sites and therefore, it can quantify the composition of an organic blend. For carbon NMR, however, it has a much lower resolution than proton NMR because isotope ^{13}C has a natural abundance of 1.1%, while in most cases, all the hydrogen atoms in organic compounds consist of the isotope ^{1}H. In the cases where there are no hydrogen atoms in the molecules, carbon NMR can be used to characterize the carbon skeleton structure

of the compound, although more scans, longer acquisition time and relaxation delay are required to get a relatively high resolution for the quantitative analysis. For the most common types of proton NMR and carbon NMR, samples are usually dissolved in a solvent, however it is difficult to get equally well-resolved spectra from solid NMR based on magic angle spinning (146).

For the model compound characterized by FTIR above, there is no hydrogen in neither isocyanates nor isocyanurates, so proton NMR is not suitable for characterizing the isocyanurate-to-oxazolidone transformation. Instead, carbon NMR technique is an ideal choice to characterize this transformation as it can identify the carbon structure of the compound. For quantitative measurements of the reaction products, a Varian vnmr 500 MHz instrument with a Varian 5 mm PFG OneNMR probe is used. Proton decoupling is used to eliminate the nuclear Overhauser effect (NOE). A spectrum window of 40 to 210 ppm is used to ensure that all peaks of interest fall within 60% in the center of the spectrum. For quantification analysis, an acquisition time of 5 seconds and a 90° pulse with a relaxation delay of 25 seconds are used. Each sample is dissolved in dimethyl sulfoxide (DMSO)-d_6 and is scanned 256 times to get an optimal signal to noise ratio. As can be seen from the carbon NMR spectrum of the product in Figure 2.3 (a), after the 80 °C reaction, the peak at 149 ppm is detected at high field, which is assigned to the isocyanurate (147). After the reaction temperature is raised to 150 °C, the peak at 149 ppm disappears, while the peak at 154 ppm which is assigned to the oxazolidone is observed in the carbon NMR spectrum, as shown in Figure 2.3 (b), which indicates the consumption of the isocyanurate and the formation of oxazolidone during the process.

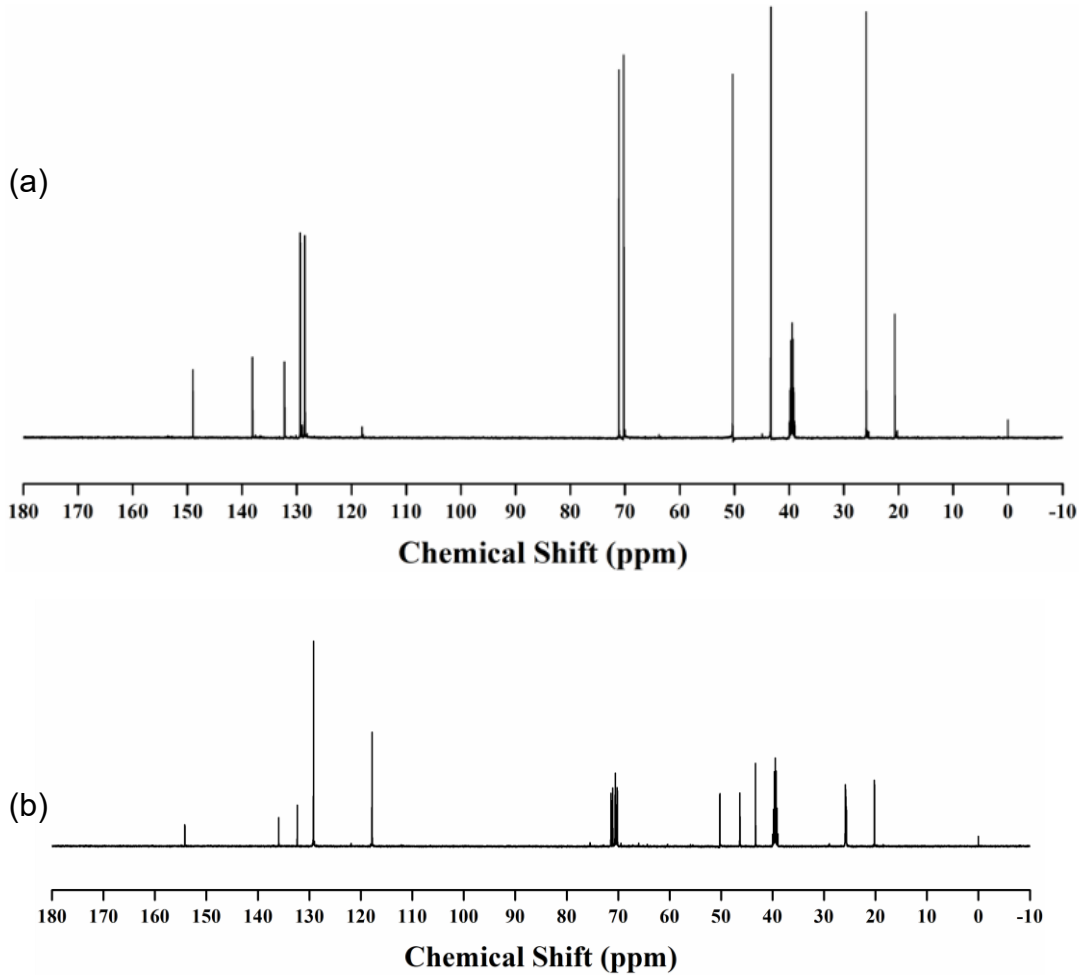

Figure 2.3. (a) Carbon NMR spectrum for 1PTI/1BDE/BDMA after 80 °C reaction (500 Hz, DMSO-d6, 149.01, 138.12, 132.26, 129.38, 128.55, 118.10, 71.05, 70.24, 50.32, 43.35, 25.92, 20.69 ppm). (b) Carbon NMR spectrum for 1PTI/1BDE/BDMA after 150 °C reaction (500 Hz, DMSO-d6, 154.22, 135.97, 132.36, 129.20, 117.83, 70.56, 50.25, 46.37, 43.32, 25.88, 20.21 ppm).

For the carbon NMR spectrum of the model compound after the 80 °C reaction as shown in Figure 2.3 (a), the peak at 149 ppm corresponds to isocyanurate carbonyl carbons; the peak at 138 ppm corresponds to aromatic carbons para to isocyanurate-substituted aromatic carbons; the resonance at 132 ppm corresponds to isocyanurate-substituted aromatic carbons; the peak at 129 ppm corresponds to unsubstituted aromatic carbons meta to isocyanurate-substituted aromatic carbons; the resonance at 128 ppm corresponds to aromatic carbons ortho to isocyanurate-substituted aromatic carbons; peaks at 71 and 70 ppm correspond to the two aliphatic carbons of the linear ether in the diepoxide; peaks at 50 and 43 ppm correspond to the

two aliphatic carbons of the epoxide; the resonance of 26 ppm corresponds to aliphatic carbons of methylene group centered in the diepoxide; the resonance of 20 ppm corresponds to aliphatic carbons of methyl group para to the isocyanurate-substituted aromatic rings.

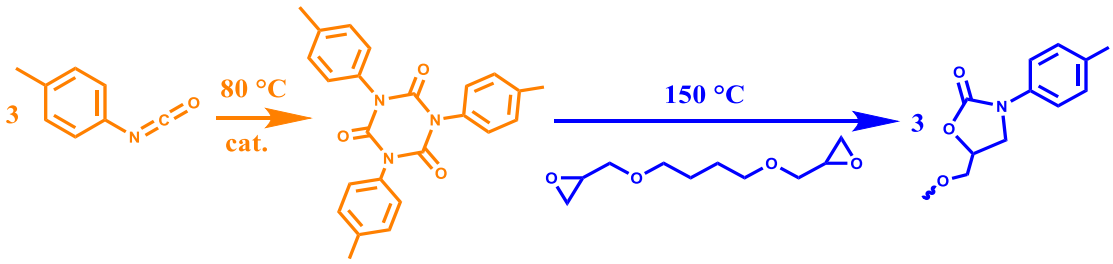

Figure 2.4. Reaction scheme of the 1 mmol p-tolyl isocyanate (PTI) / 1 mmol 1, 4-butanediol diglycideyl ether (BDE) in dimethyl sulfoxide (DMSO) with (benzyldimethylamine) BDMA as catalyst.

The isocyanurate-to-oxazolidone transformation is then studied in the polymeric system in the presence of heavy steric effect, in contrast to the unrestricted molecular mobility of the model compound in solution discussed above. Toluene diisocyanates (TDI) are first trimerized into TDI polymer under the catalytic effect of 1 wt% BDMA at 100 °C for 12 h. Under FTIR, a large amount of isocyanate and isocyanurate is detected in the TDI polymer, as shown in Figure 2.5, and the detected isocyanate is from the partially trimerized TDI trapped within the polymer network because of the heavy steric effect derived from the dense cross-link structure of the TDI polymer. In contrast with the TDI polymer, no isocyanate is detected in the model compound in neither FTIR or carbon NMR spectrum as discussed above, due to the full conversion of the isocyanate facilitated by higher molecular mobility. The TDI polymer is a light-yellow solid with a three-dimensional polymer network structure as shown in Figure 2.6, where isocyanurate is the cross-link in the network. The TDI polymer is then mixed with an excessive amount of bisphenol F diglycidyl ether (DGEBF), an reactant with two epoxide groups as shown in Figure 2.6. The mixture of the TDI polymer and DGEBF is then treated at 200 °C overnight and it ends up as an orange, transparent, and homogenous liquid. This whole process is demonstrated in the scheme in Figure 2.7. Under FTIR, only oxazolidone is detected while no isocyanate or isocynuarate

remains, as shown in Figure 2.5. Comparing the FTIR results of the TDI polymer and the heat treated TDI polymer/DGEBF mixture, the instability of the isocyanurate in the presence of epoxides under thermal stimulus is unaffected, despite the significantly increased steric effect in the polymer network. Again, this instability of the isocyanurate is promising as a new healing chemistry for new bond formation required by self-healing purposes.

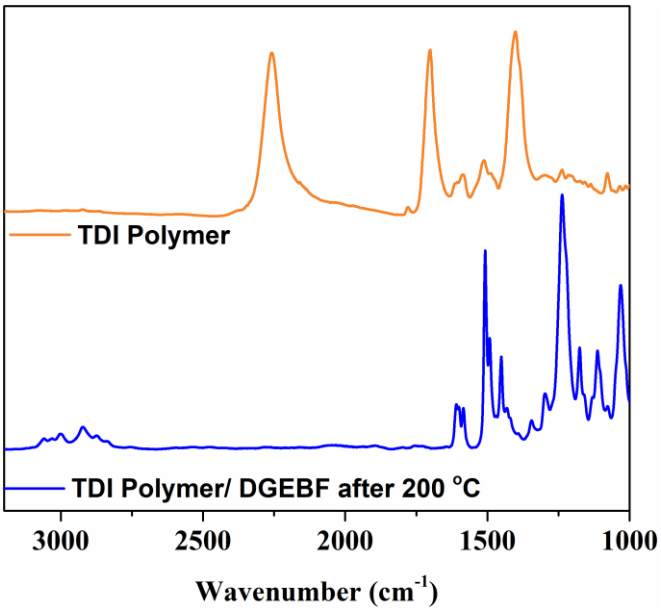

Figure 2.5. FTIR spectra of TDI polymer trimerized from toluene diisocyanates (TDI), and TDI polymer/DGEBF mixture heat treated at 200 °C overnight.

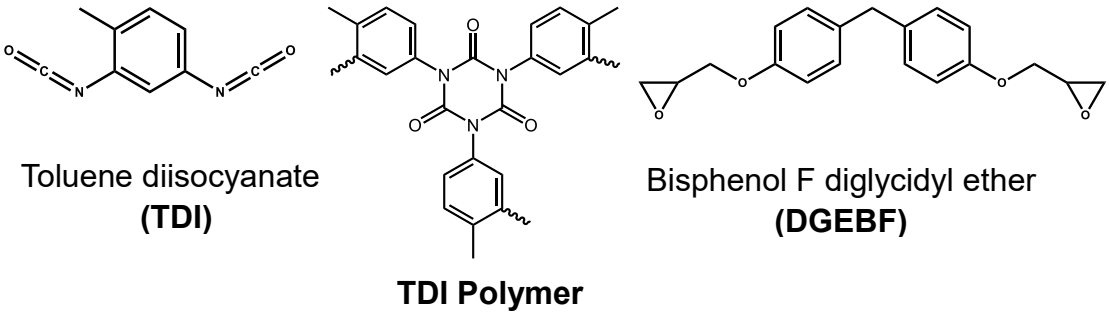

Figure 2.6. Reactants investigated for the study of the isocyanurate-to-oxazolidone transformation in the polymer network.

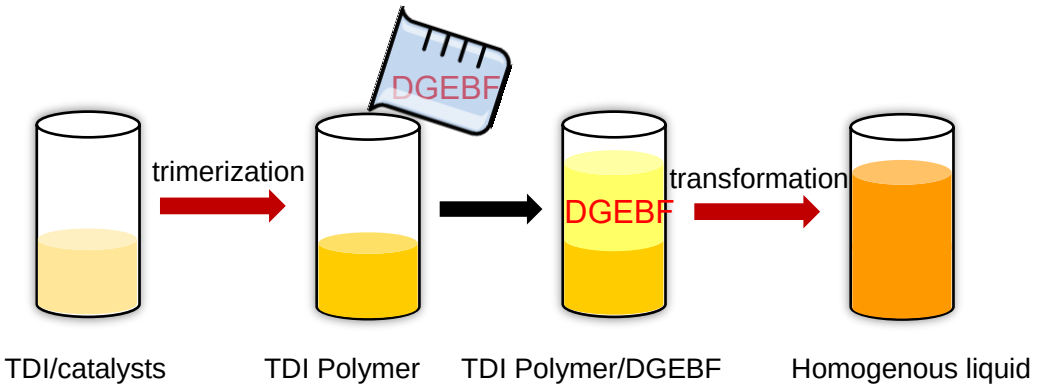

Figure 2.7. Scheme of the isocyanurate-to-oxazolidone transformation in the TDI polymer network.

2.3 Polymerization of the Isocyanurate-Oxazolidone (ISOX) Polymers

The polymerization mechanism of isocyanurate-oxazolidone (ISOX) polymers is investigated first to further understand the isocyanurate-to-oxazolidone transformation in the polymer network. The initiation stage of the polymerization, isocyanurate formation, isocyanate-to-oxazolidone and isocyanurate-to-oxazolidone transformation, are studied under the catalytic effect of tertiary amines and pyridines. 1,4-diazabicyclo [2.2.2] octane (DABCO), benzyldimethylamine(BDMA) and 2-dimethylaminopyridine (2-DMAP), are added individually to catalyze the polymerization. Lewis basicity of the utilized nucleophiles, DABCO, BDMA and 2-DMAP decreases from left to right in Figure 2.8, as indicated by their *pKa* values (148, 149).

.

As the polymerization proceeds, the viscosity of the ISOX resins increases with time, and the viscosity increase is slow at the early stage of the curing until there is a sudden and large increase in viscosity, and the time needed to reach this point is called gel time (150). The gel time is an important molding parameter, since the processing of resin becomes increasingly difficult when approaching the gel time. When epoxide or isocyanate is solely present in the reaction, the catalysts cannot efficiently initiate the polymerization and the gel time is longer than 24 hours. However, in the presence of epoxide and isocyanate together, the gel time for the isocyanurate-oxazolidone

polymers catalyzed with BDMA is around 20 minutes, as shown by the gel point measurement results for the three ISOX polymers in Figure 2.9. The initiation of the polymerization, started by the zwitterion formation from the nucleophiles, epoxide and isocyanate, is discussed in detail in the following paragraphs.

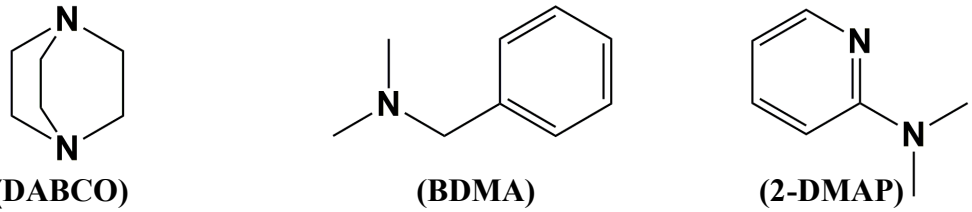

(DABCO)

1,4-Diazabicyclo [2.2.2]octane

(BDMA)

Benzyldimethylamine

(2-DMAP)

2-Dimethylamino pyridine

Figure 2.8. Tertiary amines and pyridine investigated for the polymerization of isocyanruate-oxazolidone (ISOX) polymers.

For the polymerization of the ISOX polymers, DGEBF and TDI are purchased from Momentive and Acros Organics, respectively. For the three catalysts, benzyldimethylamine (BDMA, 99%) is purchased from Acros Organics, 1,4-diazabicyclo [2.2.2] octane (DABCO, 99%) is purchased from Sigma Aldrich and 2-dimethylaminopyridine (2-DMAP, 98%) is purchased from TCI America™. 1,4-butanediol diglycidyl ether (BDE), phenyl glycidyl ether (PGE) and p-tolyl isocyanate (PTI) are purchased from Fisher and all the chemicals are used as received. A DV2T viscometer from Brookfield is used to conduct viscosity tests on the ISOX resins under ambient conditions. A fixed volume of TDI and DGEBF with a 1 to 1 ratio are mixed thoroughly for 10 minutes before the addition of 0.1 wt% of each catalyst, and then a rotating spindle is immersed in the resin immediately to monitor the gelling process.

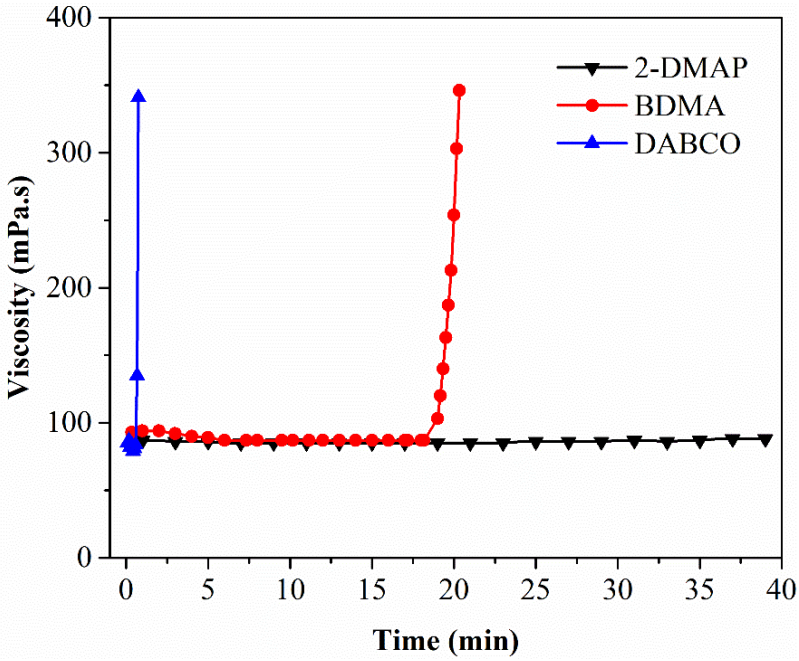

Figure 2.9. Viscosity measurements during the gelling process of ISOX polymers with three polymerization catalysts: DABCO, BDMA and 2-DMAP.

During the initiation stage of the polymerization, two zwitterions can be active depending on the initial nucleophilic reaction induced by the nucleophiles. The nucleophiles attack the epoxide first and zwitterion 1 forms, while the nucleophiles attack the isocyanate first and zwitterion 2 forms, as shown in Figure 2.10. Zwitterion 1 is the true active species during the initiation, suggested by both experimental evidence and simulation evidence. At room temperature, 1 mmol p-tolyl isocyanate (PTI), 1 mmol phenyl glycidyl ether (PGE), and 0.1 wt% benzyldimethylamine (BDMA) are mixed in DMSO-d_6 and immediately characterized by proton NMR. Based on the proton NMR spectrum of the mixture, the formation of the ring-opening product of PEG is confirmed by the presence of three new peaks at 3.57 ppm, 3.72 ppm, and 5.12 ppm, as by comparison of Figure 2.11 and Figure 2.12. The proton signal of CH in the epoxide ring showed a downfield shift from 3.33 to 5.12 ppm, suggesting zwitterion 1 as the active species. In the case of zwitterion 2, a new chemical shift at lower field would be expected, however it is not observed. Previous research (151) has reported a lower activation energy of 14.6 kcal/mol for zwitterion 1 and 34.3 kcal/mol for zwitterion 2, which further supports that zwitterion 1 is the true initiating species for the polymerization. For nucleophiles with varied nucleophilicity, the

stronger ones lead to faster formation of the initiating species, resulting in significantly reduced gel time. As can be seen in Figure 2.8, the polymer with DABCO catalyst, the strongest nucleophile, gels in less than one minute, making it difficult to mold the polymers and it is not further utilized as the polymerization catalyst in the following study.

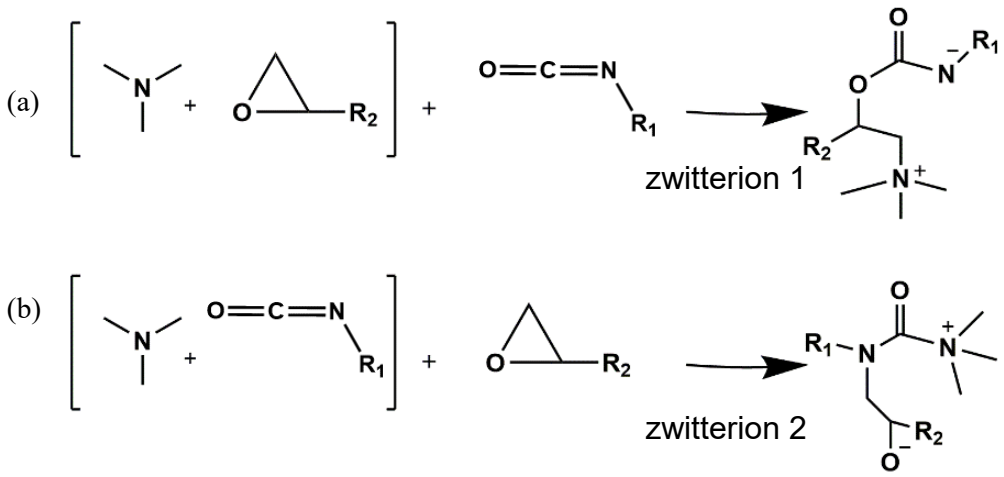

Figure 2.10. Zwitterion formation as initiation mechanism of (a) tertiary amines/pyridine attacks the epoxide first; (b) tertiary amines/pyridine attacks the isocyanate first (122).

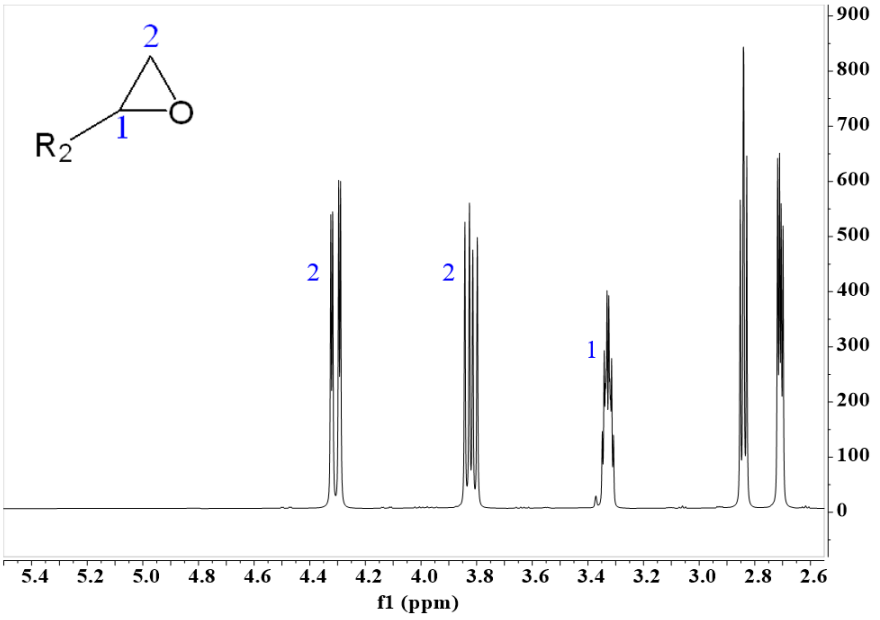

Figure 2.11. Proton NMR spectrum for phenyl glycidyl ether (500 Hz, DMSO-d_6, 4.31, 3.82, 3.33, 2.84, 2.71 ppm).

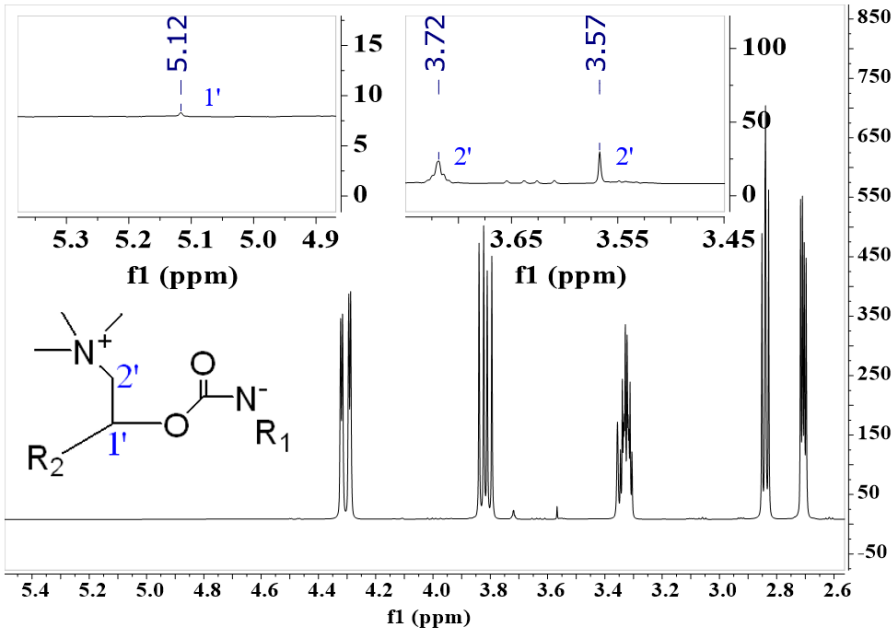

Figure 2.12. Proton NMR spectrum for 1 mmol phenyl glycidyl ether /1 mmol p-tolyl isocyanate /0.1 wt% benzyldimethylamine (500 Hz, DMSO-d_6, 5.12, 4.79, 4.31, 3.82, 3.33, 2.84, 2.71 ppm).

Following the formation of the catalytic species, trimerization of the isocyanates dominates the first stage of the polymerization because isocyanurate is the only species detected after the first curing step at 80 °C. As shown in Figure 2.13, the nitrogen anion of the isocyanate acts as the nucleophile, attacks two free isocyanates and forms the cyclic isocyanurate ring, releasing the epoxide/tertiary amine for the formation of another isocyanurate. Unlike the full conversion in the model compound cases to be discussed in this section, the isocyanate-to-isocyanurate conversion in the polymer network is hard to reach 100%, as the steric effect caused by the increasing crosslinking density gets stronger during the trimerization. As a result, a large portion of isocyanate remains trapped in the polymer network, which enables the formation of oxazolidone at elevated temperatures. It should be noted that the trimerization rate increases with stronger nucleophiles due to the more rapid formation of the zwitterions. In other words, more isocyanurate forms during the first stage of the polymerization given the same polymerization time at 80 °C, due to the enhanced catalytic effect of stronger nucleophiles.

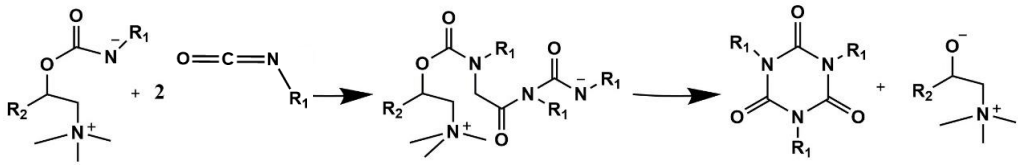

Figure 2.13. Trimerization mechanism (isocyanate to isocyanurate).

Steric effects in the ISOX polymers get weakened as the temperature increases from 80 °C to 200 °C, leading to higher molecular mobility, allowing for more isocyanurate formation with the remaining isocyanate after the trimerization stage. Meanwhile, oxazolidone formation predominates at 200 °C, which is demonstrated by two model compounds discussed below. As shown in Figure 2.14, after the formation of isocyanurate, the released zwitterion combines with epoxide and isocyanate to give oxazolidone in the polymer network at 200 °C. For the ISOX polymers polymerized under the stronger nucleophiles, less oxazolidone is expected to form during this stage as more isocyanate has been converted to isocyanurate at the trimerization stage with faster trimerization rate. For the isocyanurate-to-oxazolidone transformation, the speculated mechanism is shown in Figure 2.15, where the residual nucleophiles attack the isocyanurate ring and yield oxazolidone and isocyanate. The resulting free isocyanate then further transforms into oxazolidone in the presence of nucleophiles and epoxides, leading to more oxazolidone formation. As this process continues, more oxazolidone is obtained in the polymer network, before equilibrium between the isocyanurate and oxazolidone is finally reached at this temperature.

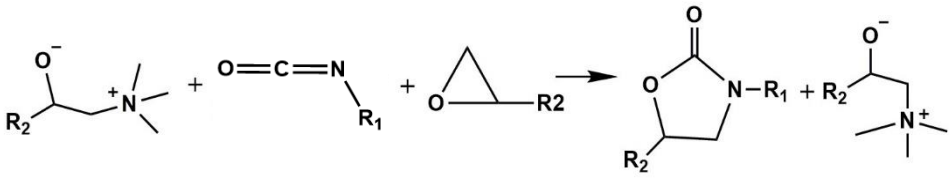

Figure 2.14. Isocyanate-to-oxazolidone transformation.

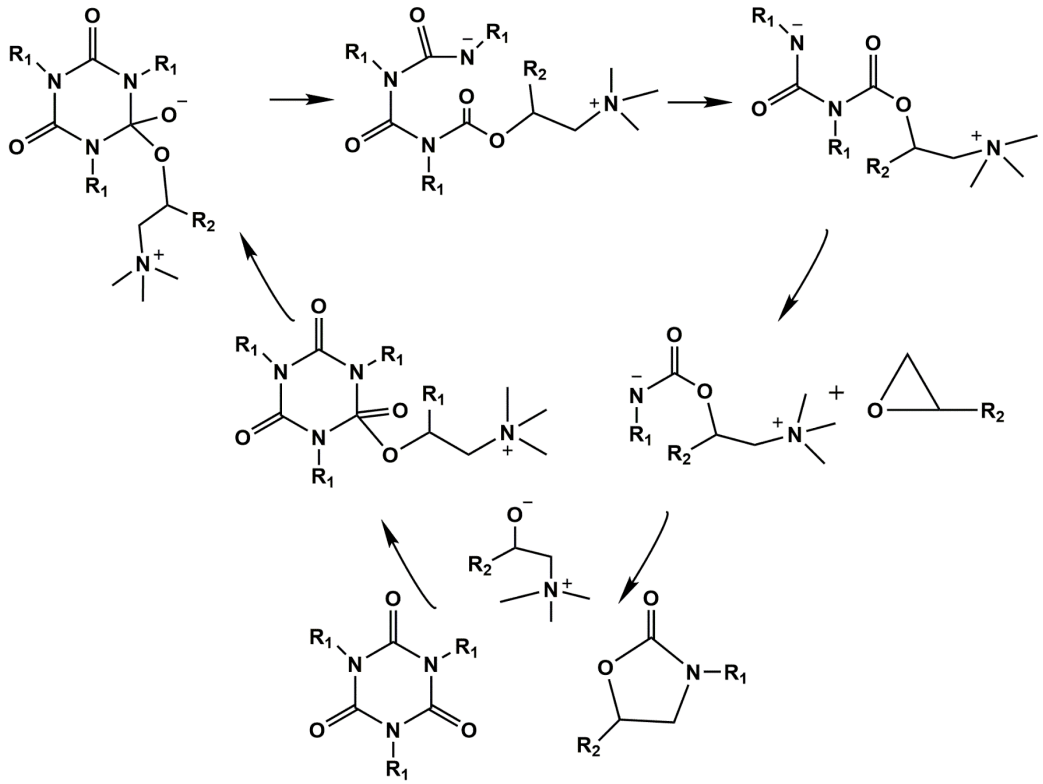

Figure 2.15. Isocyanurate-to-oxazolidone transformation.

To ensure that a large amount of isocyanurate and epoxide is present in the polymer network, a two-step curing is designed for the polymerization of the ISOX polymers. The ISOX resins, consisting of bisphenol F diglycidyl ether (DGEBF), tolylene-2, 4-diisocyanate (TDI), and catalysts including benzyl dimethylamine (BDMA) and 2-dimethylaminopyridine (2-DMAP), are cured at 80 °C for 1 h during the first curing step. During this stage, only part of the isocyanate trimerizes into isocyanurate under the catalytic effect of initiation species, as further trimerization is prevented by the rising steric effect, leaving the unreacted isocyanate trapped in the polymer network. The unreacted isocyanate then reacts with epoxide and forms the oxazolidone, when the molecular mobility gets improved at an elevated temperature during the second curing step at 200 °C. The purpose of the second curing step is to exhaust all the isocyanate in the ISOX polymers through either transformation into isocyanurate ring or oxazolidone ring. The network structure of the ISOX polymers is shown in Figure 2.16, where isocyanurate is the crosslink and the oxazolidone is the chain extender in the polymer network.

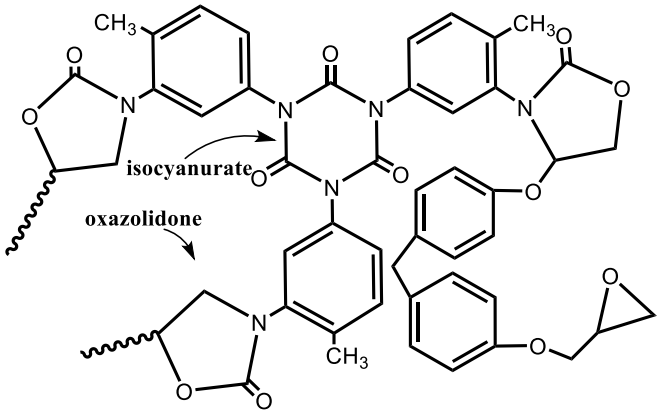

Figure 2.16. Network structure of the isocyanurate-oxazolidone (ISOX) polymers.

The two monomers of the polymerization, DGEBF and TDI are mixed with molar ratios of 1:1, 1:1.5, and 1:2, respectively, before the addition of 0.1 wt% of BDMA/2-DMAP. The purpose of the stoichiometry variation is to tune the ring concentrations of isocyanurate and oxazolidone for the study on the structure-property relationship of the ISOX polymers. After the applied two-step curing of the ISOX resins, three polymers of 1TDI/1DGEBF, 1.5TDI/1DGEBF and 2TDI/1DGEBF are fabricated, and FTIR is used to monitor the curing of the ISOX polymers. As can be seen from the FTIR spectra of the TDI/DGEBF mixture and the three ISOX polymers, the TDI /DGEBF mixture without the curing process shows a strong peak at 2260 cm^{-1}(carbonyl of isocyanate). However, this absorption at 2260 cm^{-1} disappears in three ISOX cured polymers, indicating full conversion of isocyanate during the two-step curing process. Strong characteristic peaks at 1710 cm^{-1} (carbonyl of isocyanurate) and 1750 cm^{-1} (carbonyl of oxazolidone) are both detected in the cured ISOX polymers. The peak at 1100 cm^{-1} is attributed to ether in DGEBF (C-O-C) and the peak at 910cm^{-1} attributed to epoxide, are observed in all the samples. This change in spectra confirms the formation of the polymer network via trimerization of isocyanates to isocyanurate rings, the formation of oxazolidone as chain extenders by reaction of DGEBF with isocyanurate rings, and the formation of ether through homopolymerization of DGEBF as a side reaction (122).

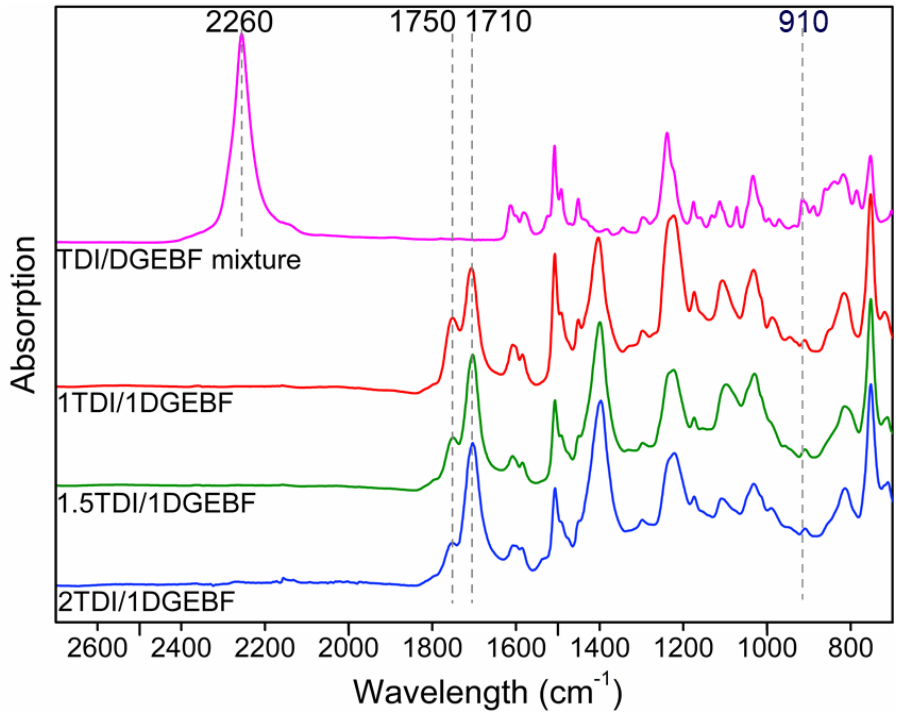

Figure 2.17. FTIR spectra for the TDI/DGEBF mixture and the three ISOX polymers, 1TDI/1DGEBF, 1.5TDI/1DGEBF and 2TDI/1DGEBF.

As expected, the absorption intensity at 1710 cm^{-1} increases with more TDI in the ISOX resins, indicating more isocyanurate in the corresponding polymers. In contrast, the absorption intensity at 1750 cm^{-1} decreases with less TDI in the ISOX resins. Besides the stoichiometry of the monomers, the ring concentrations of the ISOX polymers can also be tuned by the post-cure of the polymers at 250 °C after the initial two-step curing, because the post-cure allows for further isocyanurate-to-oxazolidone transformation within the polymers. Another important parameter for tuning the polymer composition is the nucleophilicity of the polymerization catalysts. Based on the polymerization mechanism, the initiation species derived from the polymerization catalyst participate in each curing step and determine the formation of both the isocyanurate ring and oxazolidone ring. To promote a deeper understanding of how these factors together determine the ultimate network structure of the ISOX polymers, 1TDI/1DGEBF is polymerized with BDMA and 2-DMAP individually, and the resulting polymers are then post-cured at 250 °C for durations of 0, 1 and 3 h.

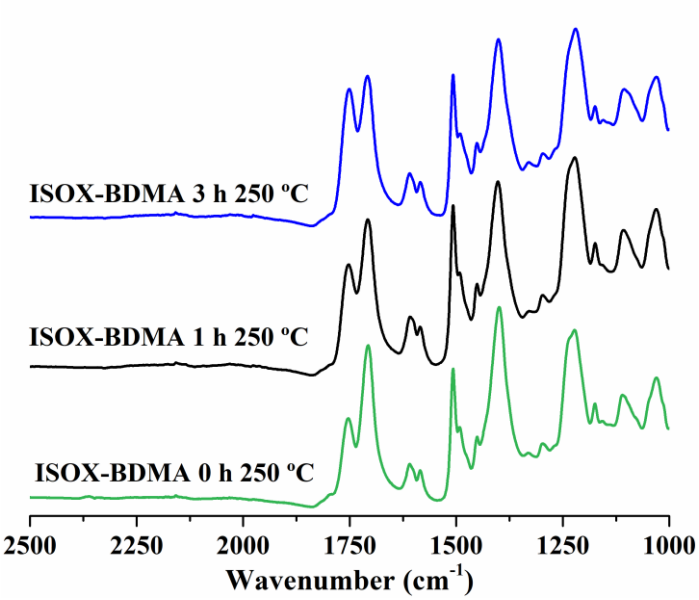

Figure 2.18. FTIR spectra for the 1TDI/1DGEBF polymers with BDMA after post-cure at 250 °C for 0, 1 and 3 h.

As can be seen in Figure 2.18, for the 1TDI/1DGEBF polymers polymerized under BDMA (ISOX-BDMA), a significant amount of oxazolidone forms during the post-cure and the proportion is increasing with elongated post-cure time. As there is no isocyanate present in the ISOX-BMDA after the initial two-step curing, the oxazolidone can only be formed from the isocyanurate-to-oxazolidone transformation, which is promoted at a much faster rate at 250 °C than at 200 °C. FTIR spectra of the 1TDI/1DGEBF polymers polymerized under 2-DMAP (ISOX-2DMAP) is shown in Figure 2.19, where a similar trend that oxazolidone fraction increases with increased post-cure time is found. However, comparing the results of 0 h and 1 h at 250 °C, the post-cure has a more significant effect on the ring concentrations of the 2-DMAP polymers, resulting in very different FTIR spectra of the 2-DMAP polymers and that of the BDMA polymers. Comparing Figure 2.18 and Figure 2.19, more oxazolidone (1750 cm^{-1}) is observed in the 2-DMAP polymers in each case, and this variation in the ring concentrations is derived from the different nucleophilicity of BDMA and 2-DMAP.

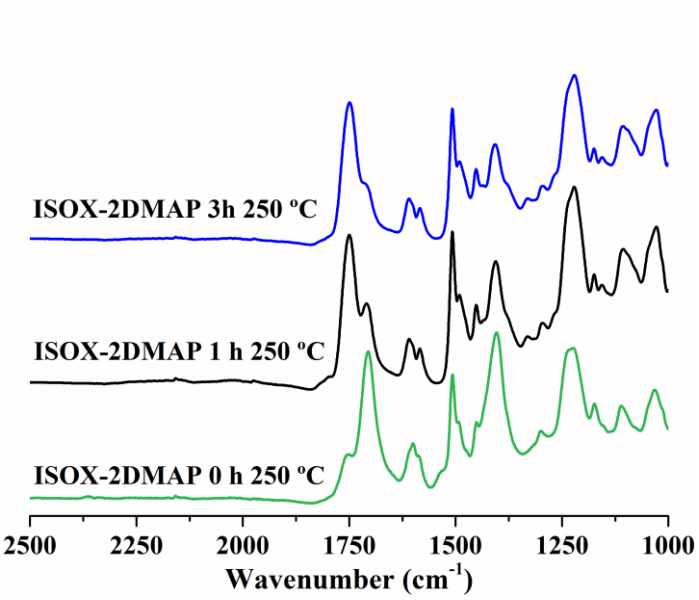

Figure 2.19. FTIR spectra for the 1TDI/1DGEBF polymers with 2-DMAP after post-curing at 250 °C for 0, 1 and 3 h.

The electronic structures of BDMA and 2-DMAP are shown in Figure 2.20, where the initiation species formed with the corresponding catalysts are also shown. BDMA is more nucleophilic than 2-DMAP because the tertiary amine in BDMA retains its electron density, whereas the tertiary amine of 2-DMAP donates part of the electron density to the pyridine due to the conjugation (152). The lower nucleophilicity slows down the nucleophilic attack of the 2-DMAP towards epoxide and isocyanate during the initiation stage of the polymerization. The more nucleophilic BDMA forms more efficient catalytic species for trimerization, and thus more isocyanate trimerizes into isocyanurate during the first curing step. In other words, more unreacted isocyanate is left in the 2-DMAP case, which further reacts with epoxide at elevated temperatures to give more oxazolidone.

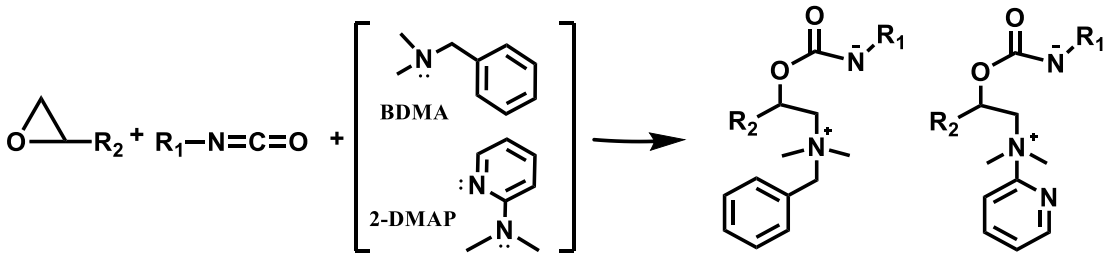

Figure 2.20. Electron structures of the polymerization catalysts of BDMA and 2-DMAP and the corresponding initiation species.

Although it is concluded that the oxazolidone fraction increases with increased post-cure time, the exact concentrations of isocyanurate and oxazolidone are still unknown because FTIR by itself cannot be used as for quantitative analysis, as discussed ealier in this chapter. In other words, the isocyanurate fraction and oxazolidone fraction in each case with variation in monomer stoichiometry, polymerization catalyst and post-cure time, are only apparent numbers obtained from the FTIR spectra instead of real ring concentrations. However, it is important to quantify and control the oxazolidone and isocyanurate concentrations in the ISOX polymers, especially the isocyanurate concentration, as it determines the extent of isocyanurate-to-oxazolidone transformation for the potential healing performance of the developed ISOX polymers. In the following section, a quantitative method combining FTIR and carbon NMR is developed to measure the true oxazolidone and isocyanurate concentrations of the ISOX polymers, and further utilization of this method is presented in the later chapters.

2.4 Characterization of Isocyanurate Fraction in the ISOX Polymers

To quantify the isocyanurate concentration in the ISOX polymers, carbon NMR, which is used to characterize the model compound in the section 2.2, is no longer a suitable technique for the characterizing the ISOX polymers, as the polymers cannot be dissolved in solvent. Given the low sensitivity and high cost of solid carbon NMR, it is neither considered in the study for quantitative analysis of the polymer composition. The isocyanurate fraction can be measured from FTIR, however, it is only an apparent number instead of real isocyanurate concentration (153). In this section, a working curve is developed through combined FTIR and carbon NMR characterizations of three model compounds. With the working curve, the apparent oxazolidone and isocyanurate concentrations in the ISOX polymers measured by FTIR, can be interpreted into the real concentrations. Also, the compositional change during the isocyanurate-to-oxazolidone transformation can be conveniently measured through

FTIR with the assistance of the working curve, which serves to instruct the development of novel self-healing polymers in the following chapter. Detailed discussion is given in the following paragraphs on the development of the working curve with the combined characterization method.

Three model compounds, specifically 3PTI/1BDE/BDMA (model compound 1), 1PTI/1PGE/BDMA (model compound 2), and 1PTI/1BDE/BDMA (model compound 3), are first prepared. The p-tolyl isocyanate (PTI), 1,4-butanediol diglycidyl ether (BDE), and phenyl glycidyl ether (PGE) are purchased from Fisher and all the chemicals are used as received. The reactants in the three model compounds are first dissolved in DMSO and 0.1wt% of BDMA is used as the catalyst. The three model compounds are treated under heat with pre-determined procedures specified in Table 2.1 and then characterized under both FTIR and carbon NMR. Model compound 1 and 2, represent the case of excessive isocyanate and the equivalent stoichiometry case respectively, while model compound 3 represents the case of excessive epoxide.

Table 2.1. Three model compounds used for the development of a working curve.

	Reactant Molar Ratios	Heat Treatment
Model Compound 1	3PTI/1BDE/BDMA	80 °C 1 h, 150 °C 3 h, 200 °C 1 h
Model Compound 2	1PTI/1PGE/BDMA	80 °C 1 h, 150 °C 3 h, 200 °C 1 h
Model Compound 3	1PTI/1BDE/BDMA	80 °C 1 h, 150 °C 3 h

The reaction products after the applied heat treatment, are characterized by both FTIR and carbon NMR. A Varian vnmr 500 MHz instrument with a Varian 5 mm PFG OneNMR probe is used for the carbon NMR tests in this work. Proton decoupling is used to eliminate the nuclear Overhauser effect (NOE) (154). A spectrum window of -40 to 210 ppm is used to ensure that all peaks of interest fall within 60% of the center of the spectrum. For quantification analysis, an acquisition time of 5 seconds and a 90° pulse with a relaxation delay of 25 seconds are used. Each sample is dissolved in DMSO-d_6 and is scanned 256 times to get an optimal signal to noise ratio. FTIR spectra are recorded over a range from 600 to 4000 cm^{-1} with a Nicolet iS50 spectrometer using a diamond ATR from Thermo Scientific. Each

spectrum is collected under 16 scans with a resolution number of 4.

The product of the model compound 1 after the 80 °C 1 h, 150 °C 3 h, 200 °C 1 h reaction, is characterized by FTIR first, as shown in Figure 2.21. The peak corresponding to the oxazolidone has a corrected peak height, (A (ν_{CO} 1750cm^{-1}) of 0.185, and the peak corresponding to isocyanurate has a corrected peak height, A (ν_{CO} 1710cm^{-1}) of 0.339. The ratio of these two peak heights, A (ν_{CO} 1750cm^{-1}) / A (ν_{CO} 1710cm^{-1}), is 0.546, which represents the apparent concentration ratio of the two rings of oxazolidone and isocyanurate in the model compound 1.

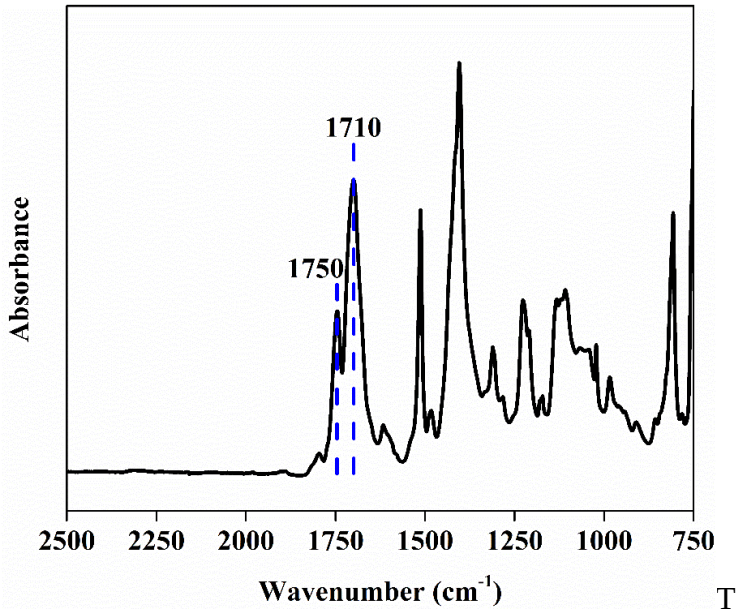

Figure 2.21. FTIR absorbance spectrum for 3PTI/1BDE/BDMA after 80 °C 1 h, 150 °C 3 h, 200 °C 1 h reaction (A (ν_{CO} 1750cm^{-1}) = 0.185, A (ν_{CO} 1710cm^{-1}) = 0.339, A (ν_{CO} 1750cm^{-1}) / A (ν_{CO} 1710cm^{-1}) = 0.546).

For the same product, its carbon NMR spectrum is shown in Figure 2.22, where the integration of the peak corresponding to oxazolidone at 154 ppm is normalized, and the integration of the peak corresponding to isocyanurate at 149 ppm is calculated as 2.61 accordingly. The ratio of these two integrations is calculated as 0.383 (1/2.61), which represents the real concentration ratio of the two rings of oxazolidone and isocyanurate in the model compound 1.

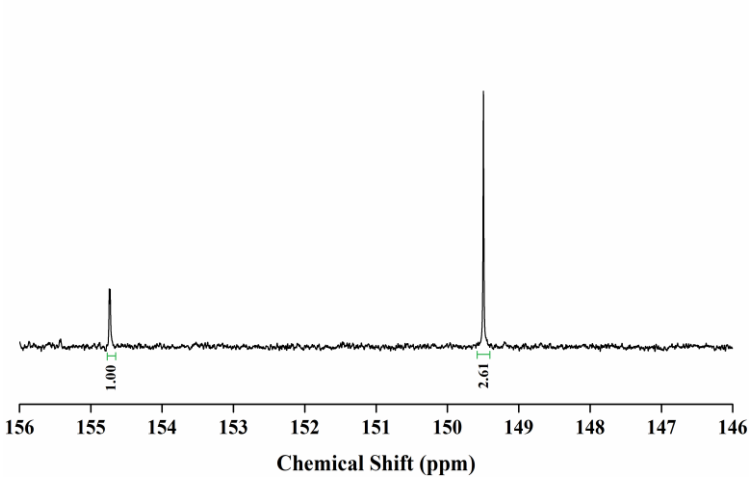

Figure 2.22. Carbon NMR spectrum for 3PTI/1BDE/BDMA after 80 °C 1 h, 150 °C 1 h, 200 °C 1 h reaction (500 Hz, DMSO-d_6, 154.73, 149.50 ppm), OXA/ISO = 0.383.

The apparent ring concentrations from the FTIR spectra and the real ring concentrations from the carbon NMR spectra in the model compound 1 are then calculated from the concentration ratio of the two rings of oxazolidone and isocyanurate in the model compound 1. The resulting ring concentrations obtained from FTIR and carbon NMR are then correlated and used to define a data point in a working curve developed in this section. The collection of three data points, following the same procedure as illustrated above, is discussed in detail in the following paragraphs. These data points are measured from the prepared model compounds with varied ring concentrations adjusted by reaction temperature and time. With four data points in total, a working curve correlating the FT-IR and carbon NMR results is established using linear regression analysis, as shown in Figure 2.23. With the assistance of the working curve, the polymer composition of the ISOX polymers can be measured from FTIR in a fast and cost-efficient way.

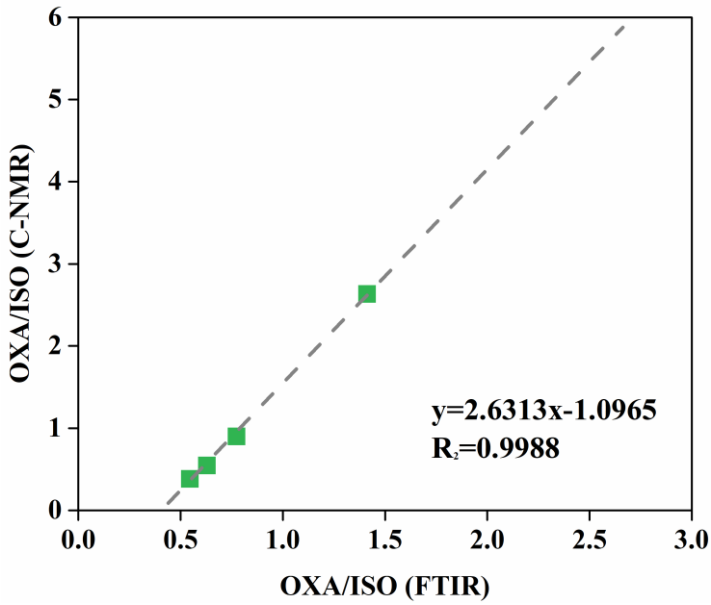

Figure 2.23. A working curve for quantification of the compositions of ISOX polymers developed by the combination characterization of FTIR and carbon NMR techniques on three model compounds.

For model compound 2, equilibrium between isocyanurate and oxazolidone is observed with a lower molar ratio of epoxide reactant, where PTI reacts with a stoichiometric ratio of a mono-epoxide, phenyl glycidyl ether (PGE). In this isocyanate/epoxide equivalent case, both isocyanurate and oxazolidone are detected in the product by FTIR and carbon NMR after the heat treatment of 80°C 1 h, 150 °C 3 h, and 200 °C 1 h. The coexistence of isocyanurate and oxazolidone indicates that the conversion between these two rings reach an equilibrium. Similar to the analysis for model compound 1, the ratio ring concentrations from both the FTIR and NMR are first measured and then converted into ring concentrations of the isocyanurate and oxazolidone. The FTIR spectrum of the product of model compound 2 is shown in Figure 2.24, exhibiting very similar absorption bands with that of model compound 1. The carbon NMR spectrum is shown in Figure 2.25, based on which the integration of the signal at 149 ppm and 154 ppm is measured. With the integration data, the conversion of isocyanate to oxazolidone is calculated to be 36% and the conversion of isocyanate to isocyanurate is 64% in the product of model compound 2 after the heat treatment at 200 ˚C.

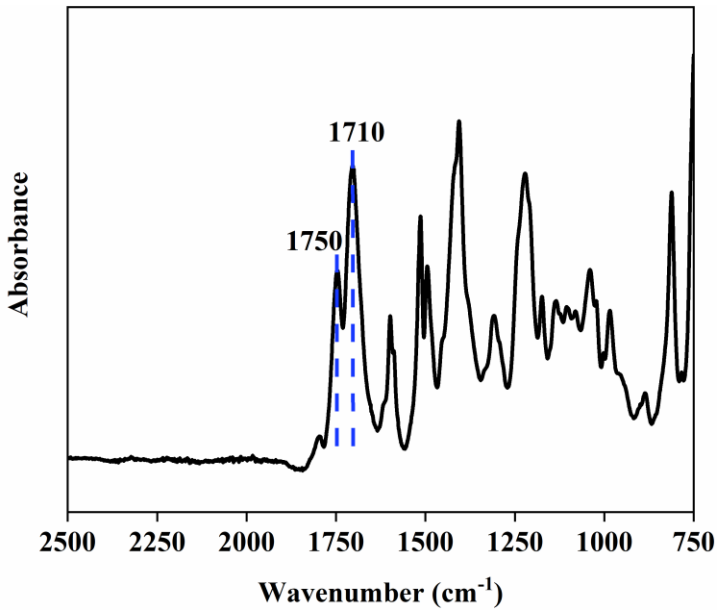

Figure 2.24. FTIR spectrum for 1PTI/1PGE/BDMA after 80 °C 1 h, 150 °C 3 h, 200 °C 1 h reaction.

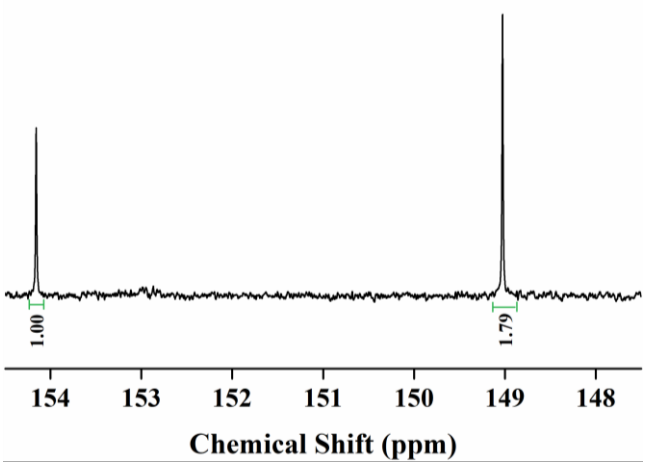

Figure 2.25. Carbon NMR spectrum for 1PTI/1PGE/BDMA after 80 °C 1 h, 150 °C 3 h, 200 °C 1 h reaction (500 Hz, DMSO-d_6, 154.17, 149.04 ppm).

With the assistance of the developed working curve, the polymer compositions of the BDMA polymers and 2-DMAP polymers are then interpreted from the corresponding FTIR spectra in Figure 2.18 and Figure 2.19. Through the ratio of the two peak heights from the specific FTIR spectrum, which is equal to A (vCO 1750cm-1) / A (vCO 1710cm-1), the corresponding point on the working curve is targeted. The y value of the targeted point is the real ratio between the two rings of oxazolidone and isocyanurate, and the real ring concentrations of the ISOX polymers can then be calculated utilizing this ratio. Following the same calculation method for the

isocyanurate/oxazolidone conversion in the model compounds, the conversion to oxazolidone/isocyanurate in the ISOX polymers can be calulated. The results of oxazolidone fraction representing the correspoing oxazolidone conversion within the ISOX polymers is shown in Figure 2.26, where the change in the oxazolidone fraction of the 1TDI/1DGEBF polymers catalyzed by BDMA/2-DMAP with increased post-cured at 250 °C is tracked. As can be seen in Figure 2.26, without post-cure, the oxazolidone content in the 2-DMAP polymers is 25% higher than that in the BDMA polymers, which confirms the previously made conclusion in the last section that more nucleophilic catalyst leads to lower oxazolidone fraction. Both of the two ISOX polymers have about a 40% increase in oxazolidone fraction after post-cure at 250 °C for 3 h, and this increase comes from the accerlerated isocyanurate-to-oxazolidone transformation at the elevated temperatures.

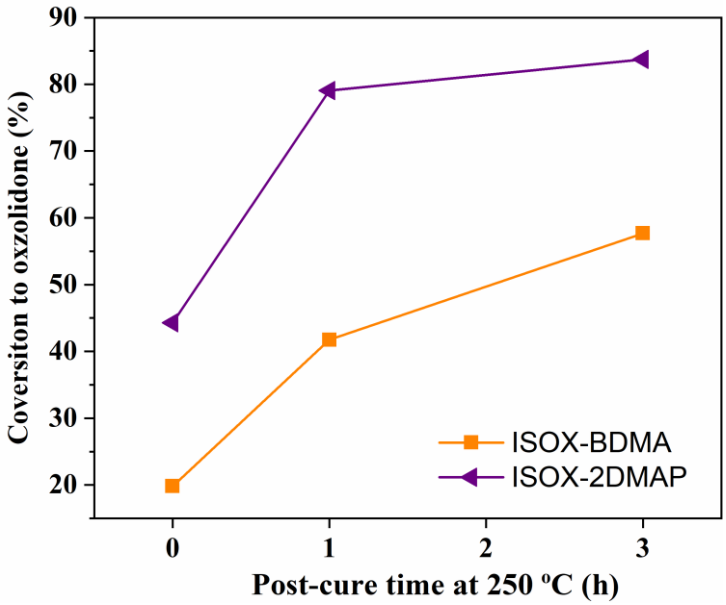

Figure 2.26. Oxazolidone fraction of the BDMA polymers and 2-DMAP polymers after post-cure for 0, 1, and 3 h.

2.5 Structure-Property Relationship of the ISOX Polymers

Several factors including the monomer stoichiometry, nucleophilicity of catalyst, and post-cure time, are studied to tune ring concentrations of the ISOX polymers and

the resulting polymer composition. In this section, the structure-property relationship of the ISOX polymers is further investigated to see how the variation in the polymer composition would affect the material properties of the ISOX polymers. Since the development of the high-temperature performance polymers is one of the most important motivations of this research, the high-temperature stability of the ISOX polymers is examined first in this section. Thermal stability of the three polymers 1TDI/1DGEBF, 1.5TDI/1DGEBF, 2TDI/1DGEBF is characterized by thermogravimetric analysis with a TA Instruments SDT Q600 thermogravimetric analyzer (TGA). The polymers are tested over a temperature range from 25°C to 600°C at a heating rate of 20°C/min and a sample purge flow rate of nitrogen at 60 mL/min is used.

The decomposition onset temperature (Td), which is defined as the temperature at 5% weight loss of the sample from the TGA test (155), is an important parameter to determine the thermal stability of polymeric materials. The measured values of Td for 1TDI/1DGEBF, 1.5TDI/1DGEBF and 2TDI/1DGEBF are 365.4°C, 363.1°C, and 359.9°C respectively, which reveals the high-temperature-resistant nature of the ISOX polymers. The T_d of ISOX polymers increases with decreased TDI fraction in the polymer formulation, and the highest Td is measured from the 1TDI/1DGEBF, which has the highest oxazolidine fraction. This increased thermal stability comes with more oxazolidones, which are believed to show higher thermal stability compared to isocyanurates (156), while the char formation increases with a higher proportion of isocyanurates, as can be seen in Figure 2.27.

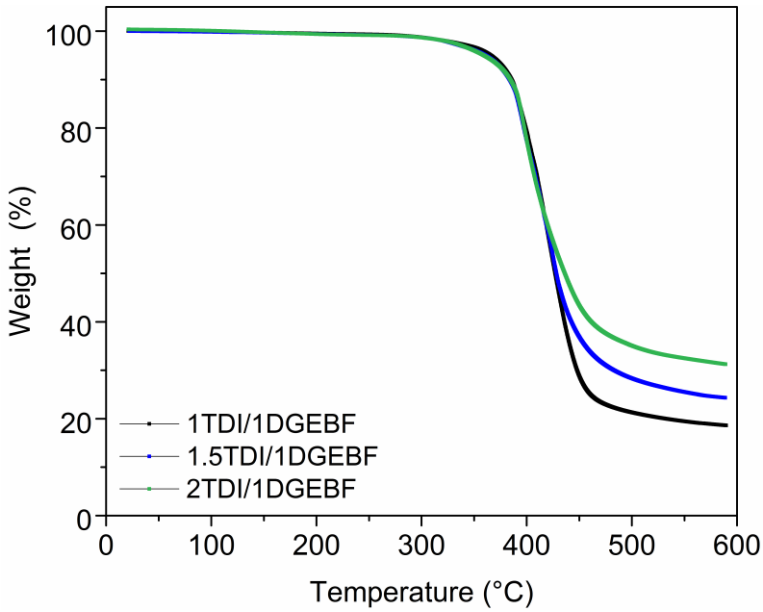

Figure 2.27. Thermogravimetric analysis (TGA) results of 1TDI/1DGEBF, 1.5TDI/1DGEBF, and 2TDI/1DGEBF.

Another important parameter for evaluating the thermal stability of polymeric materials is the glass transition temperature (Tg). Tg of a polymer defines the point where the polymer transforms from a "glassy" state into a flexible rubbery state, above which the material loses most of its strength and stiffness (157). At temperatures below Tg, the molecular movement is higly inhibited; however, at temperatures above Tg, only a small force is required to deform the polymer. Therefore, Tg usually determines the upper-limited use temperature for a polymer for structural applications. Dynamic mechanical analysis is one of the most common methods to measure the Tg of polymers. Generally, Tg can be easily identified from dynamic data because of the sharp drop in the storage modulus, and the corresponding loss modulus and tan delta. The criterion for the Tg measurement is either the peak temperature of loss modulus or tan delta (158), although the the latter one is the more prevalent in literature and the corresponding Tg is usually several degrees higher than that measured from the peak temperature of loss modulus. The Tg assignment in this work is based on the peak tan delta value, and a TA Instruments Q800 dynamic mechanical analyzer (DMA) is used to measure the Tg of the three ISOX polymers, which are molded into rectangular DMA samples with a dimension of 28mm x 6.5mm x 0.6mm. The samples are then loaded at 1Hz under tension in DMA over a temperature range from 25°C to 320°C at a heating

rate of 2°C/min. The representative DMA results of the three polymers are shown in Figure 2.28, and the Tg of the polymer is defined as the temperature when the Tan Delta peaks in the study.

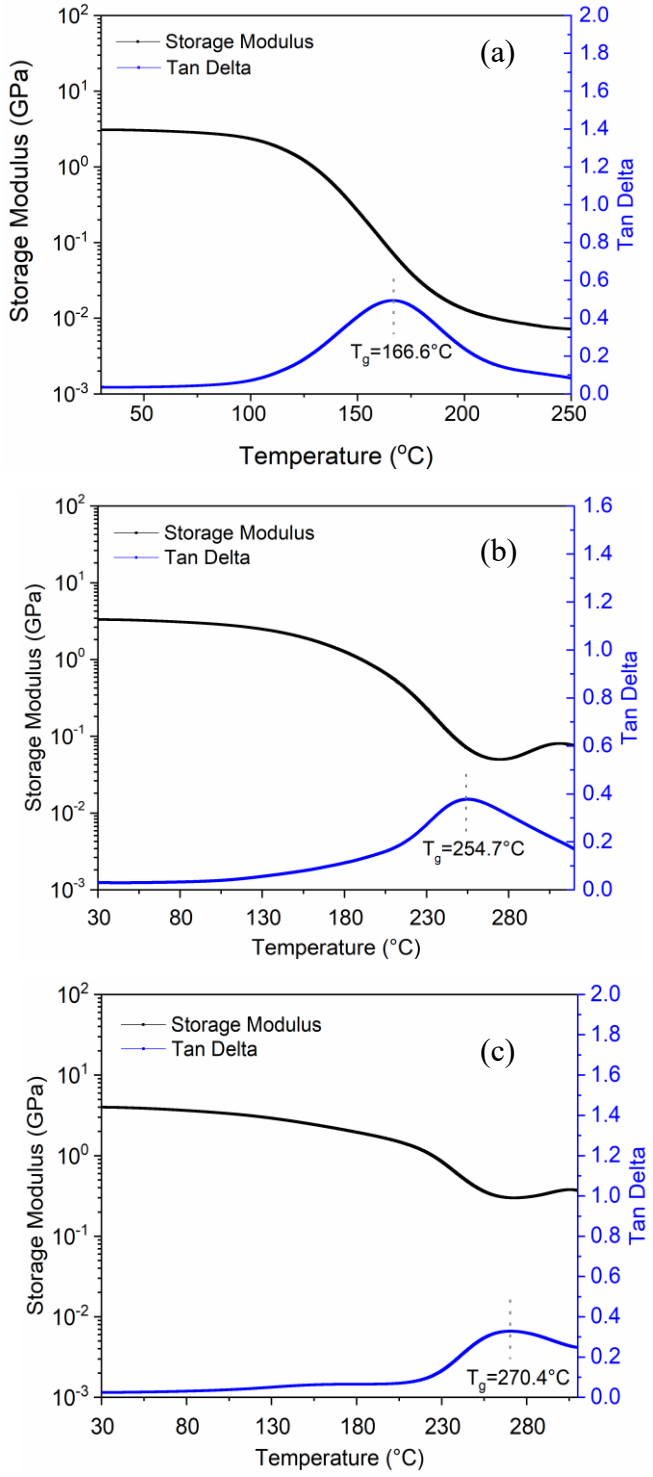

Figure 2.28. Representative dynamic mechanical analysis (DMA) results of (a) 1TDI/1DGEBF, (b) 1.5TDI/1DGEBF and (c) 2TDI/1DGEBF.

At least three samples are tested by DMA for each ISOX polymer to determine the

Tg, and the results are shown in Table 2.2, where the highest Tg is measured form the 2TDI/1DGEBF. Two epoxy polymers DGEBF/EPIKURE 3230 and DGEBF/curing Agent W, are polymerized from the same DGEBF epoxy resin and measured under DMA for Tg. Compared to the two epoxy reference samples, the ISOX polymers show significantly increased Tgs, which indicates their higher use temperatures. Opposed to the trend observed in Td, higher Tg is measured for the ISOX polymers with higher TDI fraction in the polymer formulation. As shown by the graphic comparison in Figure 2.29 (159), the Tgs of ISOX polymers are comparable to that of poly(bismaleimides) and polyimides, which are well known as high-temperature specialty polymers with an upper service temperature ranging from 197°C to 247°C (160). However, the ISOX polymers are more cost-effective than these commercial counterparts, which indicates their potential as high-temperature performance polymers for large-scale production and application.

Table 2.2. Glass Transition Temperature (Tg) of the ISOX polymers and two epoxy reference polymers.

	ISOX Polymers			**Epoxy Reference**	
	1TDI/ 1DGEBF	1.5TDI/ 1DGEBF	2TDI/ 1DGEBF	DGEBF/EPIKURE 3230	DGEBF/curing Agent W
Tg (°C)	166.4 (±0.8)	252.3 (±2.4)	270.4 (±1.8)	78	121

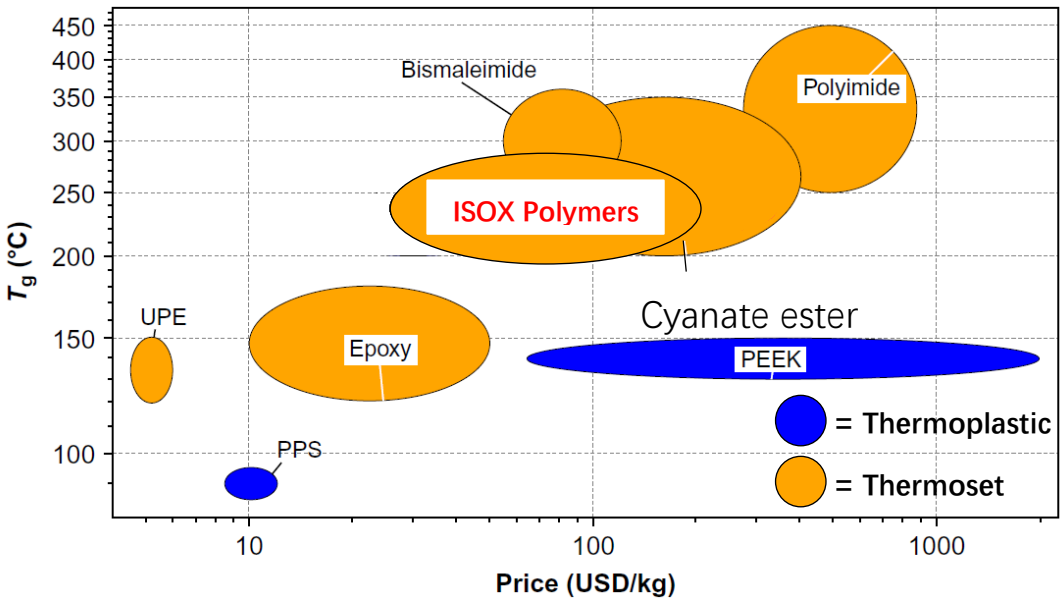

Figure 2.29. Graphic comparisons of the ISOX polymers with other high-temperature performance polymers (159).

The high Tg of the ISOX polymers are derived from its dense network, which is crosslinked by a large amount of isocyanurate rings. To further verify this explanation, an important parameter, molecular weight (Mc) between crosslinks, or number of cross-links per unit length, is measured for the ISOX polymers. Smaller Mc represents smaller molecular weight between crosslinks and therefore indicates a denser network structure. For the ISOX polymers, a smaller Mc then represents higher isocyanurate fraction in its polymer network and therefore can provide an important perspective for the structure-property relationship of the ISOX polymers. Equation 1 below is used to calculate Mc according to Kessler et al., (161) where q represents the front factor (q=1 is used here), d is the density of the material ($d \approx 1.3 g \cdot cm^{-3}$ is measured for the three ISOX polymers), R is the universal gas constant ($R=8.314 J \cdot K^{-1} \cdot mol^{-1}$), T is equal to Tg+50K, and C represents the storage modulus at Tg+50K measured from DMA. These parameters of each ISOX sample are listed below in Table 2.3. To note, both Tg and Tg+50K are also measured from DMA. The density of the 1.3 $g \cdot cm^{-3}$ is calculated from the measured weight and volume of a molded ISOX polymer and then used for calculation of the Mc of the polymers. The characterization results of Mc are shown in Table 2.3, where the 1TDI/1DGEBF is measured to have the largest Mc of 1713 g/mol while the 2TDI/1DGEBF has the smallest Mc of 79 g/mol. The Mc results provide a strong explanation for the Tg trend measured from the DMA, as the highest Tg is measured from the ISOX polymer with the smallest Mc. The Mc, which can be conveniently measured from DMA, can serve as a useful parameter to obtain the required Td or Tg of the ISOX polymers as it directly correlates with the polymer composition of the ISOX polymers.

$$\mathrm{Mc} = \frac{3qdRT}{E'(T_g + 50K)} \qquad Equation\ 1$$

Table 2.3. Results of the molecular weight between cross-links (Mc) of the ISOX polymers.

	Tg + 50K (K)	E' (Tg + 50K) (MPa)	Mc (g/mol)
1TDI/1DGEBF	489.78	9.27	1713
1.5TDI/1DGEBF	577.57	77.54	242
2TDI/1DGEBF	593.47	244.7	79

2.6 Chapter Summary

The isocyanurate-to-oxazolidone transformation, which is demonstrated in both small model compounds and in a polymeric network, is shown to be a promising healing chemistry with high thermal stability in this chapter. The presence of both isocyanurate and epoxide as the two reactive components for this transformation is verified in the isocyanurate-oxazolidone (ISOX) polymers to serve the healing purpose, which is further discussed in the next chapter. The ISOX polymers, synthesized from commodity reactants through the formation of the isocyanurate-oxazolidone network, exhibit excellent high-temperature performance, as demonstrated by their glass transition temperature (Tg) up to 270°C and decomposition temperature (Td) up to 365°C. These properties are determined by the polymer composition of the ISOX polymers, which can be tuned by several factors based on the understanding of the polymerization mechanism. Polymerization of ISOX polymers begins with nucleophiles attacking the epoxide before the zwitterion of the nucleophile/epoxide/isocyanate initiates polymerization. By using catalysts with various nucleophilicity, ISOX polymers with different chemical compositions can be prepared. Another two factors including post-cure time and monomer stoichiometry between diisocyanates and diepoxides can also be tuned to control the polymer composition to achieve required material properties. The polymer composition is characterized through a working curved developed from the combination of FT-IR spectroscopy and carbon NMR spectroscopy. The developed working curve is further used in the following chapter to study the important structure-healing property relationship.

CHAPTER 3

Self-Healable ISOX Polymers with Repeatable Strength Recovery

3.1 Chapter Introduction

The study in the last chapter has shown the great potential of the isocyanurate-to-oxazolidone transformation incorporated in the ISOX polymers, as a high-temperature stable self-healing chemistry. In this chapter, this isocyanurate-to-oxazolidone transformation is further utilized to develop novel self-healable ISOX polymers. The healing performance of the ISOX polymers after the introduction of macroscopic cracks is demonstrated in this chapter by the measurements of the strength recovery of the polymers after crack removal under heat stimulus. Their capability of multiple-time repair is also an important prospective for intrinsically self-healable polymers and therefore it is also evaluated. The healing properties of the ISOX polymers are optimized by studying the healing performance with respect to a variety of healing temperatures and healing time. Healing of the polymers both below and above the Tg is also studied in this chapter to explore the possibility of achieving crack repair while preserving the mechanical strength and stiffness of the ISOX polymers. The healing mechanism of the polymers is fully investigated by direct characterization of the fracture surfaces which are induced through crack initiation. The developed self-healable polymers withstanding high temperatures will greatly impact the application of thermosetting polymers in the field of structural laminates and electronics packaging.

3.2 Characterization of Self-Healing Performance of the Developed ISOX Polymers

3.2.1 Fabrication of ISOX polymers for self-healing characterization

Diglycidyl ether of bisphenol F (DGEBF) is purchased from Momentive. Tolylene-2, 4-diisocyanate (TDI) and benzyldimethylamine (BDMA) 99% are purchased from Acros Organics. All the chemicals are used as received. 1TDI/1DGEBF is prepared by mixing 1 mole of TDI, 1 mole of DGEBF and 0.1 wt% BDMA as a catalyst; 1.5TDI/1DGEBF and 2TDI/1DGEBF are prepared in the same way with 1.5 moles TDI and 2 moles TDI respectively. TDI and DGEBF are mixed thoroughly by a vortex mixer for 10 minutes and the mixture is degassed under vacuum for 30 minutes until no bubbles are visible before the BDMA is added, yielding a transparent ISOX liquid resin. The blended resin is transferred to an RTV664 silicone mold and placed in a vacuum oven under a nitrogen atmosphere before it is cured under heat in an oven.

The 1TDI/1DGEBF, 1.5TDI/1DGEBF and 2TDI/1DGEBF samples are cured at 80 °C for 1 h and then at 200 °C for 20 h, with another 20 h of annealing at 200 °C. The additional 20 h annealing for the ISOX polymers is designed to achieve a higher conversion of the isocyanate in the polymers, especially for the 2TDI/1DGEBF within which the heaviest steric effect is expected because of its highest isocyanurate fraction. A 2TDI/1DGEBF sample, cured under the two-step curing procedure developed in the last chapter, is pulverized and subsequently analyzed through FTIR, after which the peak at 2260 cm^{-1} is observed for the powder sample. Then the sample is annealed at 200 °C for 10 h, 15 h, and 20 h, respectively. The peak at 2260 cm^{-1} is detected for the 10 h and 15 h ones, but not for the 20 h one, as shown in Figure 3.1.

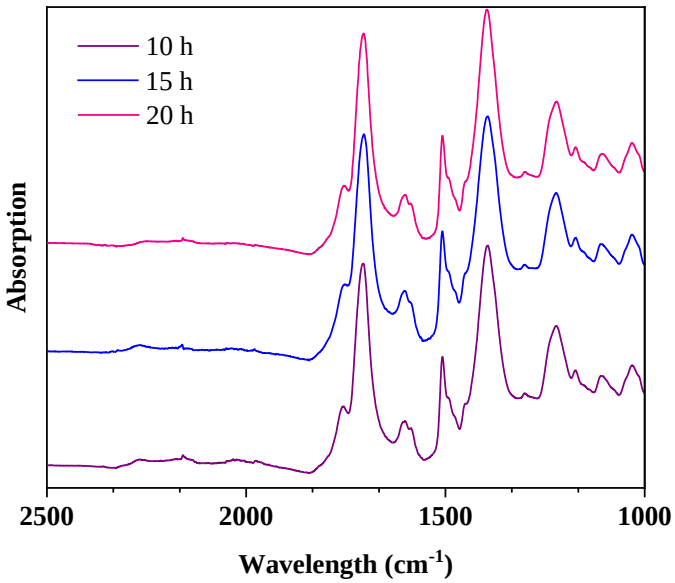

Figure 3.1. FTIR spectra of the 2TDI/1DGEBF powder after annealing for 10, 15 and 20 h.

The ISOX polymers after annealing are characterized by differential scanning calorimetry (DSC). DSC can measure the difference in the amount of heat required to increase the temperature of a sample and its reference during a temperature ramping process where both the sample and the reference are maintained at the same temperature. Through DSC, any exothermal and endothermal reactions can be directly observed from the heat flow measured from the sample and therefore it is one of the most extensively used characterization techniques to monitor reaction processes including polymerization process. DSC is used in this study to confirm the complete polymerization of the cured ISOX polymers before they are further evaluated for their healing potential. As can be seen in the DSC results of the three polymers in Figure 3.2, the absence of any exothermal peaks around 200 °C indicates a complete polymerization although two reactive components of isocyanurate and epoxide are both present in the polymers.

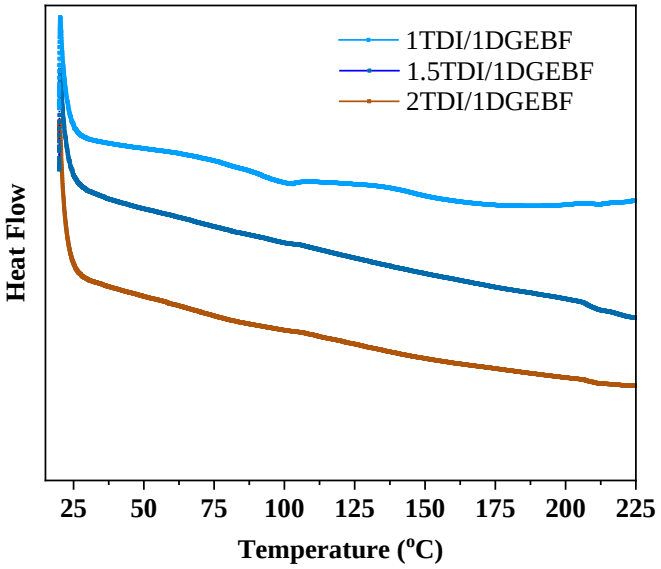

Figure 3.2. Differential scanning calorimetry (DSC) results of the three ISOX polymers after annealing at 200 °C.

Two sample configurations are used for characterizing the healing performance of the ISOX polymers in this work. The first one is compact tension test (CT) configuration which has average dimensions of 1.30 in. x 1.20 in. x 0.32 in., and a computer numerical control (CNC) mill is then used to machine the samples to the specific dimensions for a CT specimen defined in ASTM D5045 as shown in Figure 3.3. The specimen geometry is modified slightly through the addition of a resting hole along the crack path to stop the crack from uncontrolled crack growth. Uncontrolled crack growth is not wanted because it complicates the measurement of the strength recovery of the polymers as perfect mating of the two fractured surfaces during healing is generally not possible leading to unnecessary variability in healing behaviors. The notch length is also shortened to stop the crack at the resting hole due to the brittle nature of polyisocyanurate rings (139). The fracture load is measured for the initial sample, and then healed and retested three successive times to determine the repeated healing efficiencies using an Instron 5956 with a constant opening rate of 0.1 mm/min under ambient conditions. The average fracture load values are obtained from six specimens, based on the general procedure of ASTM D5045.

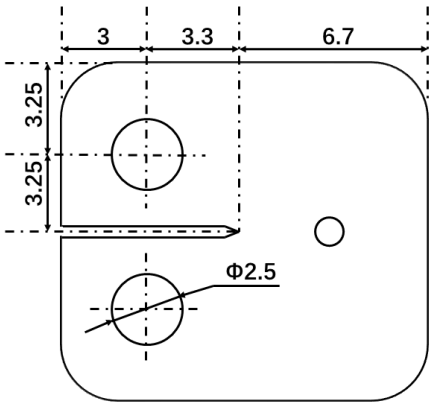

Figure 3.3. Compact tension (CT) configuration for self-healing performance characterization (unit in inch/10).

The second configuration to characterize the healing performance of the ISOX polymers is a single edge notched bending (SENB) geometry as shown in Figure 3.4. This three-point bend fracture testing according to ASTM D5045 is also extensively used to study the healing mechanism of the ISOX polymers in the later section because of its simplicity and effectiveness. The cured ISOX polymers molded using RTV664 silicone molds are individually machined into this SENB configuration, where a sharp notch is then introduced to the specimen by repeatedly sliding a fresh razor blade on the pre-crack before placing the specimen on the two stationary rollers for the SENB test. The SENB specimen is loaded at a low displacement rate of 0.1 mm/min, and the test is stopped once the specimen is fractured into two pieces. It should be noted that a piece of high-temperature resistant Kapton tape is applied on the top of each specimen (under the middle loading pin), to allow the specimen to be assembled without dislocation between the two pieces of the fractured specimen. The fractured specimen is wrapped in aluminum foil to help create a uniform temperature throughout the specimen during the heat treatment. The healed samples with the two rejoined surfaces are then retested using the three-point bend test under the same conditions, as the maximum loading during the first SENB test and the result of the second SENB test are recorded for each specimen for quantification purpose. It should be noted that the load is applied in the direction perpendicular to the crack during the healing procedure, to solely maintain contact between the two fracture surfaces of the SENB specimen.

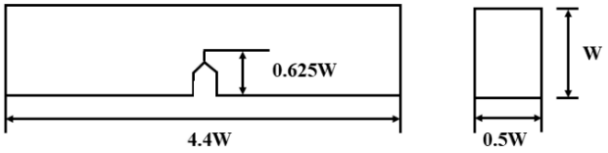

Figure 3.4. Geometry of single edge notched bending (SENB) samples, W = 15 mm.

3.2.2 Healing performance of the ISOX polymers below and above Tg

After the crack initiation in the CT samples, these fractured samples are placed in the oven under a nitrogen atmosphere at 200 °C for 20 h before a CT test is performed. A comparison of representative graphics of a CT sample (1.5TDI/1DGEBF) with an initiated crack and the same sample after the heat treatment for crack removal is shown in Figure 3.5. As can be seen in the CT sample on the left, a crack in length of 1 cm is observed in the middle of the sample, which is created intentionally under the tension applied to the sample during the CT test. However, this macroscopic crack gets effectively removed after the annealing indicated by the disappearance of the crack in the middle of the sample on the right. It should be noted that a light pressure is needed for the CT sample during the heat treatment to ensure the two fracture surfaces are in contact so the reactive components on the interface can form new bonds to achieve the apparent crack removal. The disappearance of the crack in the middle of the polymer does not come from the melting as thermosets do not melt at high temperatures while they directly decompose when the temperature reaches its decomposition temperature. From the data in the previous chapter, the 1.5TDI/1DGEBF does not decompose until around 360 °C so decomposition of the polymer is not an issue either.

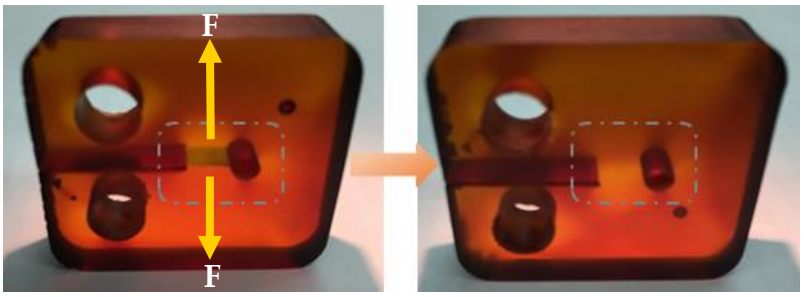

Figure 3.5. Comparison of fractured sample and healed compact tension (CT) sample.

For the 1.5TDI/1DGEBF shown in Figure 3.5, its Tg is measured to be 252 °C following the characterization steps with DMA described in Chapter 2. The crack removal within the polymer is the first demonstration of healing achieved below Tg where mobility of molecular chains is highly restricted by the dense distribution of isocyanurates as crosslinks. In other words, the polymer is in its "glassy" state where most of its strength and stiffness are preserved when the healing of the polymer is proceeded at 200 °C. There is little compromise on the mechanical properties of the polymers because of the healing conditions. This mechanical stability during the healing process is rare in literatures because most existing self-healing polymers developed over the past decade require a high degree of flexibility to overcome steric issues to allow active interactions of reactive components on the interface. These low-modulus polymers are not suitable for structural applications where high mechanical strength, stiffness and toughness are significant for the materials to perform load-bearing functions. The capability of crack removal under heat is also achieved for both the 1TDI/1DGEBF and the 2TDI/1DGEBF under heat stimulus. The Tg of the 1TDI/1DGEBF and the 2TDI/1DGEBF is measured and averaged from three specimens to be 187 °C and 270 °C, respectively. The 2TDI/1DGEBF has the highest reported Tg for an intrinsically healing thermoset and thus shows its great potential as a multifunctional material with high use temperature for extreme environments.

3.2.3 Quantification of the self-healing performance of the ISOX polymers

For a CT sample after crack removal under heat, it is tested under a second CT test where a crack is initiated again at the same spot within the sample. The sample after the second CT test is then heat treated for the second time, after which it is tested under a third time CT test. A CT sample is tested for four times in totals, and the load-extension curves during the initial loading and three post-healing loadings are recorded. Representative demonstrations of the load-extension curves of the three polymers are shown in Figure 3.6. The sudden drop of the recorded load of the curves represents the presence of the crack in the CT sample, which is stopped by the small hole introduced in the center of the sample. This drop also represents the end of the test where the Instron instrument is set to be stopped given this large drop in the load-bearing capacity of the sample. For the three ISOX polymers, after each damage-healing cycle, considerable strength is recovered although the strength recovery decreases slightly with more damage-healing cycles indicated by the slightly reduced maximum load recorded during the crack initiation. The slope of the load-extension curves which reflects the stiffness of the samples, however, is unchanged even after three damage-healing cycles, suggesting full recovery of the stiffness of the polymers. Similar trends are observed in the load-extension curves of the three polymers, however, we can see that the highest strength recovery is from the 2TDI/1DGEBF.

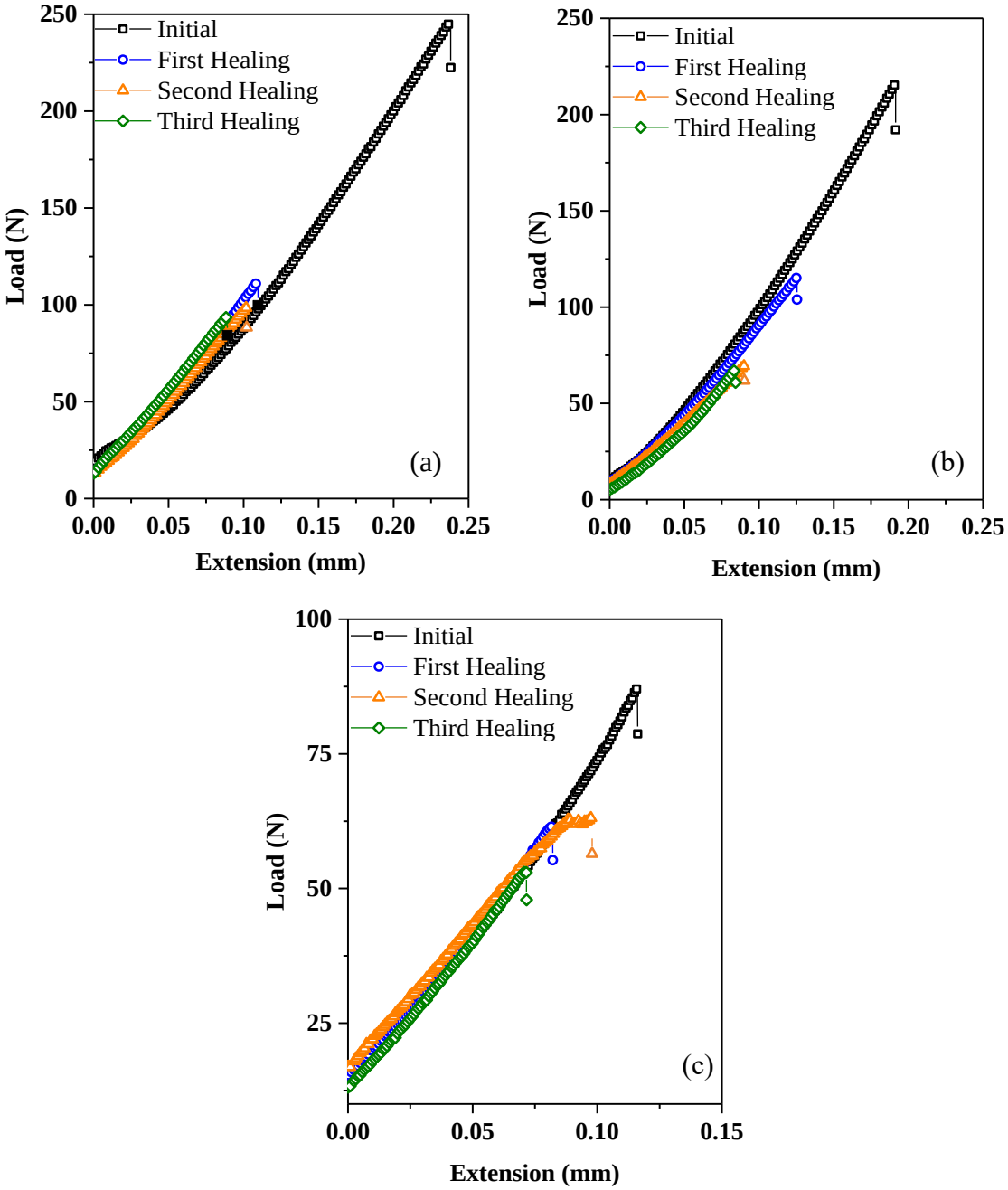

Figure 3.6. Examples of failure load plot for (a) 1TDI/1 DGEBF, (b) 1.5TDI/1DGEBF, and (c) 2TDI/1 DGEBF, respectively.

The healing performance of 1TDI/1DGEBF, 1.5TDI/1DGEBF and 2TDI/1DGEBF is further quantified through the evaluation of their healing efficiencies during each damage-healing cycle. The recorded maximum load to induce fracture in the original samples and the three successively healed samples are used to calculate the healing efficiencies of the three polymers. The healing efficiencies are obtained according to *Equation 2* using the initial and post-healing maximum loads. The first,

the second, and the third healing efficiencies for 1TDI/1DGEBF samples are 43.52%, 31.63% and 26.49%, respectively; for 1.5TDI/1DGEBF samples, they are 49.33%, 33.38%, and 32.55%, respectively; for 2TDI/1DGEBF samples, they are 50.98%, 42.00%, and 42.85% respectively, with the error bars representing the standard deviation shown in Figure 3.7.

$$\text{Healing Efficiency (\%)} = 100\times \frac{\text{Maximum Load of Mended Sample}}{\text{Maximum Load of Original Sample}} \quad \textit{Equation 2}$$

As can be seen in Figure 3.7, considerable strength recovery is observed for each ISOX polymer and multiple-time repair is achievable even after four times of macroscopic crack initiation at the same spot within the sample. Reduced healing efficiencies are calculated for each polymer with increased damage-healing cycles and this decreased healing performance can be caused by two factors. The first factor is that the rupture of bonds induced by external mechanical stress is unselective, and most of these bond scissions are irreversible under heat treatment, for example, N-C bonds that connect isocyanurate rings to the benzene rings. These ruptured bonds cannot provide strength for the polymers and therefore they partially account for the loss of the measured healing efficiencies. The second factor is that after the first time a CT sample is fractured, the crack in the sample becomes sharper after each healing cycle; thus, a higher stress concentration exists in the specimen. Due to this reason, the subsequent healing samples cannot reach the original maximum load even with 100% healing. It is notable that the healing efficiency between fractured samples is high with the healing efficiency being 73%, 68% and 82% for 1TDI/1DGEBF, 1.5TDI/1DGEBF, and 2TDI/1DGEBF, respectively, when comparing the first healing cycle to the second one.

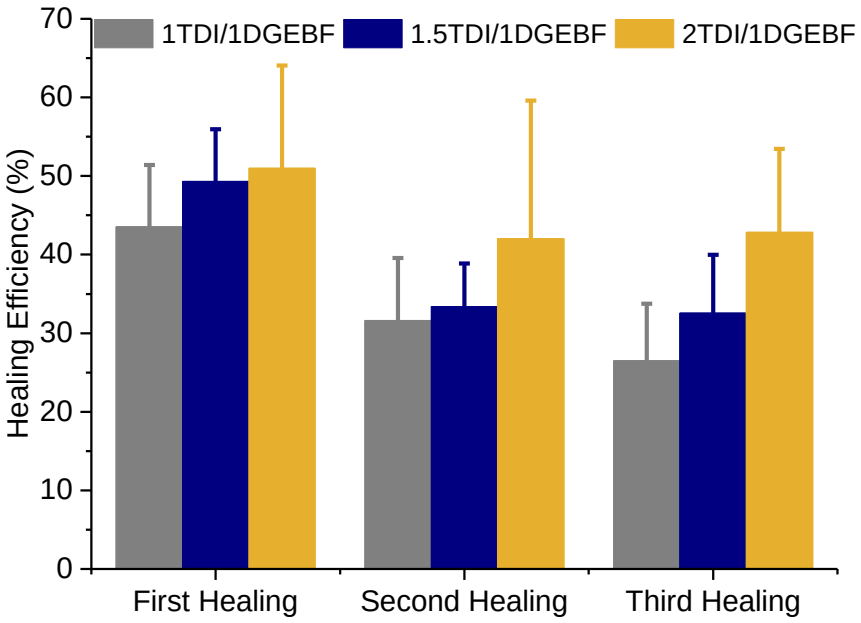

Figure 3.7. Average healing efficiencies of 1TDI/1DGEBF, 1.5TDI/1DGEBF and 2TDI/1 DGEBF during the first, second and third damage-healing cycles.

Comparing the results of healing efficiencies measured for the three ISOX polymers, no correlation between the healing performance and the T_g of the polymers is observed. Although the 1TDI/1DGEBF is heat treated at 200 °C which is higher than its T_g of 187 °C for crack removal, the strength recovery of 1TDI/1DGEBF is lower than that of the 2TDI/1DGEBF during each round. For the 2TDI/1DGEBF, it is heat treated at the same healing temperature after the crack initiation, but it has a much higher T_g of 270 °C. For the 1.5TDI/1DGEBF with a medium T_g and, it has a decent healing performance in between. It can be concluded that T_g is not a determining factor for the healing performance of the ISOX polymers, instead, the strength recovery of the polymers is decided by the bond formation under the heat treatment. More insight into the surface chemistry of the ISOX polymers is discussed in the next section, to explain the trend observed in Figure 3.7, where higher TDI in the polymer formulation leads to higher strength recovery of the ISOX polymers.

3.3 Investigation of Self-Healing Mechanism of the ISOX Polymers

To fully elucidate the healing behaviors of the ISOX polymers and study the origin

of their inherent healing capability, the surface chemistry on the fracture surfaces of the ISOX polymers after crack initiation is further investigated. The effect of polymer composition on the fracture surfaces is first studied and then the compositional change during the healing process is tracked. Upon cracking, the scission of unselective bonds, rather than intermolecular slippage or damage of Van der Waals forces occurs, and the chain scission on the fracture surfaces is studied through FTIR in the first part of this section. In the second part, all forms of the covalent bond formation including the isocyanurate-to-oxazolidone transformation, are carefully examined on their effects on the healing performance of the ISOX polymers.

3.3.1 Characterization of reactive components on the fracture surfaces

Figure 3.8 shows a 2TDI/1DGEBF compact tension (CT) sample which is fractured completely under the CT test without a resting hole. The bulk surfaces as well as the fracture surfaces of the sample are first characterized and then compared under FTIR to study the surface composition of the polymer and identify the presence of reactive functional groups that yield healing. The FTIR spectrum of the fracture surfaces of the CT sample is collected prior to each healing process which is kept consistent with the healing procedure applied for the CT samples for the measurement of healing efficiencies in the last section. The FTIR results are shown in Figure 3.9, where the isocyanate peak at 2260 cm^{-1} can be observed on every fracture surface created after the first, the second, the third fracture, but not on the bulk surface before the fracture.

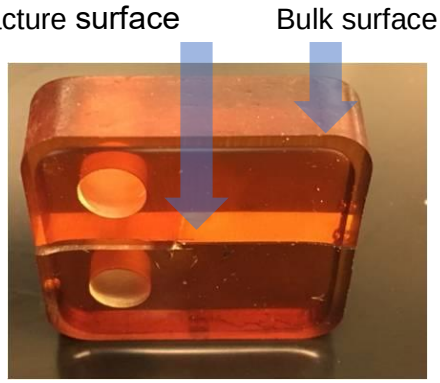

Figure 3.8. Demonstration of a completely fractured compact tension (CT) specimen.

In comparison, a second 2TDI/1DGEBF sample, is prepared as a reference under the same procedure and then it is fractured completely through the specimen. However, the fractured reference sample is then placed in an oven under a nitrogen atmosphere under thermal annealing at 200 °C for 20 h before the two separate pieces of the same CT sample are brought back together under pressure and the same healing procedure is applied for the reference sample. After the healing treatment, the visual presence of a crack in the reference sample is obvious, and it shows little to no recovery of the mechanical strength. The FTIR spectrum of the reference sample's crack surfaces, before the sample is placed on the hot press under pressure for healing purpose, but after the heat treatment in the oven at 200 °C for 20 h, has no isocyanate peak, as shown in Figure 3.9. The poor healing performance for this reference sample can be explained by the fact that heat treatment leads to the reaction of active functional groups across the crack surfaces of the reference sample. This observation also eliminates the possibility that diffusion and entanglement of the polymer across the crack surface as the healing mechanism.

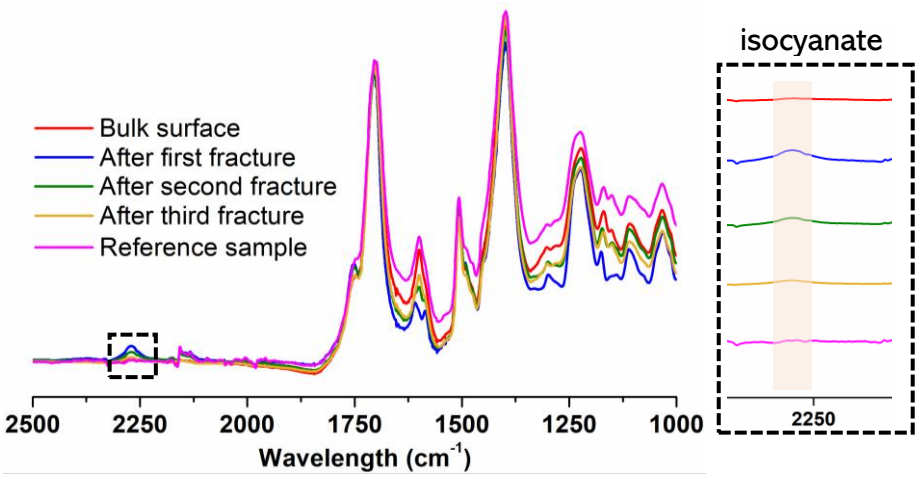

Figure 3.9. (a) FTIR spectra of surfaces for 2TDI/1DGEBF in comparison with a reference after heat treatment at 200 °C 20 h. (b) Enlarged view of the boxed region in (a).

The detected isocyanate under FTIR on the fracture surfaces can have two possible origins. Firstly, it can come from the unreacted isocyanate which is trapped in the polymer due to the heavy steric, which is exactly the case of the 2TDI/1DGEBF with its highest isocyanurate fraction. Another important explanation is that isocyanurate may cleave into three isocyanates upon crack initiation, as a mechano-responsive degradation. Mechano-responsive moiety, also called mechanophores, are reactive moieties whose reactivity depends on externally applied load and they have been incorporated into a variety of polymer systems to develop stress-responsive materials (162, 163). Many studies have reported reversibility that utilized mechano-responsive polymers (164) . Marx et al. (165) used a constant external force to open the benzocyclobutene cores as the mechanophores in the polyethylene oligomers. FTIR was used to confirm the reversion of cyclobutane to the original cinnamoyl structure from grinding 1,1,1-tris-(cinnamoyloxymethyl) ethane (TCE) polymers(166). Oya et al. (81) proved the mechano-chemical reversibility of anthracene-maleimide Diels–Alder adducts by UV/vis spectroscopy. Chung et al. (156) verified mechanical damage and thermal repair of perfluorocyclobutane (PFCB) groups by FTIR, and Craig et al. (167) utilized ^{19}F-NMR to further confirm this mechano-chemical reversibility. Moller et.al (168) studied the fracture nucleation in cross-linked epoxy networks through an analysis of dihedral angle activity, and the result showed that bond scission

took place after significant plastic strain, principally at cross-link sites, and between phenyl rings in the bisphenol moiety over short strain intervals. Their theory was also confirmed through physical experiments performed by other researchers (169). Moller's simulation results indicate a possible route of producing isocyanate through cycloreversion of isocyanurate rings upon fracture under large mechanical stress. This assumption is verified by analyzing a ground 2TDI/1DGEBF polymer through FTIR. Since FTIR has been widely used in studying mechano-responsive moiety in the literatures and our study in the chapter 2 has shown its convenience in detecting the isocyanate and isocyanurate groups in the ISOX polymers, it is a suitable technique to study the potential cycloreversion of isocyanurate upon cracking.

The 2TDI/1DGEBF polymer is pulverized and subsequently analyzed through FTIR spectroscopy. To get a fine powder, a small piece of bulk 2TDI/1DGEBF polymer is initially pulverized through impact and subsequently ground in a mortar pestle for 30 min which creates a high density of fractured surfaces allowing the IR spectrum to be used to identify the structural change with greater fidelity. The IR spectrum after grinding and subsequent heat treatment at 200 °C is shown in Figure 3.10 with the ground material showing a characteristic isocyanate peak at 2260 cm^{-1} while the bulk specimen prior to grinding shows no apparent isocyanate peak. The ground sample is then placed in the oven under nitrogen atmosphere at 200 °C for 20 h to simulate the healing treatment of the bulk sample in the last section. Through the healing process, the powder sample transforms from a state of loose powder to an aggregated mass and it is then tested with FTIR which shows that the isocyanate peak at 2260 cm^{-1} completely disappears after the annealing at 200 °C. The aggregated mass is then ground for a second time for 30 min before retesting, at which point the isocyanate peak at 2260 cm^{-1} is once again observed. The same grinding and healing treatments are applied successively with the disappearance and reappearance of the isocyanate peak at 2260cm^{-1} being repeatable. This repeatable cycle indicates that the mechano-chemical cycloreversion of isocyanurate is an important reason for the appearance of free isocyanate on the crack surfaces of the polymer.

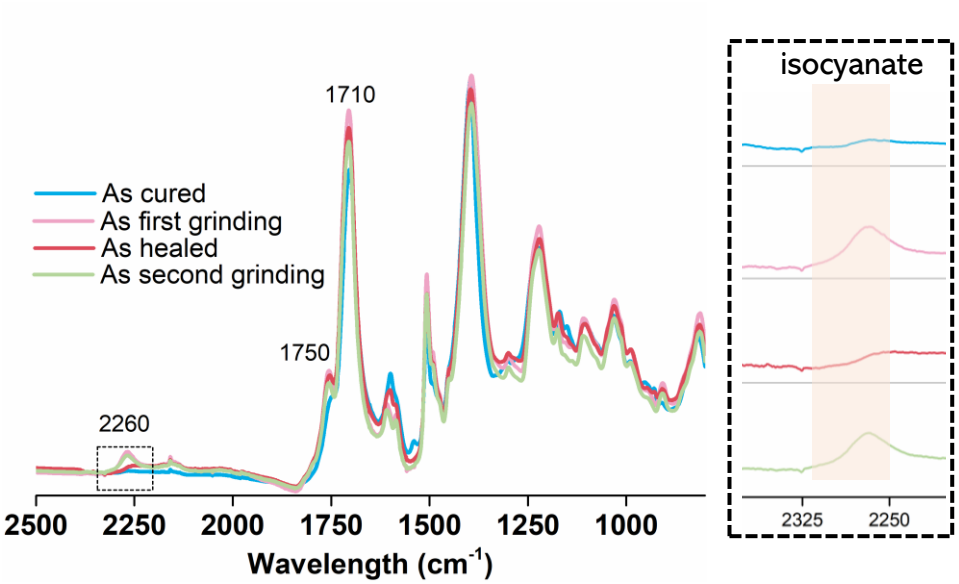

Figure 3.10. (a) FTIR spectra of powder 2TDI/1DGEBF samples. (b) Enlarged view of the boxed region as seen in (a).

The cleavage of isocyanurate is one of the many chain scissions on the fracture surfaces upon cracking, possible scission between phenyl rings in the bisphenol moiety in the ISOX polymers, according to Moller's simulation, can account for the irreversible bond scission, as discussed in the previous section, resulting in a healing efficiency less than 100%. Given the fact that tolylene-2,4-diisocyanate owning benzene ring connected to two isocyanate functional groups at the 2 and 4 positions is used, the space around isocyanurate cross-links is crowded due to the 3 benzene rings surrounding a single bulky 6-member-ring with pendant ketones. When large mechanical stress is applied, these rings are believed to be ruptured firstly because they have much less space to relax stress compared to homopolymerized epoxy chains. Secondly, isocyanurate rings are also more prone to dissociate compared to benzene rings because benzene rings are more stable with the homogeneity of carbon atoms.

The mechano-reversibility of this mechanical degradation of isocyanurate contributes to the healing process as the dissociated isocyanurate ring under mechanical chain scission at the crack surfaces, results in free isocyanrate as one of the active components on the crack surfaces. To the best of the authors' knowledge, this work is the first to show the mechano-responsive characteristic of isocyanurate. The reversibility of isocyanurate formation was reported to take place at very high

temperature, approximately 300 °C, by thermal dissociation of isocyanurate rings to isocyanates (170-173). Due to the extreme temperature where thermal reversibility is expected, the mechano-reversibility of the isocyanurate is then useful to produce isocyanate for healing purpose. According to this concept, greater density of isocyanurate in the bulk sample would yield more cleavage of isocyanurate under external mechanical stress. As a result, there is more isocyanate created during the crack initiation with more TDI in the polymer formulation. In the case of 2TDI/1DGEBF, the largest amount of free isocyanate can be produced among the three ISOX polymers, which is an important reason for its highest strength recovery measured from the compact tension tests in the last section. With more reactive components on the fracture surfaces, more bond formation is available during the heat treatment under the same period. The nature of the new bonds is further investigated in the next section.

3.3.2 New covalent bond formation on the fracture surfaces

In section 3.3.2, the presence of isocyanate is detected through FTIR and the origin of the isocyanate is also investigated. The detected isocyanate functional groups, during the heat treatment of the polymers, can trimerize back to isocyanurate; alternatively, it can react with epoxide to give more oxazolidone in the polymer network. Both cases contribute to the new covalent bond formation on the fracture surfaces, which accounts for the observed strength recovery of the ISOX polymers. To further investigate the nature of these bonds formed during the healing process, the compositional change of the crack surfaces is studied in this section to give a direct perspective on healing mechanism of the ISOX polymers. The ISOX polymer, 1TDI/1DGEBF is molded into the single-edge notched beam (SENB) configuration which is introduced previously. The ISOX resin is first prepared by first mixing TDI and DGEBF in a 1/1 molar ratio using a vortex mixer for 10 minutes; then a 0.1 wt% of BDMA/2-DMAP is added and mixed thoroughly with the TDI/DGEBF mixture before transferring the resin into an RTV664 silicone mold and degassing the resin

under vacuum. It should be noted that the polymerization catalyst of BDMA and 2-DMAP are both applied for the 1TDI/1DGEBF polymer, however, they are added separately into the ISOX resins and the corresponding ISOX polymers are named BDMA and 2-DMAP polymers, respectively. The ISOX resin is then cured at 80 °C for 1 h and then 200 °C for 12 h as a two-step curing. To continuously track the transformation to oxazolidone under high temperatures, the cured BDMA polymers and 2-DMAP polymers are further post-cured at 250 °C for varying durations ranging from 0 to 3 h. After the thermal curing of the polymer, a crack of 0.56 cm is then introduced into each SENB specimen through a bending test.

After the crack initiation of each SENB specimen, the two separate parts of the fractured SENB specimen are brought together and then heat treated at 200 °C for 4 h. After this step, the SENB specimen is tested again for crack initiation, and the maximum loads recorded during the initial loading and post-healing loading are recorded and used to quantify the healing performance of the polymers. For each SENB specimen tested for the measurement of healing efficiencies, a reference specimen is prepared under the consistent conditions, but it is tested for the measurement of compositional change during the healing process. This reference specimen, in SENB configuration, is fractured in the same manner and then FTIR spectra are collected for the fracture surfaces of the reference specimen. The two separate pieces of the fractured reference specimen are not brought back together although they are also heat treated at 200 °C for 4 h to investigate the representative chemistry during the healing process. After the heat treatment, the fracture surfaces of the reference specimen are characterized under FTIR again, meanwhile, the healed SENB specimen is tested again under the bending test to quantify the healing performance of the polymers.

The healing performance after a first-time crack initiation of the BDMA polymers is shown in Figure 3.11. Duration of heating at 250 °C is varied from 0 to 3 h to tune the polymer composition of the BDMA polymers. When the post-cure time at 250 °C is increased from 0 to 3 h, reduced strength recovery is observed from the BDMA polymers which are characterized by the calculated healing efficiencies. The

corresponding compositional change during the healing process is first characterized through FTIR and then the FTIR spectra are interpreted by the working curve to analyze the corresponding polymer composition. The compositional change of the BDMA polymers during the healing process is demonstrated in Figure 3.12. Comparing the composition of the BDMA polymers before and after the healing process, higher conversion to oxazolidone is observed within the healed samples than that of the cured samples in each case. Increased oxazolidone fraction is observed during healing for all cases, with 17% of oxazolidone formed during the heat treatment for the BDMA polymer without post-cure. For the BDMA polymers post-cured with 1 h and 3 h, 17% and 7% of oxazolidone formation are measured, respectively.

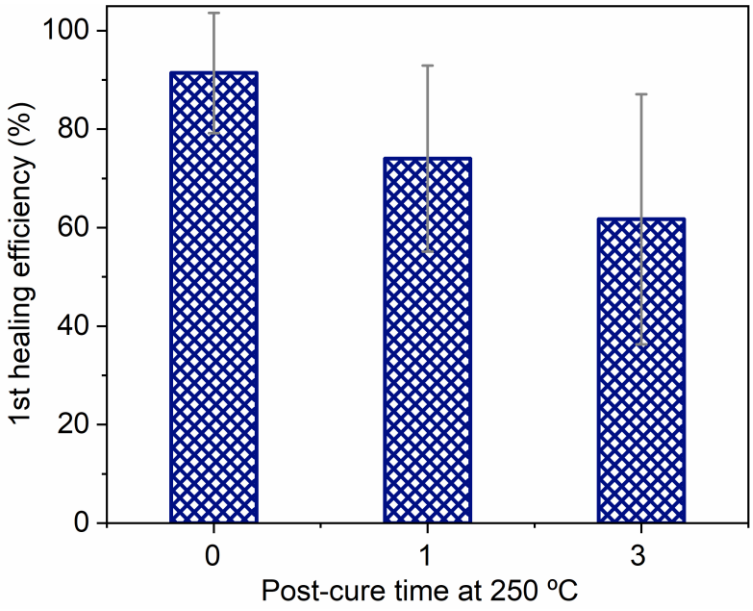

Figure 3.11. The corresponding healing efficiencies measured for the BDMA polymers post-cured at 0, 1, 3 h.

Correlating the healing performance and the compositional change during the healing process, it can be concluded that oxazolidone formation on the fracture surfaces determines the healing performance of the polymers. While the isocyanate detected on the fracture surfaces in the last section is believed to contribute to the oxazolidone formation during the healing process, the isocyanurate-to-oxazolidone transformation is believed as the dominating pathway for producing new covalent bonds on the fracture

surfaces for the healing of the ISOX polymers. This transformation is restricted in the cured polymers due to the heavy steric effect which is significantly reduced in the presence of a large amount of chain scissions at the fracture surfaces and thus it accounts for the strong healing behaviors of the ISOX polymers.

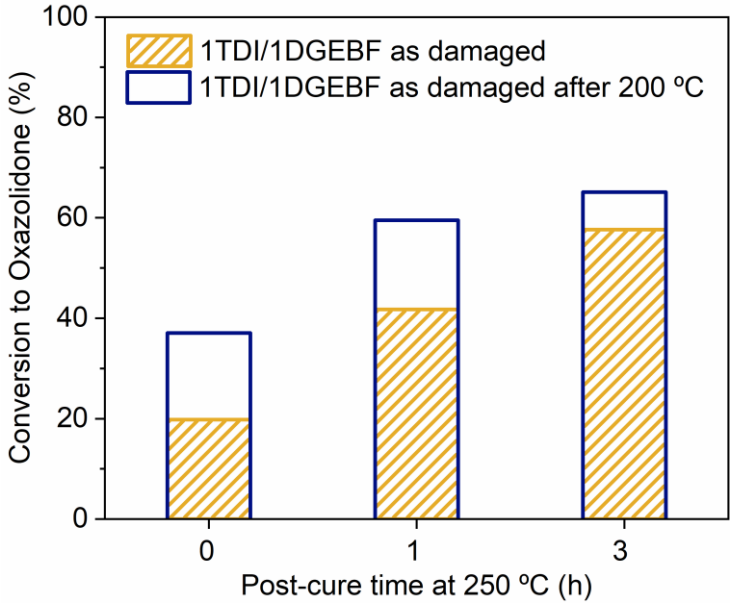

Figure 3.12. The corresponding compositional change during the healing process measured for the BDMA polymers post-cured at 0, 1 and 3 h.

When the polymerization catalyst is changed to 2-DMAP, a similar trend is observed for the calculated healing efficiencies, where reduced strength recovery is observed with increased post-cure time at 250 °C, as can be seen in Figure 3.12. However, the healing efficiencies of the 2-DMAP polymers are lower than that of the BDMA polymers in each case. With a weaker nucleophile added during the polymerization stage in the case of 2-DMAP polymers, varied healing performance is observed due to the difference in the capacity of the ISOX polymers to accomplish the isocyanurate-to-oxazolidone transformation at the fracture surfaces under the heat treatment. For the BDMA polymers, stronger zwitterions formed with more nucleophilic BDMA promote faster isocyanurate-to-oxazolidone transformation, resulting in more oxazolidone formation and a corresponding higher strength recovery of the BDMA polymers.

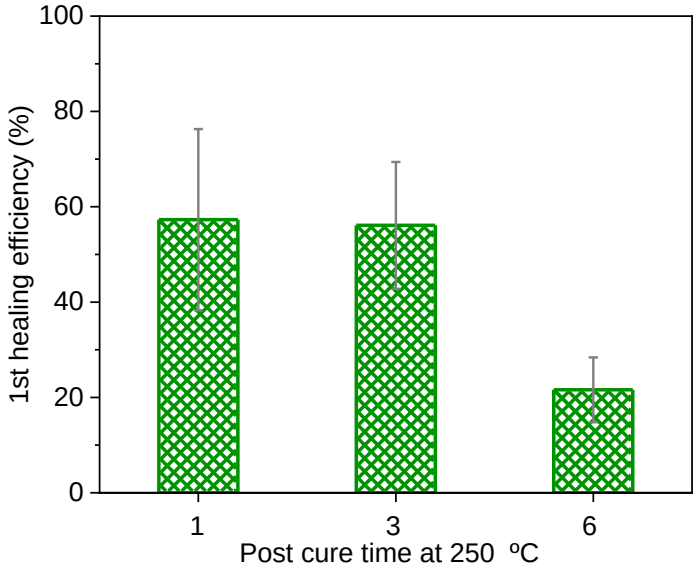

Figure 3.13. The corresponding healing efficiencies measured for the 2-DMAP polymers post-cured at 1, 3 and 6 h.

The corresponding compositional change of the 2-DMAP polymers during the healing process is characterized and interpreted following the method applied for the BDMA polymers. The compositional change of the 2-DMAP polymer is demonstrated in Figure 3.14. Higher conversion to oxazolidone is also observed within the healed samples than that of the cured samples in each case for the 2-DMAP polymers. Oxazolidone formation of 17%, 1%, 3% during the heat treatment is measured for the 2-DMAP polymers with post-cure time of 1, 3 and 6 h, respectively. Compared the amount of oxazolidone formation during the heat treatment, the oxazolidone formation within the 2-DMAP polymers during the 200 °C 4 h healing process is less than that of the BDMA ones for post-cure times at 1 h and 3 h. This lower amount of oxazolidone formation accounts for the lower strength recovery measured from the 2-DMAP polymers observed in Figure 3.14.

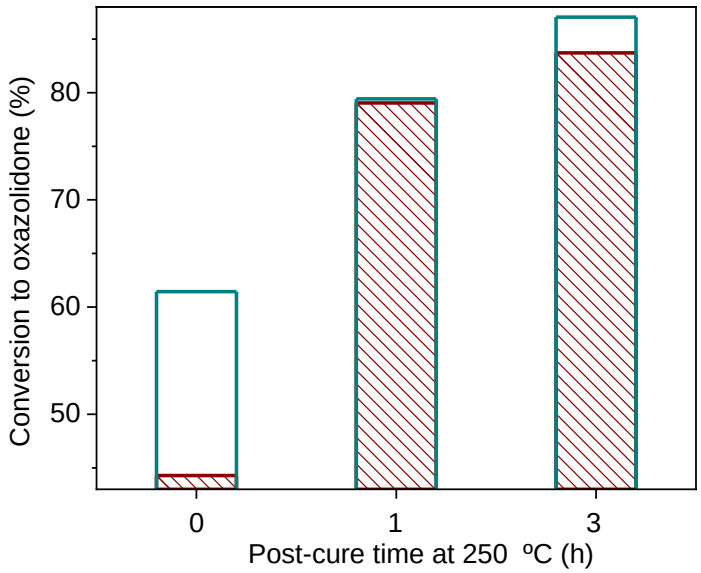

Figure 3.14. The corresponding compositional change during the healing process for the 2-DMAP polymers post-cured at 1, 3 and 6 h.

Regarding the nucleophiles applied for the polymerization, the healing efficiencies of the ISOX polymers increase with the increased isocyanurate fraction of the polymers, which is available for the isocyanurate-to-oxazolidone transformation upon damage. From the trend observed in the healing performance of 1TDI/1DGEBF, 1.5TDI/1DGEBF and 2TDI/1DGEBF in the last section, the 2TDI/1DGEBF one has the highest strength recovery, and this is because of its highest isocyanurate fraction. ISOX polymers with further increase in the molar fraction of diisocyanate as reactants are expected to have increasing healing efficiencies; however, they are not prepared here since the 2TDI/1DGEBF sample already has a high cross-link density and stalling the crack will be more difficult due to its brittleness. This brittleness can explain why the 2TDI/1DGEBF compact tension sample shows much lower failure load and extension compared to 1TDI/1DGEBF and 1.5TDI/1DGEBF samples which have a lower cross-link density characterized by the molecular weight (Mc) between cross-links in Chapter 2. The improved healing performance with higher isocyanurate fraction, as shown in Figure 3.15, further validates that the isocyanurate-to-oxazolidone transformation as a dominant contributing factor in the healing mechanism of the ISOX polymers.

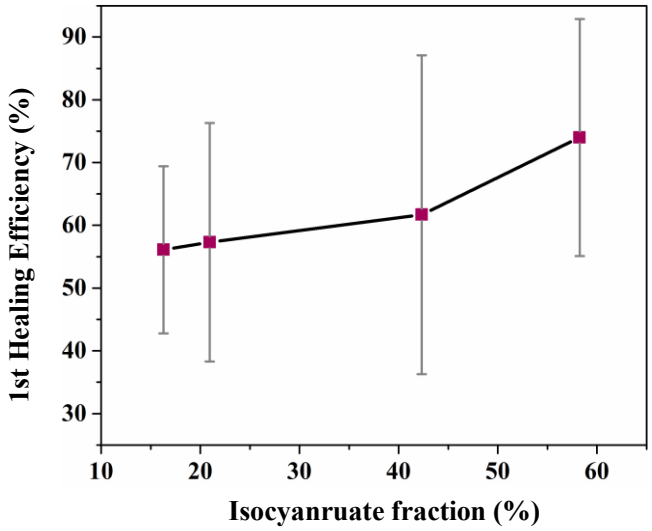

Figure 3.15. Healing efficiency measurements for the BDMA polymers with varying isocyanurate fractions.

It is worthwhile to note that the purpose of post-cure applied to the ISOX polymers in this section is to understand the relationship between the polymer composition and the healing performance of the polymers. To achieve an optimal healing performance of the ISOX polymers, post-cure at 250 °C is not preferred as it leads to decreased isocyanurate conversion. Although the post-cure is expected to improve the toughness of the polymers because of the increased amount of oxazolidone in the network as chain extenders, it is considered a trade-off between healing capacity and the mechanical properties of the polymers. The trade-off between the healing property and other material properties of the ISOX polymers are further studied in the next section to optimize the overall performance of the self-healing ISOX polymers.

3.4 Optimization of Material Properties of the ISOX Polymers

3.4.1 Evaluation of overall thermal and mechanical properties of the ISOX polymers

The healing performance of the ISOX polymers is dependent on the isocyanurate-to-oxazolidone transformation in the polymers, so more isocyanurate available in the polymers leads to higher strength recovery of the polymers after healing. This is a typical structure-property relationship studied for the ISOX polymers in the last section,

and it is useful to instruct self-healing applications of the polymers by tuning the isocyanurate ring concentration within the polymer network. The polymer compositions of the ISOX polymers, however, does not only determine the healing performance of the polymers, but also the mechanical properties of the polymers as well as thermal properties. Further understanding of the structure-property relationship can be used to instruct optimization of overall performance of the ISOX polymers including mechanical strength, stiffness, stability, and more importantly, the healing capacity. Mechanical properties of the 1TDI/1DGEBF, 1.5TDI/1DGEBF and 2TDI/1DGEBF are first evaluated and analyzed in this section.

To evaluate the tensile properties of the polymers, the three ISOX polymers are first molded into a dog-bone shaped configuration which is decided according to Type IV in ASTM D638. The molded tensile samples are cured following the same procedure applied for the compact tension samples. At least five flat specimens are tested for every sample to measure the ultimate tensile strength, ultimate tensile strain and Young's modulus of the polymer. The specimens are first tested under ambient conditions and then at 125 °C, the testing speed of 1 mm/min is used in both conditions. Average values of ultimate tensile strength, strain at failure and Young's modulus of the 1TDI/1DGEBF, 1.5TDI/1DGEBF and 2TDI/1DGEBF are listed in Table 3.1, and the standard deviations are listed in brackets. Under ambient conditions, the tensile strength of ISOX polymers is close to the reported tensile strength of intrinsic self-healing polyurethane based on furan-maleimide Diels-Alder adducts (81), while three ISOX polymers show superior Young' s modulus compared to these prior materials (81, 82). Furthermore, the tensile strength, strain at failure and Young's modulus of ISOX polymers are within the range of those reported for composite grade epoxy (14), indicating the potential of these ISOX polymers as a self-healing replacement to thermoset epoxies. Comparing the tensile properties among the three ISOX polymers, the 1.5TDI/1DGEBF has both the highest tensile strength and stiffness, although its strain at failure is very close to that of the 1TDI/1DGEBF. For mechanical properties at room temperature, higher isocyanurate fraction does not necessarily result in higher strength or stiffness, however, more isocyanurate leads to higher strength recovery of

the ISOX polymers. The 1.5TDI/1DGEBF with the optimal equilibrium between isocyanurate and oxazolidone indicates that the oxazolidone as the chain extender also plays an important role in determination of the mechanical properties of the polymers as it allows larger tensile strain at fracture.

Table 3.1. Comparison of mechanical properties between ISOX polymers under ambient conditions, self-healing polyurethane (PU) based on DA reaction (80) , and commonly used epoxy.

Properties	**1TDI/1DGEBF**	**1.5TDI/1DGEBF**	**2TDI/1DGEBF**	**PU**	**Epoxy**
Ultimate Tensile Strength (MPa)	74.84 (±9.74)	84.43 (±14.47)	76.06 (±4.48)	87.8	80.02
Strain at Failure (%)	2.23 (±0.47)	2.22 (±0.62)	2.07 (±0.39)	5.4	2-6[21]
Young's Modulus (GPa)	4.11 (±0.11)	4.47 (±0.16)	4.40 (±0.13)	2.57	2.48

The tensile properties of the ISOX polymers at an elevated temperature of 125 °C are also characterized to study the high-temperature performance of the polymers. 125 °C is chosen because our previous study on self-healing polymers based on the Diels Alder (DA) reaction undergo significant degradation through the dominating retro-DA reaction at the temperature range of 120 °C to 130 °C. As we can see from the results in Table 3.2, the ISOX polymers demonstrate their good mechanical stability, with the highest Young's modulus of 3 GPa and tensile strength of 65 MPa measured from the 2TDI/1DGEBF at 125 °C. The trend for both the strength and stiffness of the three polymers at this high temperature follows the trend of the healing performance of the polymers. Calculated percentages of preserved strength for the three polymers from the data in Table 3.1 and Table 3.2, are 47%, 71%, and 86% for 1TDI/1DGEBF, 1.5TDI/1DGEBF and 2TDI/1DGEBF, respectively. In terms of stiffness, 49%, 56%, and 70% of stiffness are retained for the 1TDI/1DGEBF, 1.5TDI/1DGEBF and 2TDI/1DGEBF, respectively. Their advantage over the reference epoxy which is polymerized from epoxides can be seen by comparing the preservation of the reference epoxy in terms of both tensile strength and stiffness, as only 27% of the strength of the epoxy reference is sustained when the testing temperature is raised to 125 °C. It should be noted that there is no data for the polyurethane network polymers based on the DA reaction in Table 3.2, as the materials have already started significant

degradation at this temperature and thus it is not applicable around this temperature range. Again, this comparison reveals the superior high-temperature performance of the ISOX polymers.

Table 3.2. Comparison of mechanical properties between ISOX polymers at 125 °C, self-healing polyurethane (PU) based on DA reaction (81), and commonly used epoxy (174).

Properties	**1TDI/1DGEBF**	**1.5TDI/1DGEBF**	**2TDI/1DGEB**	**PU**	**Epoxy**
Ultimate Tensile Strength (MPa)	35.52 (±2.55)	60.13 (±4.89)	65.37 (±5.52)	/	21.55
Strain at Failure (%)	3.60 (±0.27)	2.98 (±0.46)	2.61 (±0.38)	/	13.63
Young'S Modulus (GPa)	2.01 (±0.14)	2.51 (±0.05)	3.07 (±0.06)	/	1.52
Tg (°C)	187	252	270	45.6	180
Td (°C)	365.4 (±1.2)	363.1 (±3.7)	359.9(±2.8)	130	343

The higFh-temperature performance of the ISOX polymers, derived from the dense network structure of the polymers, can be further verified through the measured Tg of the polymers, which are also listed in Table 3.2. With increased TDI in the polymer formulation, there is a higher Tg measured for the polymers, which follows the same trend observed for the healing performance. In comparison, Td, the decomposition temperature of the polymers, measured for the three polymers, has shown the opposite trend where more TDI in the polymer formulation leads to the slightly reduced thermal stability of the ISOX polymers.

3.4.2 Temperature/time dependence healing of the ISOX polymers

The effect of both healing temperature and healing time on the below Tg healing performance of the ISOX polymers is further investigated in this section. The 1.5TDI/1DGEBF polymers, which are cured using a two-step curing process of 80 °C 1 h, 200 °C 12 h, are molded into SENB specimens in order to perform healing efficiency measurements. The reason why 1.5TDI/1DGEBF polymers are chosen instead of 2TDI/1DGEBF polymers is their superior mechanical strength and stiffness among the three ISOX polymers, as it was discussed in the previous section. The Tg of the 1.5TDI/1DGEBF polymers is measured to be 252.5 °C through the dynamic

mechanical analysis, using the same Tg measurement procedure described in Chapter 2. After crack initiation, the specimens are healed according to the standard healing procedure at varied temperatures ranging between 140 °C to 240 °C, thus allowing for the evaluation of temperature dependence in the healing behavior of the 1.5TDI/1DGEBF polymers. The results can be seen in Figure 3.16, where (a) shows the fraction of the samples healed in each data set pertaining to a specific healing temperature, while (b) displays the corresponding healing efficiency measured for these samples. For healing temperatures below 200 °C, a healing fraction of 100% cannot be ensured and this temperature threshold for achieving efficient healing performance of the polymers is possibly correlated to the temperature requirement for the isocyanurate-to-oxazolidone transformation on the fracture surfaces of the ISOX polymers. The unsuccessful healing at temperatures below 200 °C is the reason why the corresponding measured data points lack error bars in Figure 3.18 (b) (140 °C, 160 °C, 180 °C and 190 °C). The standard deviation of the measured healing efficiency is only calculated and reported for data sets with a 100% fraction of healed samples (Figure 3.16). The 1.5TDI/1DGEBF samples healed at 200°C demonstrate considerable strength recovery with an average healing efficiency of 68.9%, while those healed at 220 °C and 240 °C show higher but less consistent strength recovery, with healing efficiencies exceeding 100% measured from the SENB tests. Strength recovery greater than 100% is not desirable, as it would reduce the potential healing cycles of the ISOX polymers, due to greater degree of isocynaurate-to-oxazolidone transformation proceeding in one cycle. Therefore, the healing temperature of 200 °C is optimal, as it can ensure efficient first healing performance as well multiple-time healing performance of the ISOX polymers. The effect of healing time on the healing performance of the polymers at a healing temperature of 200 °C is then further studied.

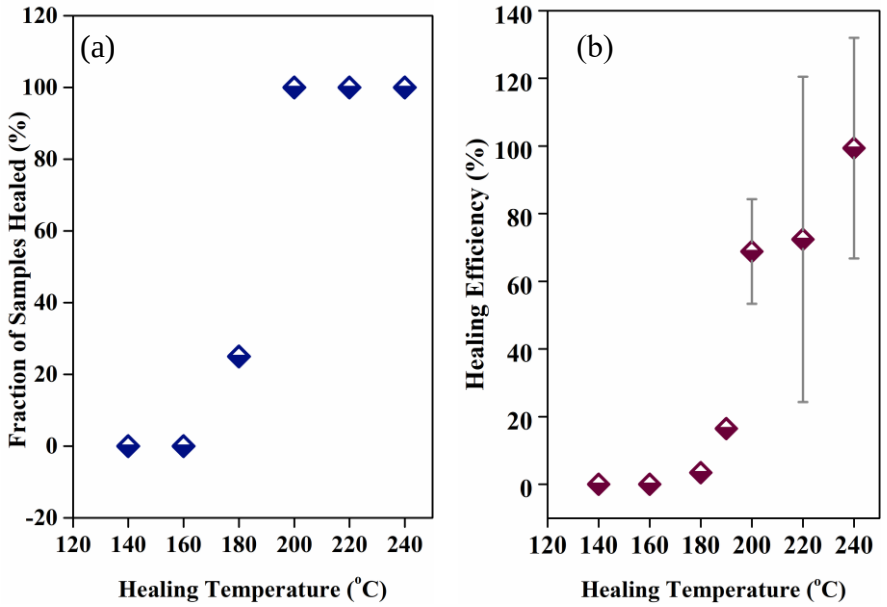

Figure 3.16. Healing performance of 1.5TDI/1DGEBF polymers under varied healing temperatures: (a) fraction of samples healed (b) and the corresponding healing efficiency.

For the 1.5TDI/1DGEBF samples healed at 200 °C, healing time is ranged between 0 h and 16 h to further investigate the time dependence of the healing performance of the ISOX polymers. As can be seen in Figure 3.17 (a), minimum healing time of 4 h is necessary to heal 100% of the heat treated samples. Again, the standard deviation of the measured healing efficiency is only calculated and reported for data sets with a 100% fraction of healed samples, as can be seen in Figure 3.17 (b) where samples with healing time of 0 h, 1 h and 2 h have no error bar. When incrementing healing duration from 0 h to 16 h, increasing healing efficiency is measured for the 1.5TDI/2DGEBF polymers; when however, healing efficiencies greater than 100% is measured for samples healed at 200 °C for 16 h. Again, strength recovery exceeding 100% is not desirable for multiple-time repair capability of the ISOX polymers, as discussed in the last paragraph. The results of the effect of both the healing temperature and healing time on the healing performance evaluated for the ISOX polymers can be used to further optimize the material properties of the self-healable ISOX polymers.

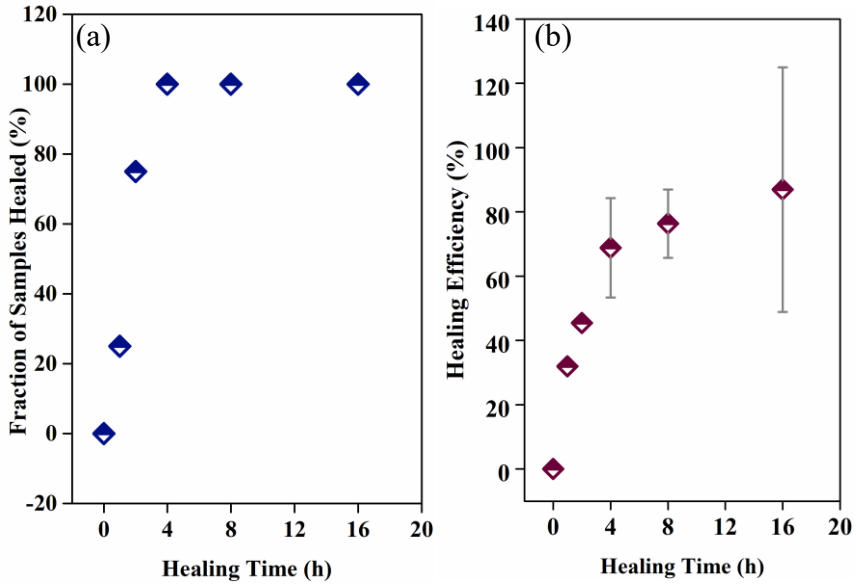

Figure 3.17. Healing performance of 1.5TDI/1DGEBF polymers under varied healing durations: (a) fraction of samples healed (b) and the corresponding healing efficiency.

3.5 Chapter Summary

The development of novel self-healing polymers exhibiting stability at extreme temperatures and retaining mechanical properties as well as mechanical stability comparable to widely used engineering plastics is fully discussed in this chapter. We demonstrate that the network polymers are repeatedly self-healable in the presence of macroscopic cracks, yielding considerable recovery of the polymer's strength and full stiffness after thermal annealing. The healing mechanism is studied by direct characterization of compositional change on the fracture surfaces during the healing process. New oxazolidone formation, accounting for the considerable strength recovery of the polymers comes from both the isocyanurate-to-oxazolidone transformation and induced isocyanate as a result of mechano-chemical cycloreversion of isocyanurate. The healing is achieved for the ISOX polymers below Tg, so the mechanical strength and stiffness of the polymers are still preserved during the healing process, which is hard to achieve through other healing mechanisms. The developed 2TDI/1DGEBF has the highest Tg of 270 °C, which is the highest reported value for intrinsically healing thermosetting polymers.

This chapter has also shown that the isocyanurate and oxazolidone fractions in the polymer together determine the overall material properties of the ISOX polymers including the healing performance, mechanical properties and thermal properties. A high isocyanurate fraction leads to a small cross-link density of the ISOX polymers. Material properties including modulus, glass transition temperature and healing performance are improved by increasing the cross-link density, but the strain at failure and thermal stability are reduced. Increased healing performance of the ISOX polymers comes with higher extent of isocyanurate-to-oxazolidone transformation during the healing process. This transformation is restricted in the cured ISOX polymers because of the heavy steric effect given the high density of isocyanurate cross-linkers in the polymer network. However, the weakening of the steric effect on the crack surfaces at high temperatures in the presence of epoxide is an important reason for the occurrence of the isocyanurate-to-oxazolidone transformation during the healing and is therefore concluded to be important for the preparation of polymers with excellent healing performance. To conclude, trade-off is shown between healing performance and thermal stability, mechanical properties under ambient conditions; however, other important properties including both glass transition temperatures and high-temperature performance follow the same trend with increased isocyanurate fraction. The study on these structure-property relationships of the ISOX polymers is important to instruct the future applications of the self-healing ISOX polymers.

CHAPTER 4

Carbon Fiber Reinforced ISOX Polymer Composites

4.1 Chapter Introduction

Building on the work demonstrated in the last two chapters, novel carbon fiber reinforced polymer (CFRP) composites are developed in this chapter by incorporating the intrinsically self-healable isocyanurate-oxazolidone (ISOX) polymers as thermosetting matrices. The ISOX polymers can provide a solution for internal damage within the composites through a combination of two damage management strategies, which are improving damage resistance and improving damage tolerance of the composites. The excellent mechanical strength and stiffness of the ISOX polymers can effectively prevent damage in the polymer matrix from occurring within the composites at the beginning of use. Since major impact damage typically occurs in the polymer matrix for CFRP composites, such as microcracks or delamination, the inherent self-healing capability of the ISOX polymers can reverse this damage in-place under thermal stimulus. This improved damage tolerance of the CFRP composites can suppress the propagation and accumulation of the cracks and keep the damage level low. The low damage level achieved with the self-healing ISOX polymer matrix can effectively prevent the catastrophic failure of the composites. The two combined strategies are useful to prolong the serving time of the composites and they can improve safety and reduce maintenance of the applied structures. The damage removal is repeatable several times at the same fractured spot within the composites with no reactants or catalysts needed for the repairing process. Meanwhile, the ISOX polymer matrix, not only adds the self-healing capability into the composites, but also enables

high-temperature performance as well as excellent mechanical strength, stiffness and high thermal stability into the hybrid system.

In this chapter, three self-healable composites are developed with unidirectional carbon fibers as the reinforcement and three ISOX thermosets with increasing cross-link density as the polymer matrices, which are termed ISOX_C1, ISOX_C1.5 and ISOX_C2, respectively. These ISOX thermosets with increased cross-link density are developed by varying the amount of tolylene diisocyanate (TDI) to bisphenol-F diglycidyl ether (DGEBF) epoxy resin from 1 to 1, 1.5 to 1 and 2 to 1 in molar ratio, respectively. The matrix of the ISOX_C2 has the highest cross-link density, due to the increased amount of isocyanurate with the increasing amount of diisocyanates as the reactant. The composites are then evaluated in terms of their capability to reverse both microscopic and macroscopic damage. Each composite sample is delaminated multiple times using the short beam shear (SBS) test and treated with a standard healing procedure after each damage event, where it is heat treated at 200 °C for 12h under approximately 100 psi. Both microcracks and delamination within the composite initiated through shear loading are repeatedly eliminated under the heat treatment without any additives due to the inherent self-healing capability of the ISOX matrix. The highest average recovery of SBS strength is observed for the ISOX_C2, which is characterized by a first healing efficiency of up to 85% and a second healing efficiency above 70%. Mechanical properties of the developed self-healing CFRP composites are comparable to that of engineering grade CFRP composites with an epoxy matrix, demonstrated by their high strength and elastic modulus characterized from tensile testing. Without compromising the structural advantage of CFRP composites, both at room and elevated temperatures, the self-healing capability is successfully added into the composites, which demonstrates the great potential of the developed composites as advanced multifunctional structural materials.

4.2 Development of the Carbon Fiber Reinforced (CFR) ISOX Polymer Composites

4.2.1 Fabrication of the carbon fiber reinforced polymer composites

Commercial tolylene-2,4-diisocyanate (TDI), benzyldimethylamine (BDMA) from Acros Organics, diglycidyl ether of bisphenol F (DGEBF) in the form of EPON^{TM} 862 (EEW of 165-173 g/eq) from Hexion^{TM}, are used as received to prepare an isocyanurate-oxazolidone (ISOX) polymer matrix for carbon fiber reinforced polymer (CFRP) composites. Unidirectional carbon fabric (US Composites, FG-CFU0001) is used as reinforcement without any additional treatment. Three different ISOX thermosets with varying TDI/DGEBF ratios (1TDI/1DGEBF, 1.5TDI/1DGEBF and 2TDI/1 DGEBF) are employed as the polymer matrix for the three CFRP composites which will be referred to ISOX_C1, ISOX_C1.5 and ISOX_C2, respectively throughout this chapter. It should be noted that 0.1 wt% of BDMA is added as catalyst for the polymerization of the ISOX polymer matrix, which is consistent with the percentage utilized in Chapter 3. To prepare the CFRP composite panels, the mixture of TDI/DGEBF is first weighted and transferred to a 100 mL bottle, and then mixed thoroughly with a magnetic stir bar for at least 15 min to get a transparent and colorless resin with low viscosity. The ISOX resins have a reduced viscosity due to the addition of TDI as a reactant diluent for DGEBF. Because of the low viscosity of the ISOX resins, vacuum assisted resin transfer molding (VARTM) is used to transfer the uncured ISOX resins to the carbon fabric plies, after the lay-up of the unidirectional carbon fabric. VARTM is an adapted version of resin transfer molding, where the vacuum is applied to achieve better wetting of the fiber reinforcement. With VARTM, CFRP composites with high fiber volume fraction can be achieved, and therefore the structural performance of the parts is generally high. The fabrication procedure of the carbon fiber reinforced ISOX polymer composites is compatible with that of commonly used engineering grade composites with an epoxy matrix. The gel time for the ISOX resins reported here can be a few hours to a few minutes based on the amount of BDMA catalyst added. To note, BDMA instead of 2-DMAP is used here for the

polymerization of the ISOX polymer matrix because of the higher healing efficiencies of the ISOX polymers catalyzed with BDMA measured in Chapter 3.

A standard curing procedure of 1 h at 80 °C under the hot press with a pressure of 100 psi and then 12 h curing at 200 °C in an oven under the same pressure is used for the composites. Pressure is necessary during the curing procedure in order to get rid of voids during the fabrication process. For the preparation of short beam shear (SBS) test samples and tensile test samples, 12 plies and 3 plies of carbon fabric are used, respectively. The thickness of the samples is measured by a digital caliper, with the value of approximately 3.5 mm and 1 mm for SBS test samples and tensile test samples, respectively. Compared to traditional CFRP composites which are relatively expensive, the developed CFRP composites with the ISOX polymer matrices are commercially available and economical, without the need of additional treatment for either the matrix or the fiber reinforcement.

4.2.2 Characterization of full curing of the CFRP composites

After the thermal curing of the three CFRP composites, they are slowly cooled down to room temperature for further characterization. No voids are visible on the surfaces of the fabricated CRRP composites, indicating good bonding between the ISOX polymers and the carbon fiber reinforcement. To verify the full curing of the composites, a differential scanning calorimetry (DSC) TA Q2000 from, is used to characterize the fabricated CFRP composites. Under DSC, any incomplete reactions would lead to exothermic peaks in the thermograph. A composite specimen of approximately 2 mg is placed into a Tzero hermetically sealed aluminum pan and then tested under a N_2 atmosphere with a purge flow of 100 mL/min. A heat-cool-heat loop from 0 °C to 250 °C at a rate of 10 °C/min is used for the three CFRP composites with varying ISOX polymer matrix. Generally, the purpose of the DSC heat-cool-heat experiment is to detect any reactions/transitions during the second heating process after erasing the thermal history during the first heating process (176-178) . Potential relaxation or molecular rearrangement can occur during the first temperature ramping

process, after which the material is cooled at a known rate before it is heated again. The cooling process imparts a known thermal history and therefore, important thermal information on internal differences of similar materials can be detected during the second heating curve without the influence of previous thermal effects. The representative DSC results of the three CFRP composites are shown in Figure 4.1, where a similar trend in the heat flow curve is observed for the first and second heating loop for each composite, and there are no exothermic peaks detected under DSC. These results confirm the full curing of the fabricated CFRP composites with the two-step curing procedures on the hot press, even though the isocyanurate-to-oxazolidone transformation is still active in the polymer matrix. The absence of any measurable reactions for the three composites confirms full polymerization and thus demonstrates that unfinished polymerization cannot be a plausible explanation of the healing mechanism which occurs at 200 °C. The CFRP composites fabricated here are used for the healing property characterization in the next section.

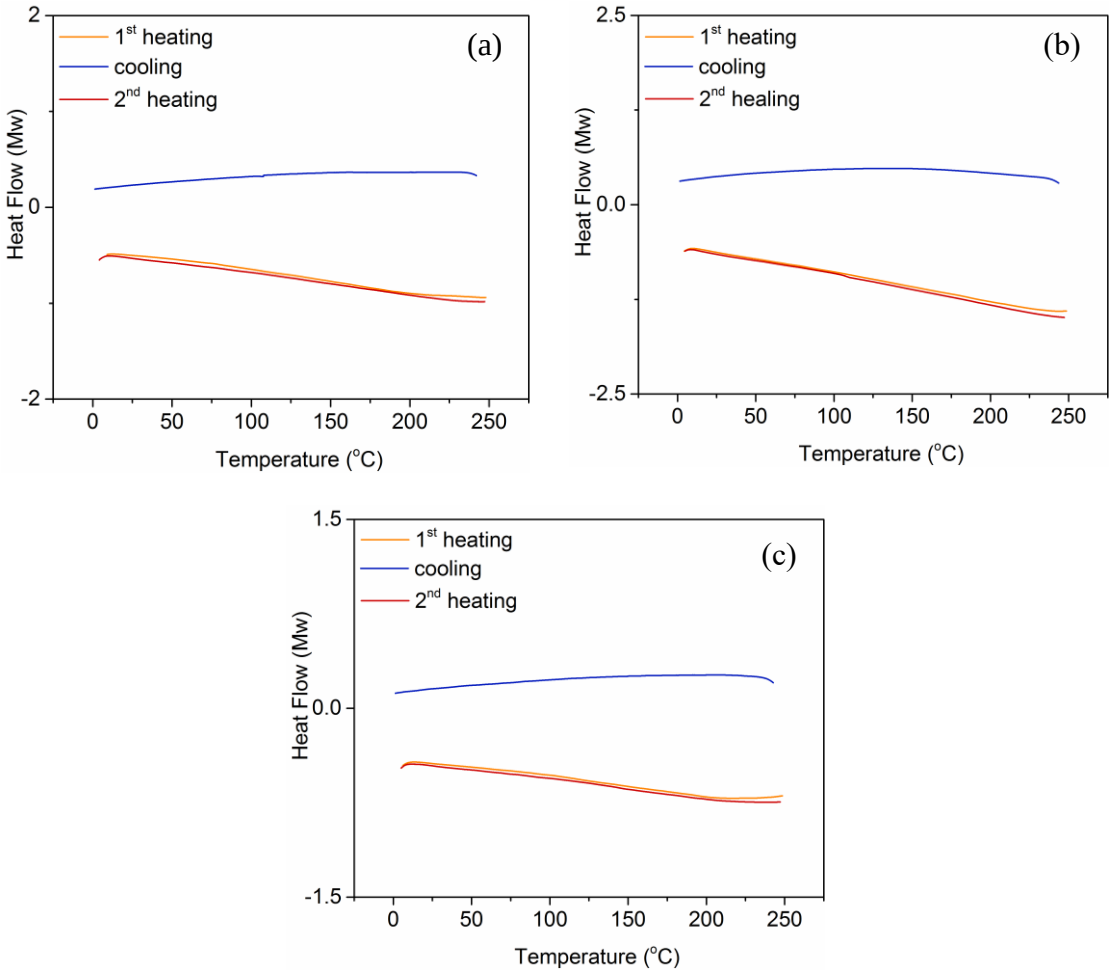

Figure 4.1. Representative differential scanning calorimetry (DSC) test results of the (a) ISOX_C1, (b) ISOX_C1.5 and (c) ISOX_C2, respectively.

4.2.3 Measurement of fiber volume fraction of the CFRP composites

Fiber volume fraction (V_f), or fiber volume ratio, is the percentage of fiber volume in the entire volume of a fiber reinforced polymer composite material. V_f is an important parameter of a composite material as it determines the overall mechanical properties of the composite. The effect of V_f on the properties of fiber reinforced polymer composites can calculated from the classic rule of mixtures, or the law of mixtures equation as shown in Equation below,

$$X_C = X_r V_r + X_m V_m$$

where X represents any particular property, the subscripts c, r, and m refer to the composite, reinforcement, and matrix, respectively. The ultimate tensile strength of a

composite as a function of V_f can be calculated based on the equation. Generally, a higher fiber volume fraction typically results in better mechanical properties of the composite (179). V_f is measured for each CFRP composite through nitric acid digestion in accordance with the ASTM D3171 procedure A. Briefly, a rectangular specimen is cut out of a composite panel and then weighed to the nearest 0.0001 g to get its initial mass (M_i) before it is placed into a 250 mL conical flask containing 30 mL of 70% nitric acid. The specimen is then heated under 60 °C for 6 h under reflux conditions. After the heating procedure, the mixture is filtered with a tared sintered glass filter under vacuum and the remaining carbon fiber in the filter is washed three times with deionized water and then acetone. Finally, the solid leftover carbon fiber is dried in an oven overnight at 80 °C and then weighed in the same way to get mass of the sintered glass filter with reinforcement (M_{cr}). The measured M_i and M_{cr}, along with the measured density (1.3 g/cm^3) of the ISOX polymers (180), are used to calculate the V_f of the specimen. The V_f of each composite sample is calculated and averaged from the test results of three specimens. The measured V_f is 76%, 72% and 70% for the ISOX_C1, ISOX_C1 and ISOX_C2, respectively, and the effect of V_f on the healing performance of these carbon fiber reinforced ISOX polymer composites is further discussed in the next section.

4.3 Healing Performance of the Self-Healable CFRP Composites

4.3.1 Characterization of matrix delamination elimination

The healing performance of the developed CFRP composites is evaluated through the short beam shear (SBS) test which subjects a beam to bending, just as flexural testing methods do, but the beam is very short relative to its thickness. The schematic of the SBS test is shown in Figure 4.2 (181). The objective of the employed SBS tests is to minimize the flexural (tensile and compressive) stresses and to maximize the induced shear stress within the tested specimen. During the SBS test, it was reported that small cracks were first developed in the resin-rich layers between plies, some fine-scale debonding occurred between fibers and a light increase in shear stress led to the

formation of intra-ply delamination (182) . Therefore, the SBS test is used to induce delamination and microcracking within the carbon fiber reinforced ISOX polymer composites in this work. Once a sudden and significant load drop is observed due to the accumulation of defects and the resulting failure of the specimen, the test is stopped, and the maximum bearing load is recorded. In accordance with the ASTM D2344, a support-span-length-to-specimen-thickness ratio of 4:1 is used and all SBS tests are performed on an Instron testing machine by means of a three-point bending fixture. The test is conducted at a crosshead speed of 1 mm/min to failure. For a composite sample with a thickness of 3.5 mm, SBS specimens with a width of 7 mm and a length of 21 mm are cut out from the fabricated CFRP composite panels. At least 6 specimens are tested for three composites under ambient conditions, for both the initial loading and the following three post-healing reloading. It should be noted that after the first, second and third loading, the SBS specimens are compressed under approximately 100 psi on a hot press at 200 °C for 12 h as the standard healing procedure in this chapter.

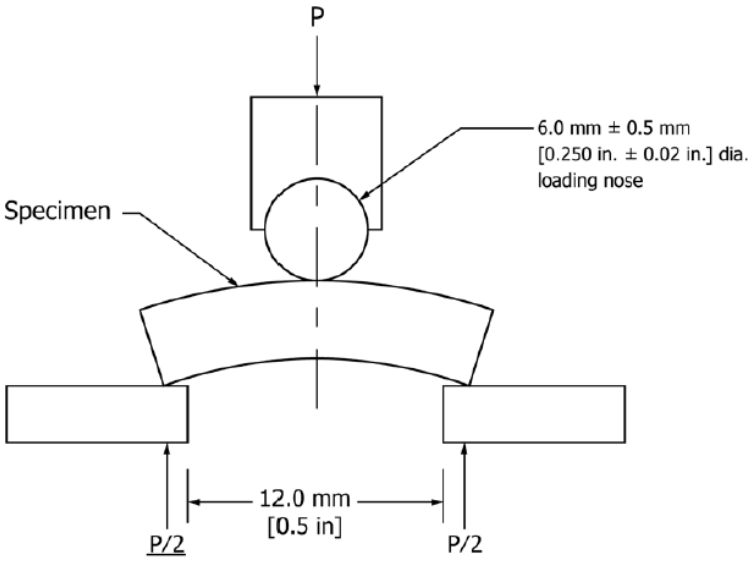

Figure 4.2. Horizontal shear loading diagram (curved beam) of the short beam shear (SBS) tests (181).

A representative schematic of an ISOX-C2 specimen after initial shear loading is shown in Figure 4.3, where significant delamination is observed under optical microscope. This induced damage mode can be seen more clearly under scanning

electron microscope (SEM), as shown in Figure. 4.4. The delaminated specimen is then subjected to the healing procedure described above and then characterized under both optical microscope and SEM for the second time to make a comparison between the delaminated and healed specimen.

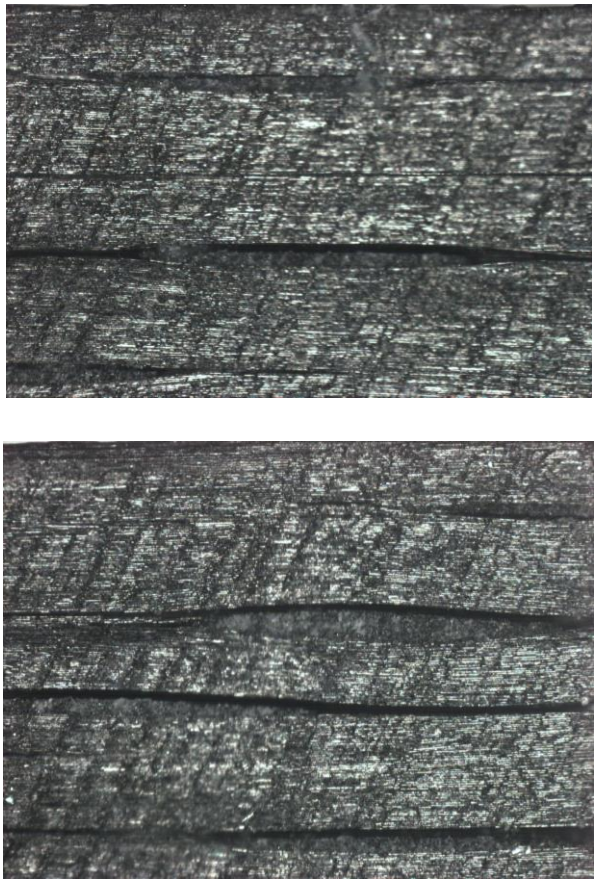

Figure 4.3. Representative delamination within the ISOX_C2 after short beam shear (SBS) tests observed under optical microscope.

The delaminated plies of the ISOX_C2 specimen are effectively bonded after the healing procedure. As shown in Figure 4.5, the delamination sites disappear after the healing process, which is observed both under optical microscope and SEM. Visible black strips in the composite specimen after healing are binders of the unidirectional carbon fibers, which are already present in the non-delaminated composite specimen. The healing response of the CFRP composites is repeatable due to the inherent healing nature of the ISOX thermosetting matrix and is repeated three times for each composite. The healing capacity of the composites comes from the self-healable ISOX polymer matrix, which in its the neat resin form can remove the macroscopic defects under

thermal stimulus. Scission of the isocyanurate ring during matrix crack propagation, overcomes the steric effect at the crack surfaces so that the subsequent transformation from isocyanurate to oxazolidone can effectively heal the cracks under annealing. To note, the steric effect comes from the large amount of isocyanurate (crosslinks) in the polymers as the reactant diisocyanate converts to either isocyanurate (at 80°C) or oxazolidone (at 200 °C). In this case, the transformation from isocyanurate to oxazolidone is non-reversible, but the healing of the polymer matrix is repeatable given the availability of this chemical transformation at 200 °C and the weakening steric effect.

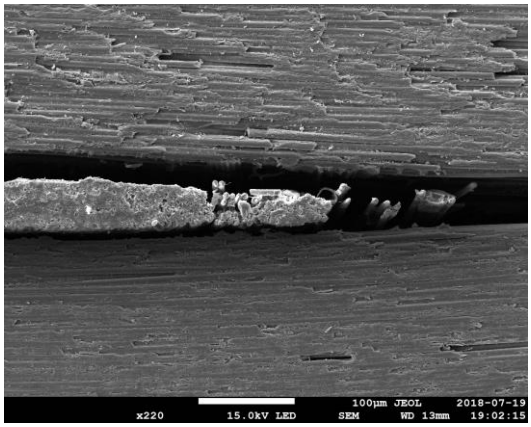

Figure 4.4. Representative delamination within the ISOX_C2 after short beam shear (SBS) tests observed under scanning electron microscope (SEM).

4.3.2 Quantification of the strength recovery of the CFRP composites

To quantify the healing performance of the CFRP composites, a healing efficiency is defined as the ratio of maximum load of the healed specimen at each healing cycle to the maximum load that the virgin specimen withstands during the initial SBS test. Representative load-displacement curves of the ISOX_C1.5 specimen for three loading cycles are shown in Figure 4.6, where considerable strength of the composite is recovered after the heat treatment. The maximum load of the virgin specimen is the highest and it reduces during the subsequent loading cycles. The SBS test is repeated for at least five specimens for each composite sample and the average value is taken to

get the healing efficiency for each composite. The results of the measured healing efficiencies of the three composites are shown in Figure 4.7, an excellent strength recovery for the self-healing composites is achieved with a first healing efficiency of 80% or above for all three cases. Specifically, a first healing efficiency of 80%, 81%, and 85% is measured for ISOX_C1, ISOX_C1.5 and ISOX_C2, respectively. The composites should not be expected to enable full recovery of strength since only the polymer can be healed, while the short span of the SBS specimen typically induces fiber failure. Figure 4.8 shows that both healable matrix delamination and non-healable fiber breakage detected under scanning electron microscope (SEM).

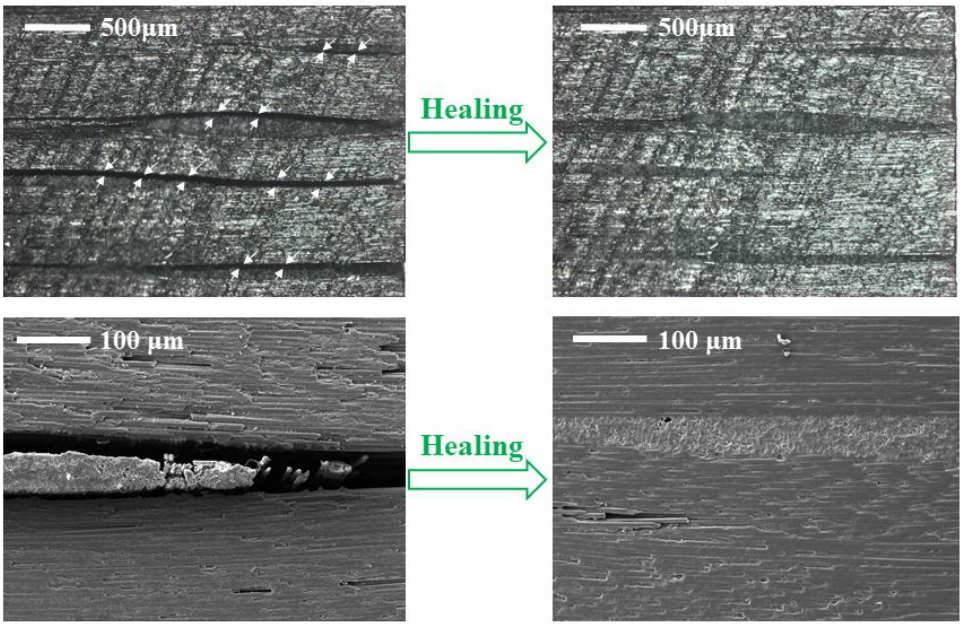

Figure 4.5. Comparison between a delaminated short beam shear (SBS) specimen after loading, with the post-healing SBS specimen for ISOX-C2 under (a) optical microscope and (b) scanning electron microscope (SEM).

There are several reasons why the second healing efficiencies of the composites fall below the initial healing efficiencies. First, the reformation of the broken chemical bonds is not 100% in ISOX polymer matrix due to irreversible bond breakage during the crack initiation and propagation process, which is also observed in pure ISOX polymers without the presence of fiber reinforcement. Figure 4.9 shows the loading curve of a neat polymer (1.5TDI/1DGEBF), where full-strength recovery of the polymer is not observed after the introduction of approximately a 5 mm crack under

three-point bending in the single-edge notched beam (SENB) test. To note, the 1.5TDI/1DGEBF polymer is polymerized and healed using the same methods as that of the polymer matrix of the ISOX_C1.5. Second, perfect contact of crack surfaces after damage is needed for 100% strength recovery; however, it is hardly possible to keep the delaminated fibers and matrix in their exact same position as they were before delamination, even with an external pressure of approximately 100 psi applied to overcome the rigidity of the fibers during the healing process. Finally, the mixed damage modes under shear loading leave more non-healable defects within the composites with increased loading cycles, which ultimately leads to reduced strength of the composites upon reloading. Decreased slope of the loading curve with the increased loading cycles for the composite is observed, where the slope of the loading curve of the ISOX polymer itself does not change when it is reloaded after healing. The decreased slope of the curve observed in the composite, which has been previously reported for unidirectional self-healing CFRP composites under short span three-point bending tests(183) (182, 184), can be explained by the fiber rupture during both the virgin loading and the post-healing reloading process, because the fiber reinforcement provides the majority of the stiffness.

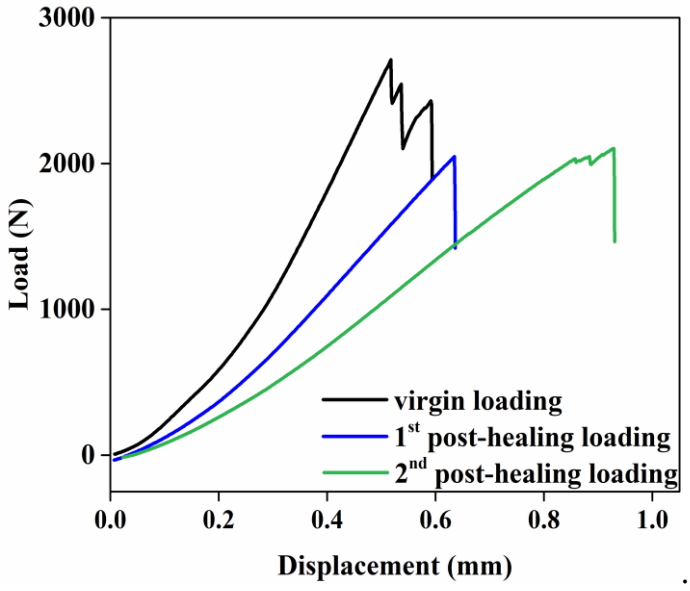

Figure 4.6. A representative short beam shear (SBS) test result of the ISOX_C1.5.

The healing efficiency results of the three CFRP composites are compared in Figure 4.7, where higher healing efficiencies are observed for the composites with more diisocyanate in the polymer formulation of the polymer matrix. The healing behavior of the self-healing composites is consistent with that of the bulk ISOX thermosets, where higher extent of strength recovery is observed for the ISOX polymers with higher TDI/DGEBF ratio. A larger fraction of TDI leads to more isocyanurate in the polymer matrix, which is available for transformation to oxazolidone at 200 °C given the weakening steric effect after the occurrence of damage, which is the nature of the matrix healing as discussed above. However, for the as-cured composites without damage (cured under the standard curing procedure of 1 h at 80 °C and then 12 h at 200 °C), this transformation is restricted and no longer detected under differential scanning calorimetry (DSC) (see details in Section 3.3). Increasing initial curing time is not expected to overcome this restriction or further facilitate this chemical transformation, so the measured healing performance of the composites should not be over-evaluated.

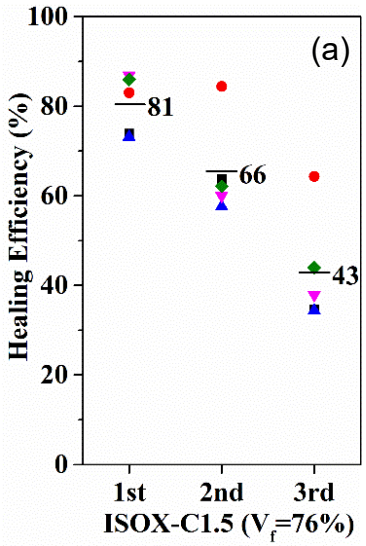

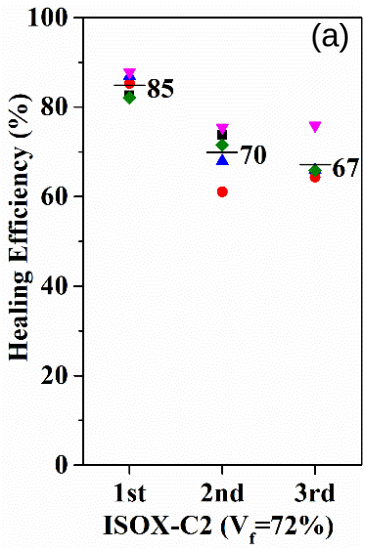

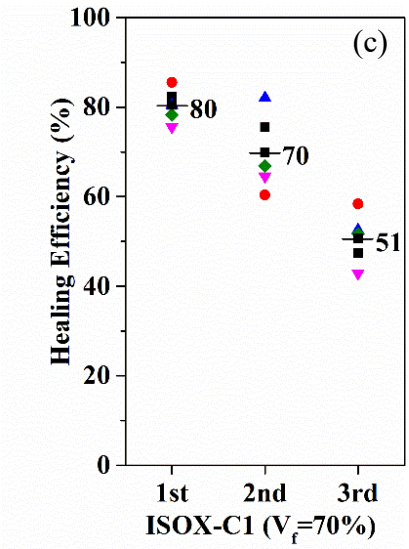

Figure 4.7. Results of multiple self-healing efficiencies of (a) ISOX_C1, (b) ISOX_C1.5 and (c) ISOX_C2, with the corresponding fiber volume fraction (V_f) specified in the bracket.

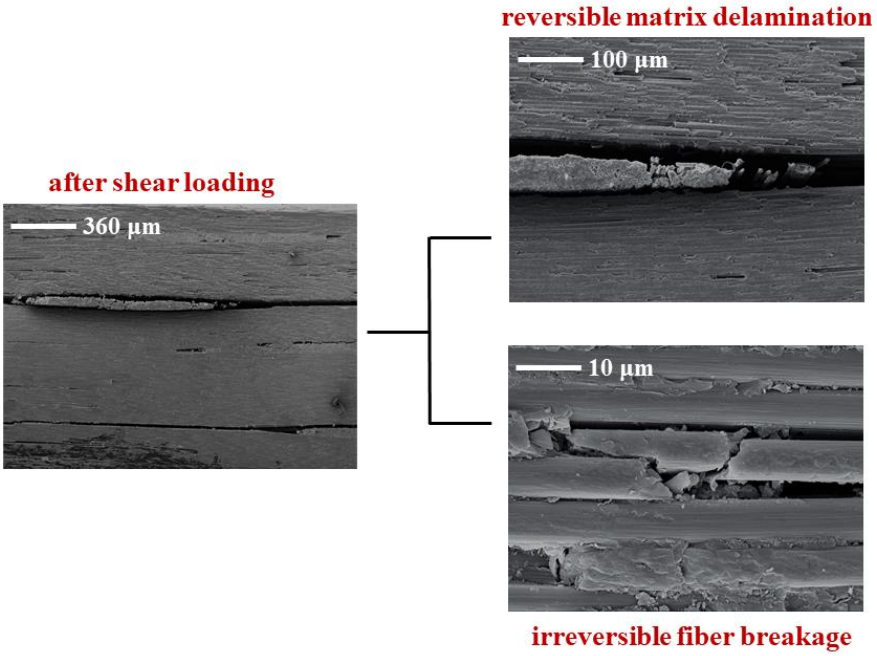

Figure 4.8. A representative damage schematic of the ISOX_C2 after shear loading under scanning electron microscope (SEM).

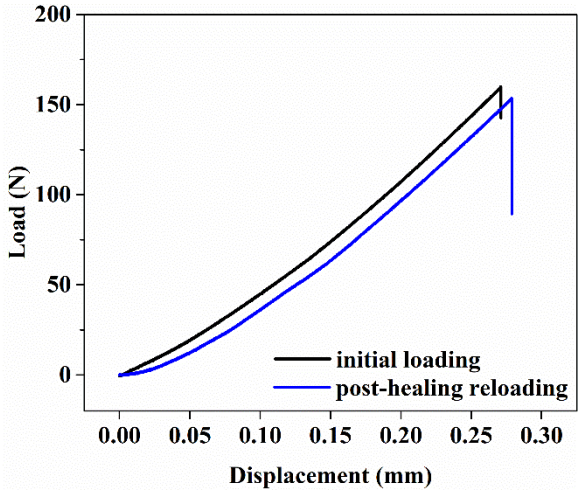

Figure 4.9. A representative single-edge notched beam test result of 1.5TDI/1DGEBF polymer.

4.3.3 Effect of fiber volume fraction and healing pressure on the healing performance of the CFRP composites

Besides the polymer composition of the ISOX polymer matrix, other factors including fiber volume fraction (V_f) of the composites, as well as applied pressure during healing are further studied for optimization of the healing performance of the composites. The V_f of each composite, as shown in the bracket at the bottom of Figure

4.7, is measured from nitric acid digestion and then analyzed to better understand the observed trend in the self-healing capacity of the CFRP composites as discussed earlier in this chapter. The V_f is expected to have a large effect on the healing performance of the CFRP composites because the level of the strength recovery is governed by the healable phase in the composite, which is the polymer matrix. In other words, for ISOX composites with the same self-healing matrix, a higher healing efficiency is expected for the one with the lowest V_f. Variation of the V_f between ISOX_C1 (V_f = 70%) and ISOX_C1.5 (V_f = 76%) can explain why the second healing efficiency of the ISOX_C1 (70%) is slightly higher than that of the ISOX-C1.5 (66%), as can be seen in Figure 4.7, while the healing efficiency of the polymer 1.5TDI/1DGEBF is always higher than that of the polymer 1TDI/1DGEBF in Chapter 3. It is worthwhile to note that the V_f of the self-healing composites is around 70%, given that a typical V_f value of unidirectional fiber reinforced polymer composites is 65% for optimized mechanical properties (67). The first healing efficiency of two ISOX_C2 composites with varied V_f of 86% and 74% are characterized and compared in Figure 4.10. The ISOX_C2 sample with the lower V_f demonstrates a higher 1st healing efficiency because it has more healable phase.

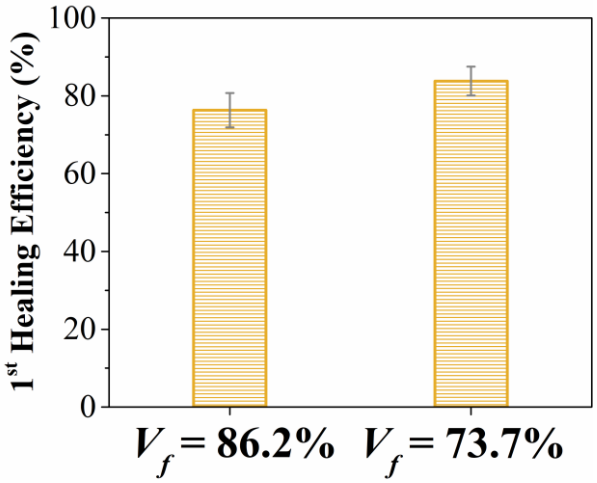

Figure 4.10. Effect of fiber volume fraction (V_f) on the healing performance of the ISOX_C2.

The healing behavior of the CFRP composites under the varying healing pressure applied during the healing process is performed on ISOX_C2 samples to study its effect

on the healing performance of the composite. ISOX_C2 is chosen as a case study since it possesses the best healing performance among the three CFRP composites. Three healing pressure of 100, 300 and 500 psi have been applied individually on the delaminated samples, with the corresponding 1st healing efficiencies shown in Figure 4.11. Increasing the healing pressure does not lead to improved healing performance of the composites, indicating that the healing pressure is only responsible for overcoming the rigidity of the fibers and achieving contact at the crack surface during the healing process. It should be noted that pressure is necessary for the healing of the composites as delamination is still observed for the samples healed under the same heat stimulus but no pressure.

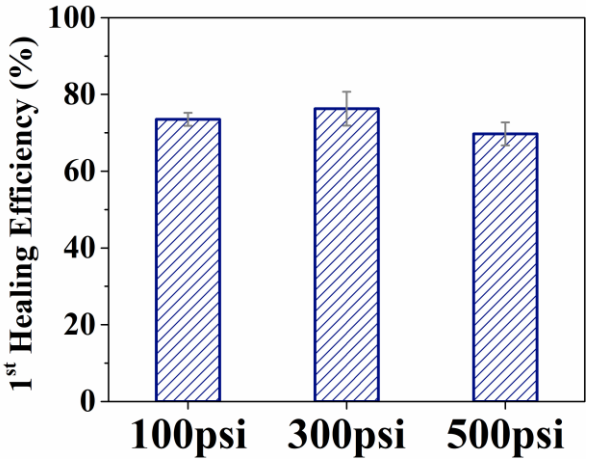

Figure 4.11. Effect of healing pressure on the healing performance of the ISOX_C2.

4.4 Characterization of Thermal Properties and Mechanical Properties of the CFRP Composites

4.4.1 Thermal analysis of the self-healing CFRP composites

Simultaneous measurements of weight change and true differential heat flow with a TA Instruments SDT Q600 are used to characterize the thermal stability of the self-healing CFRP composites. A specimen is tested under air and nitrogen atmosphere individually over a temperature range from 30 °C to 600 °C at a ramping rate of 20 °C/min. A minimum of three specimens for each sample is examined to ensure statistically relevance of the data. A TA Q800 dynamic mechanical analyzer (DMA)

is employed for the determination of the glass transition temperature (Tg) of the self-healing composites. A cantilever beam specimen, cut out of the composite panels with dimensions of 25 mm × 7 mm × 1 mm, is loaded on a dual cantilever clamp in the multi-strain module. The specimens are tested at 1 Hz over a temperature range from 30 °C to 325 °C at a rate of 2 °C/min in air atmosphere and the results obtained from three specimens are averaged to determine the average Tg for each composite sample.

The results of the simultaneous measurement of weight change and true differential heat flow are shown in Figure 4.12. A decomposition onset temperature (T_d) of 350 °C, 353 °C and 360 °C is measured for ISOX_C1, ISOX_C1.5 and ISOX_C2, respectively. The T_d of the composite is defined as the temperature where 1.5% of its weight loss is measured when subjected in nitrogen atmosphere (185)(186). More than 99.5% of the composite weight remains for three composites in both air and nitrogen atmosphere when the temperature reaches 300 °C, which demonstrates the superior thermo-oxidative stability of the self-healing composites. The excellent thermo-oxidative stability of the composites is comparable with that incorporating bismaleimides (BMIs) as the polymer matrices which are famous for their exceptional thermo-oxidative stability at temperatures higher than 300°C in the presence of air (4). The composites begin to decompose at approximately 350 °C in both air and nitrogen, where an endothermic peak is observed in the heat flow measured for each composite sample. It should be noted that the SDT Q600 used is calibrated by analyzing the heat capacity curve for sapphire over the range 200 °C to 1500 °C, so the instrument limitation in temperature range applied in the calibration process can explain the variation in the baseline of heat flow observed in Figure 4.12.

(a)

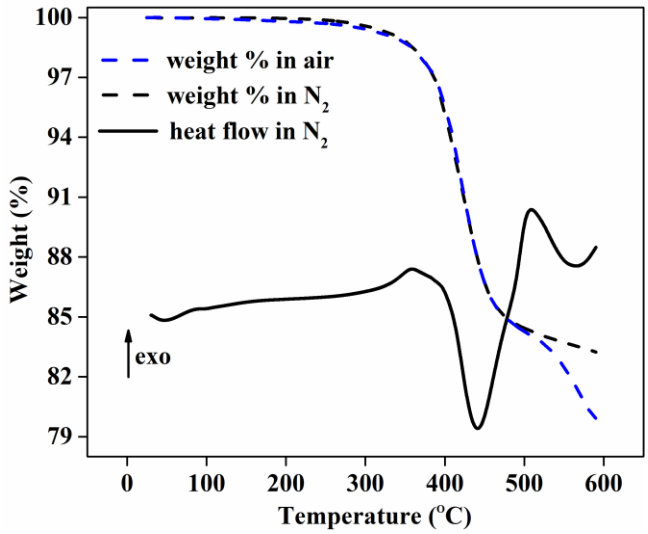

(b)

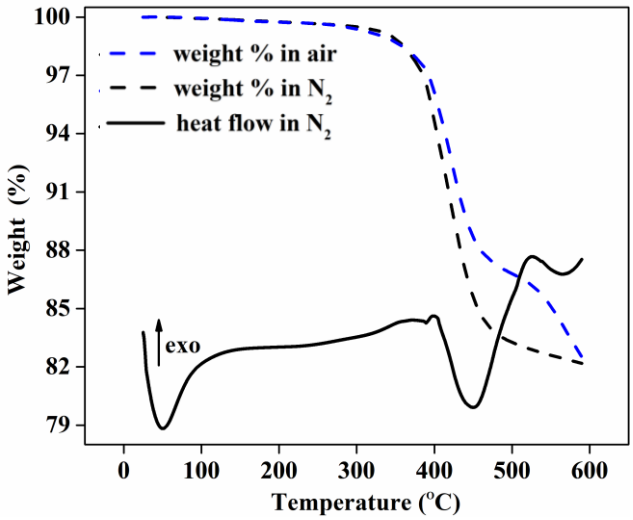

(c)

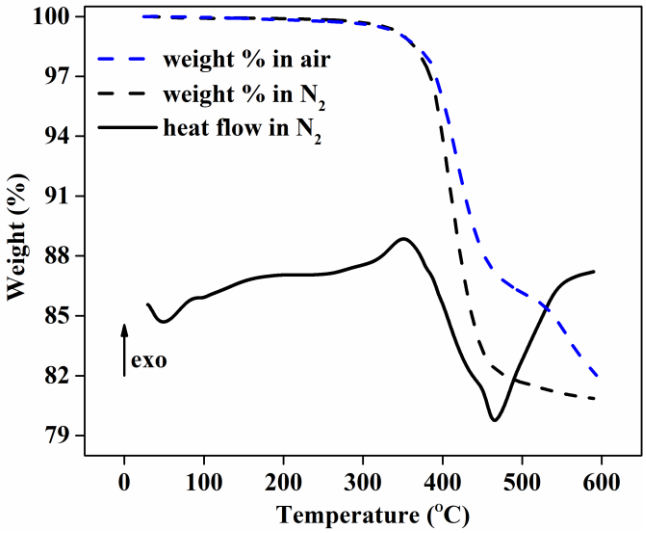

Figure 4.12. Representative simultaneous measurement of weight change and true differential heat flow test results of the (a) ISOX_C1, (b) ISOX_C1.5 and (c) ISOX_C2 in air and nitrogen.

The glass transition temperature (Tg) defines the point at which glassy polymers transform into flexible rubbers and it often determines the upper-limit use temperature of polymeric materials used in structural applications. Service temperature is often the main consideration in the selection of a matrix material. Aerospace grade epoxies are typically cured at about 177°C (350°F) and are generally not used at temperatures above 150°C (300°F) (3). Dynamic mechanical analysis (DMA) is used to detect the T_g of the three self-healing CFRP composites, where the T_g is defined as a prominent peak of Tan δ. A representative DMA test result of the ISOX_C1.5 is plotted and shown in Figure 4.13.

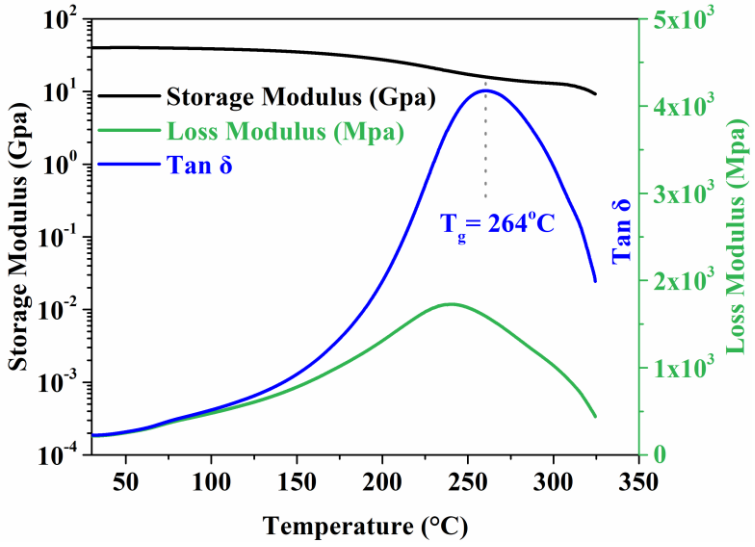

Figure 4.13. A representative dynamic mechanical analysis (DMA) result of the ISOX_C1.5 sample.

As can be seen from the results of the ISOX_C1, ISOX_C1.5 and ISOX_C2 in Figure 4.14, the Tg is measured to be 176 °C, 263 °C and 285 °C, respectively. To note, the Tg of each composite is first measured and then averaged from three specimens. The Tg of the self-healing composites is much higher than that of existing self-healable CFRP composites which have fallen below 200 °C (82, 87, 88). Moreover, compared to a structural grade CFRP composite with a commercial epoxy matrix (EPON™ 862 / EPIKURE™ Curing Agent W) which has a Tg of 150 °C represented by the gray dash line in Figure 4.14, the use temperature of the self-healing

CFRP composites in this chapter is greatly increased, although the DGEBF is a major component in the polymer matrix in both cases. The high Tg of ISOX thermosets are derived from 1) the bulky ring structure of isocyanurate and oxazolidone as one of the major components and 2) the high cross-link density of the ISOX polymers due to the crosslinking nature of the isocyanurate. The representative plots of the storage modulus measurement for the three composites from the DMA test are shown in Figure 4. 15. For comparison, the storage modulus of the three composites at 25 °C and 200 °C are reported in Table 4.1. The storage modulus of 41 GPa slightly decreased to 37 GPa when the temperature was ramped to 200 °C for the ISOX_C2. which indicates the retention of the high strength and stiffness of the composites at high temperatures.

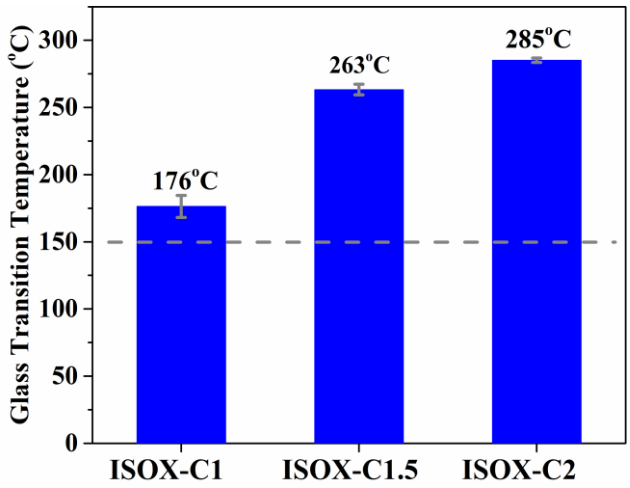

Figure 4.14. Results of glass transition temperature (Tg) for the three self-healing composites, and Tg of a composite with an epoxy matrix (EPON™ 862/ EPIKURE™ Curing Agent W) shown as the gray dash line.

(a)

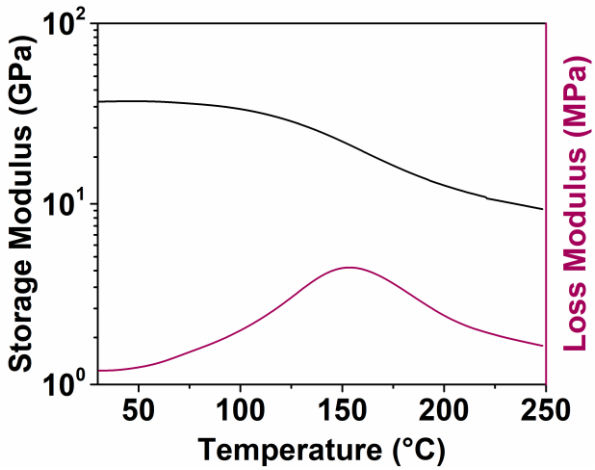

(b)

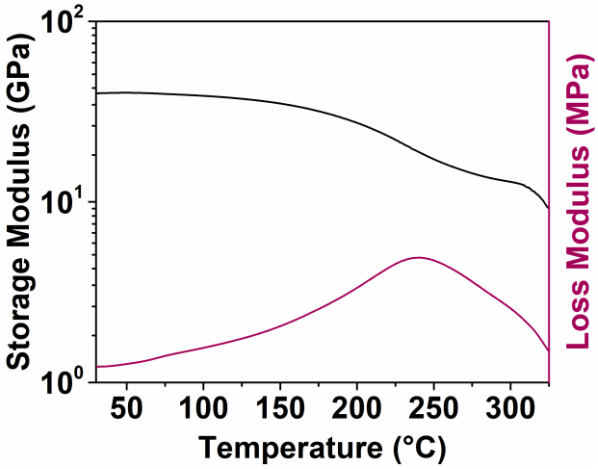

(c)

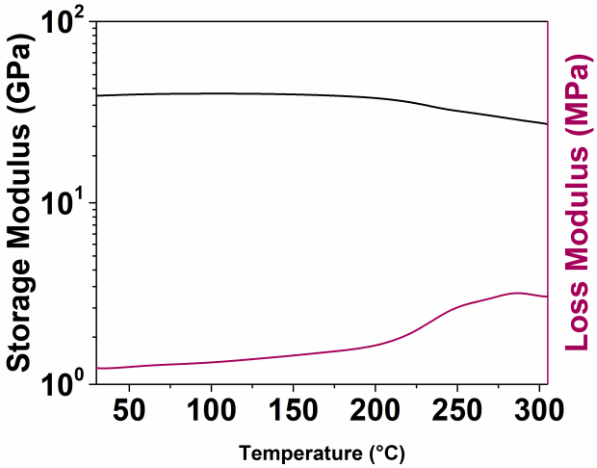

Figure 4.15. Representative dynamic mechanical analysis (DMA) results of ISOX_C1, ISOX_C1.5 and ISOX_C2.

Table 4.1. Storage modulus measured from dynamic mechanical analysis (DMA) for the ISOX_C1, ISOX_C1.5 and ISOX_C2 at varied temperatures.

Storage Modulus (GPa)	30 ºC	150 ºC	200 ºC	250 ºC
ISOX_C1	39.7 (±1.0)	26.1 (±2.9)	14.8 (±1.6)	10.9 (±1.3)
ISOX_C1.5	40.8 (±0.8)	36.2 (±0.9)	29.3 (±1.4)	19.2 (±1.4)
ISOX_C2	40.7 (±0.7)	39.0 (±0.7)	36.5 (±0.8)	30.5 (±0.4)

4.4.2 Mechanical properties of the self-healing CFRP composites

Short beam shear (SBS) strength of the carbon fiber reinforced ISOX polymer composites is measured through the procedure in accordance with ASTM D2344. The maximum apparent shear strength in the mid-plane of the composites is approximated by using the Euler-Bernoulli beam theory equation (181). The testing results are listed in Table 4.2, where the SBS strength of the self-healing composites are comparable with that of engineering grade CFRP composite with an epoxy matrix, which implies the excellent bonding between the ISOX resins and the carbon fiber reinforcement. The average SBS strength values of the self-healing composites are calculated based on the initial SBS tests for at least 6 specimens for each composite sample. As can be seen in Figure 4.16 (a), the average SBS strength of ISOX_C1 and ISOX_C1.5 is 75 MPa and 93 MPa, respectively, which are greater than that of the composite with the epoxy matrix (EPON^{TM} 862/EPIKURE^{TM} 3230) that has an average SBS strength of 65 MPa. The average SBS strength of ISOX-C2 is 40 MPa, which is attributed to the brittle nature of its 2TDI/1DGEBF polymer matrix. The brittleness can be explained by the excessive cross-link density of the 2TDI/1DGEBF thermoset characterized by its smallest Mc, as discussed above in the previous chapters.

Table 4.2. Comparison of mechanical properties among the three carbon fiber reinforced ISOX polymer composites.

Properties	ISOX_C1	ISOX_C1.5	ISOX_C2
SBS Strength of the Virgin Composites (MPa)	74.9 (±5.7)	92.8 (±5.7)	40.0 (±6.4)
SBS Strength after 1ST Healing (MPa)	60.2 (±2.7)	74.8 (±4.8)	34.0 (±1.9)
SBS strength after 2nd Healing (MPa)	52.3 (±5.5)	60.9 (±6.3)	28.0 (±3.6)
SBS strength after 3rd Healing (MPa)	37.9 (±2.6)	39.9 (±4.8)	26.9 (±2.9)

Tensile testing of the carbon fiber reinforced ISOX polymer composites is carried out in accordance with ASTM D3039, where 12 tensile specimens are cut out from composite panels with a dimension of 150 mm × 12.5 mm × 1 mm for each specimen. A composite panel with an epoxy matrix (EPON^{TM} 862 and EPIKURE^{TM} 3230 curing agent), is cured under 100 °C for 12 h and then 125 °C for 2 h and used as tabs for all tensile test specimens. The self-healing composites are tested with the Instron 5982 at a cross-head speed of 3 mm/min under ambient conditions. A 100 kN load cell and an extensometer with a 25.4 mm gauge length are used to measure the stress and strain during the tensile test. The elastic modulus is then calculated from the linear portion of the stress-strain curve and the maximum recorded stress during the test is determined as the tensile strength of the tested specimen. The elastic modulus and tensile strength of each composite sample are then calculated and averaged from the results of 12 individual specimens. The tensile properties of the three composites are demonstrated in Figure 4.16 (b) and (c), where both the tensile strength and tensile stiffness of the composites are compared with that of the reference carbon fiber reinforced epoxy composite. Tensile properties of the self-healing composites are also comparable to that of the composite with the epoxy matrix, demonstrated by the comparisons of elastic modulus and ultimate tensile strength in Figure 4.16 (b) and (c), respectively. The superior mechanical properties over traditional engineering CFRP composites with the epoxy matrix, which is derived from the ISOX thermosetting matrix, proves that the developed self-healing composites are promising candidates for advanced structural applications.

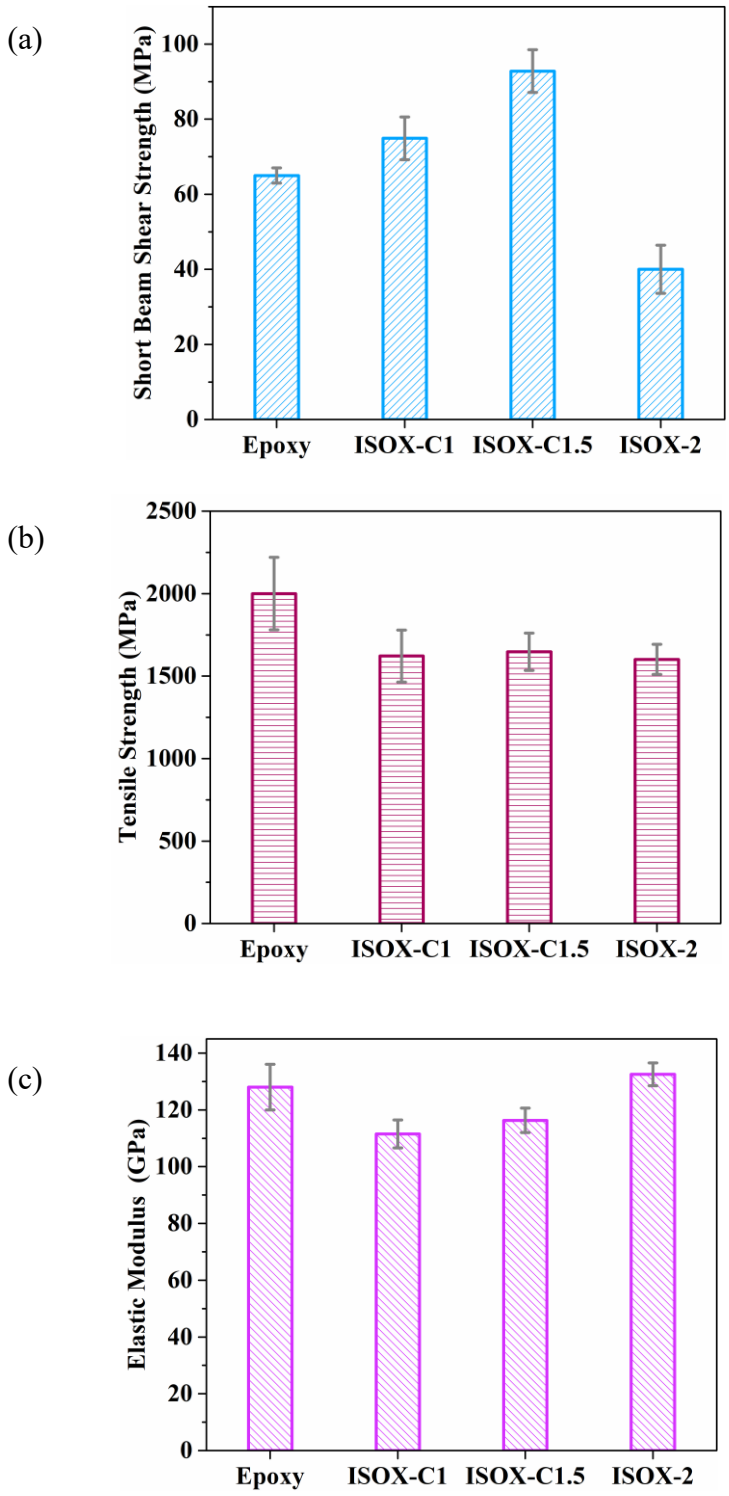

Figure 4.16. Mechanical properties: (a) short beam shear (SBS) strength, (b) elastic modulus, and (c) tensile strength of the self-healing composites and the reference composite with an epoxy matrix (EPON^{TM} 862 / EPIKURE^{TM} 3230).

4.5 Chapter Summary

The development of the self-healing ISOX composites offers a new route towards damage tolerant and longer-serving structural composites in high-temperature applications. After multiple delamination events, repeatable strength recovery of the composites has been demonstrated with a first healing efficiency up to 85% after thermal treatment. The self-healing mechanism is explained by the transformation from mechanically cleaved isocyanurate rings to oxazolidone rings under thermal stimulus. This novel ISOX polymer utilizes commercial diglycidyl ether of bisphenol F (DGEBF) and toluene diisocyanate to produce a high cross-link density thermoset with a glass transition temperature (Tg) up to 285 °C with 99.5% of the composite weight remaining at 300 °C. Structural characterization of the self-healing composites showed that their mechanical strength and stiffness are comparable with that of a structural grade epoxy matrix. The processability of the ISOX resins due to their low viscosity can benefit the manufacturing of CFRP composites. The commercially available and low-cost reactants of the self-healing composites reported are expected to expand their commercial potential as high-performance structural materials.

CHAPTER 5

Conclusions

Internal defects, such as matrix cracking and delamination, have been a longstanding issue of fiber reinforced polymer composites as they are located deep within the material resulting in a challenge in the damage detection and repair process. The development of tougher interlayers and polymer matrices by adopting the damage resistance approach has been focused to solve the problem by preventing damage initiation and propagation. For example, epoxy has been toughened through the addition of elastomers. The elastomers form a second phase in the cured matrix that restrict the formation of microcracks, yet they also reduce the Tg, stiffness, and solvent resistance of the epoxy matrix. Other toughening approaches that does not result in a tradeoff of the matrix properties is the incorporation of a thermoplastic material in the host polymer matrix. However, the uniform distribution of very fine thermoplastic particles/phase remains a challenging a difficult task.

No matter how strong and tough a composite is, defects are bound to appear within the polymer matrix due to increased loading conditions, fatigue and environmental effects such as humidity and large temperature variations. For example, ultraviolet radiation causes degradation in polymeric materials and leads to a gradual loss of their strength. The other relatively new, but equally important, philosophy for damage management in FRP composites is the damage tolerance principle, which focuses on incorporating built-in self-repair functionalities into the materials. The built-in functionality of self-healing, specifically focused in this work, can be achieved in FRP composites as individual properties of their components are preserved in the heterogeneous system. The versatility of the polymer matrix of FRP composites allows for this built-in self-healing functionality within the composites and a great

number of self-healable polymers have been developed based on newly discovered healing chemistry in the last several decades. The healing mechanism for the current self-healing polymers can be categorized into the extrinsic healing and intrinsic healing. For extrinsically self-healing polymers, there is limited times of repair for the same fracture spot within the materials. Also, the healing requires fracture of microcapsules or hollow fibers so healing agents can flow out and repair the cracks. In addition, the introduction of microcapsules and hollow fibers in the polymer matrix of the composites diminish material properties such as mechanical strength and stiffness, Tg and the resulting lower elevated temperature performance. Intrinsically self-healing polymers derive their self-healing capacity from the inherent molecular interactions on the fracture surfaces, allowing for the elimination of damage at exactly the same spot repeatedly. However, current healing chemistry lacks high temperature stability, as the developed self-healing polymers either undergo significantly thermal degradation or lose mechanical integrity at elevated temperatures.

In this work, a healing chemistry of isocyanurate-to-oxazolidone transformation exhibiting thermal stability at extreme temperatures is discovered for the development of novel, intrinsically self-healable polymers. The isocyanurate-to-oxazolidone transformation is embedded into isocyanurate-oxazolidone (ISOX) polymers, which are synthesized from the commodity monomers of toluene diisocyanate (TDI) and bisphenol F diglycidyl ether (DGEBF) in the presence of nucleophiles through the formation of an isocyanurate-oxazolidone network. The polymerization mechanism of the ISOX polymers under the effect of tertiary amines and pyridines is thoroughly investigated. It is shown that the polymerization of ISOX polymers begins with nucleophiles attacking the epoxide before the zwitterion of the nucleophile/epoxide/isocyanate initiates polymerization. Based on the understanding of the polymerization mechanism of the ISOX polymers, the chemical composition of the ISOX polymers which determines the isocyanurate fraction within the polymer network, is shown to be dependent on the monomer ratio of TDI and DEGEF, the nucleophilicity of the polymerization catalyst, and duration of the post-cure. The isocyanurate fraction of the polymers, an important parameter for the potential healing

performance of the ISOX polymers, is measured through Fourier transform infrared spectroscopy (FTIR). With the assistance of the working curve developed from combined characterization of FTIR and carbon nuclear magnetic resonance (NMR) spectroscopy on several model compounds in solution, the isocyanurate fraction of the ISOX polymers is interpreted from their FTIR spectra.

The investigated isocyanurate-to-oxazolidone transformation is used to develop novel self-healing ISOX thermosets which are repeatedly healable in the presence of a macroscopic crack without the need of any reactants or catalysts, resulting in considerable recovery of the polymer's strength after thermal annealing. This self-healing behavior is partially derived from the isocyanurate-to-oxazolidone transformation on the fracture surfaces of the polymers, as ISOX polymers with a high extent of isocyanurate-to-oxazolidone transformation during the healing process demonstrate higher strength recovery. This transformation is restricted in the cured ISOX polymers because of the heavy steric effect, given the high density of isocyanurate cross-linkers in the polymer network. However, such steric effects are weakened on the crack surfaces at high temperatures in the presence of epoxide, allowing for the isocyanurate-to-oxazolidone transformation during the healing, and heavily contributing to the resulting high healing efficiencies of the polymers. On the other hand, the high density of mechano-responsive isocyanurates, which are introduced as cross-links in the polymer network, undergo cycloreversion and produce isocyanates upon damage, leading to the formation of covalent bonds on the fracture surfaces of the ISOX polymers during the healing process. The developed self-healable ISOX polymers display a high service temperature, as shown by their Tg of up to 270 °C, which is the highest Tg reported for self-healing polymers. The high Tg, and Td of up to 365 °C allow the ISOX polymers to maintain mechanical integrity as well as mechanical properties comparable to industrially used thermosetting polyimides and BMIs designed for high-temperature applications. For example, BMIs are used for fabricating high-performance composites for military aircrafts and sports cars that can maintain their excellent mechanical properties up to 290 °C. However, these materials are primarily limited by their brittleness due to high cross-link density,

causing for their FRP composites to be prone to excessive microcracking. The superiority of the ISOX polymers over the polyimides and BMIs is highlighted by their inherent self-healing capacity, which circumvents microcracking problems within the polymer matrix of FRP composites.

Building on the developed self-healable ISOX polymers, novel carbon fiber reinforced ISOX polymer composites are fabricated, offering a novel damage management approach in the continuous CFRP composites. The development of the self-healable CFRP composites combines the two strategies of improved damage resistance and improved damage tolerance. The excellent out-of-plane and in-plane mechanical properties of the developed CFRP composites, comparable to that of aerospace grade carbon fiber reinforced epoxy composites, can offer a significantly improved damage threshold for the materials, while the built-in, inherent self-healing capacity of the ISOX polymer matrix can effectively and repeatedly eliminate of matrix cracking and matrix delamination within the composites under thermal stimulus. The ISOX polymer matrix not only introduces a self-healing functionality, but also expands the composites' operating temperature range up to 285 °C, ushering for the potential use of the self-healable FRP composites as high-performance structural materials. The exceptional strength, stiffness, light weight and in-situ repair capacity of these composites expands their potential applications including satellites, rocket motors and space stations.

5.1 Contributions

This dissertation demonstrated the isocyanurate-to-oxazolidone transformation as a novel, high temperature resistant healing chemistry. Self-healing functionality was embedded into the isoycanurate-oxazoline (ISOX) polymers to develop new, intrinsically self-healing engineering grade polymers with significantly improved thermal stability for high temperature structural applications. The developed ISOX polymers were integrated into the fabrication of continuous carbon fiber reinforced polymer (CFRP) composites, offering an alternative approach to effectively resolve

internal damage, a long-standing problem in the composite industry. The numerous contributions made in this dissertation are detailed in the following paragraphs.

Despite its high thermal stability, isocyanurate transforms into oxazolidone in the presence of epoxide moiety under thermal stimulus. This isocyanurate-to-oxazolidone transformation was first investigated in a compound solution, and then further studied in the polymeric network, where the instability of the isocyanurate when coexisting with epoxide was confirmed in both these cases using FTIR and carbon NMR. The isocyanurate-to-oxazolidone transformation was quantified through FTIR with the assistance of a working curved developed through combined characterizations of FTIR and carbon NMR. Using the developed working curve, the isocyanurate fraction within the polymeric network was accurately and quickly measured without the need for expensive, and poor quantification resolution solid carbon NMR.

The two active components of isocyanurate and epoxide moieties were then incorporated into isocyanurate-oxazolidone (ISOX) polymers. These polymers were synthesized from two commodity monomers of diisocyanates and diepoxides. The bulk polymerization mechanism of the ISOX polymers under the catalytic effect of tertiary amines and pyridines was first investigated to enhance the understanding of the potential healing chemistry of isocyanurate-to-oxazolidone transformation. The dissertation showed that high isocyanurate fraction, a preferable feature for maximizing the healing performance of the polymers, can be tuned through controlling monomer stoichiometry, the nucleophilicity of the polymerization catalysts, as well as post-cure time. The study of the polymerization mechanism was then exploited to guide the development process of the novel self-healable ISOX polymers based on the isocyanurate-to-oxazolidone transformation.

The developed self-healable ISOX polymers demonstrated efficient healing at temperatures considerably lower than their Tg. The Healing of polymers below Tg is rare and hard to achieve in currently reported self-healable polymers where significant chain mobility is a requisite. Additionally, healing below Tg allows for the preservation of the mechanical integrity of the materials throughout the healing process; thus, the healing capacity of the ISOX polymers below Tg is a very important advantage

with regards to structural applications. Multiple-time repair of macroscopic cracks initiated within the ISOX polymers was successfully achieved, as considerable portion of polymer strength and stiffness were recovered post heat treatment. The healing capacity was proven to be directly derived from the formation of covalent bonds at the crack surfaces of the polymers, specifically due to oxazolidone formation via isocyanates which are produced from cycloreversion of isocyanurate under mechanical stress, as well the isocyanurate-to-oxazolidone transformation.

The structure-property relationship of the self-healable ISOX polymers was also investigated in this dissertation. As isocyanurate fraction is increased in the ISOX polymer network, higher strength recovery was achieved, all while maintain a consistent healing procedure. The cross-link density of the polymers is found to be increased with higher isocyanurate fraction, resulting in higher Tg and improved high temperature performance. The improved high temperature performance was revealed through elevated temperature measurements of mechanical properties, where high retention of tensile strength and elastic modulus of the ISOX polymers at high isocyanurate fraction was observed. Moreover, the introduction of of a self-healing functionality does not diminish other properties of the ISOX polymers, as both their tensile strength and stiffness remain comparable with structural grade epoxy that is widely used in automobile and aerospace industries. This new class of intrinsically self-healable polymers with excellent mechanical properties and stability, as well as high thermal stability is expected to greatly impact the application of thermosets in structural laminates and electronics packaging application.

The developed self-healable ISOX polymers were then used as multifunctional polymer matrices to develop novel carbon fiber reinforced polymer composites capable of reversing matrix cracking and delamination and recovering the majority of strength and stiffness under thermal stimulus. The developed CFRP composites were shown to possess superior mechanical strength and stiffness to that of the aerospace grade CFRP composites with epoxy matrix. The fabrication process of these CFRP composites does not introduce any new requirements, as the ISOX resins have a low viscosity comparable to that of the epoxy resins, therefore allowing manufacturing of

complex-shaped parts in a relatively easy manner. Additionally, the in-situ repair capacity of the ISOX polymers can also be integrated in other fiber reinforced polymer composites to achieve such desired multifunctionality. Thus, due to their excellent structural and non-structural functions, in combination with their lightweight characteristic, the developed CFRP composites have a promising potential to achieve improved efficiency and sustainability in their end applications.

5.2 Recommendations for Future Work

The re-bonding of failed polymer surfaces under thermal stimulus offers multiple-time self-healing capacity in ISOX polymers and their corresponding fiber reinforced composites; however, the healing protocol post-damage is not autonomous. The developed in-situ damage repair approach should be incorporated in a more sophisticated system where in-situ damage detection is readily available. Damage monitoring of fiber reinforced composite materials have been extensively studied and have been achieved through both external sensors and internal sensors (187, 188), although embedded sensors are more preferred as they can detect damage in situ and eliminate the need for externally attached transducers (189). Potential in-situ damage detection using techniques such as the introduction of piezoelectric zinc oxide nanowires grown on reinforcing fibers (190) or the utilization of resistance-based damage and strain sensing via conductive carbon fiber reinforcement (191), are useful approaches for detecting a variety of damage modes in carbon fiber reinforced composites. Once damage is detected within the polymer or composite structure, the self-healing process should be initiated through a feedback loop that induces heat for repair purpose in order to achieve true “smart” materials for safety-critical applications.

Modification of the ISOX polymers to minimize their moisture absorption is another potential future direction. Water in the atmosphere can penetrate polymeric materials through diffusion, and the absorbed moisture can act as a plasticizer for the polymers, causing for a decrease in stiffness, strength, and Tg of the polymers. In the field of fiber reinforced polymer composites, moisture absorption can potentially

lead to the degradation of the polymer matrix, the fiber reinforcement, and their interface, thus resulting in premature failure of the structure. At elevated temperatures, the degradation rate of polymers is accelerated, thus low moisture absorption is an important property for the polymer matrix. The low water absorption characteristic of epoxy is an essential reason behind its use as structural polymer in the aerospace field, given that fluids such as jet fuel, hydraulic fluids, and lubricants are commonly encountered during operation (4). Unfortunately, despite the inherent self-healing capacity, excellent mechanical properties and thermal stability of ISOX polymers, relatively high water absorption is an issue in these polymers due to the large number of hydrophilic moieties in the polymer network, as indicated by our preliminary study on their moisture absorption. It is possible to chemically modify the monomers of the ISOX polymers to reduce the number of hydrophilic moieties within the resulting polymers. These chemical modifications should not affect the healing property of the polymers, while their overall material properties should be evaluated accordingly before being integrating into the design and fabrication process of the polymer based structures requiring unique mechanical, physical, and thermal characteristics.

REFERENCES

1. EERE Publication and Product Library. Fiber-Reinforced Polymer Composites: Pursuing the Promise. United States; 2014.

2. Gibson RF. Principles of Composite Material Mechanics, Fourth Edition. Boca Raton, FL: CRC Press; 2016.

3. Robert M. Jones. Mechanics of Composite Materials. New York: Taylor & Francis Group; 1999.

4. Balasubramanian M. Composite Materials and Processing. CRC Press; 2013.

5. CF and CFRP Market Worth 37.19 Billion USD by 2022 [Internet]. []. Available from: https://www.marketsandmarkets.com/PressReleases/carbon-fiber-composites.asp.

6. Marsh G. Reclaiming Value from Post-use Carbon Composite. Reinforced Plastics. 2008 July 1;52(7):36-9.

7. Bergman SD, Wudl F. Mendable Polymers. J. Mater. Chem. 2008;18(1):41-62.

8. Yuan YC, Yin T, Rong MZ, Zhang MQ. Self-Healing in Polymers and Polymer Composites. Concepts, Realization and Outlook: A Review. Express Polymer Letters. 2008;2(4):238-50.

9. Sybrand van der Zwaag. Self-Healing Materials. The Netherlands: Springer; 2007.

10. Blaiszik BJ, Kramer SLB, Olugebefola SC, Moore JS, Sottos NR, White SR. Self-Healing Polymers and Composites. Annual Review of Materials Research. 2010;40(1):179-211.

11. Delebecq E, Pascault J, Boutevin B, Ganachaud F. On the Versatility of Urethane/Urea Bonds: Reversibility, Blocked Isocyanate, and Non-isocyanate Polyurethane. Chem Rev. 2013 January 9;113(1):80-118.

12. Fu, Feng, Lauke, Mai. Effects of Particle Size, Particle/Matrix Interface Adhesion and Particle Loading on Mechanical Properties of Particulate–Polymer Composites.

13. Ahmed S, Jones FR. A Review of Particulate Reinforcement Theories for Polymer Composites. Journal of Materials Science. 1990 Dec;25(12):4933-42.

14. Balasubramanian M. Composite Materials and Processing. Baton Rouge: CRC Press; 2013.

15. Rubinstein, Michael, and Ralph H. Colby. Polymer Physics. New York: Oxford university press; 2003.

16. Saba N, Jawaid M. A Review on Thermomechanical Properties of Polymers and Fibers Reinforced Polymer Composites. Journal of Industrial and Engineering Chemistry. 2018 Nov; 67:1-11.

17. Turner P, Liu T, Zeng X. Collapse of 3D orthogonal woven carbon fibre composites under in-plane tension/compression and out-of-plane bending composite structures. Composite Structures. 2016 Feb 3,142:286-97.

18. Ray BC, Hasan ST, Clegg DW. Evaluation of Defects in FRP Composites by NDT Techniques. Journal of Reinforced Plastics and Composites. 2007 Aug;26(12):1187-92.

19. Mehdikhani M, Gorbatikh L, Verpoest I, Lomov SV. Voids in Fiber-reinforced Polymer Composites: A Review on Their Formation, Characteristics, and Effects on Mechanical Performance. Journal of Composite Materials. 2019 May;53(12):1579-669.

20. Gregory T. Kassuelke, Maple Grove, Robert E. LOng, Stephen A. Haglund, inventors; Vacuum Debulking Table for Thermoplastic Materials. 2001.

21. Donald J. Ayers, Snohomish, Wash., inventor; METHOD FOR DEBULKING PRECURED THERMOPLASTC COMPOSTE LAMINAE. patent 4,963,215. 1990.

22. Mortell DJ, Tanner DA, McCarthy CT. In-situ SEM study of transverse cracking and delamination in laminated composite materials. Composites Science and Technology. 2014 Dec 10,105:118-26.

23. WILLIAMS JG. Chapter 1 - Fracture Mechanics of Anisotropic Materials. In: Composite Materials Series.; 1989. p. 3-38.

24. Blackman BRK, Brunner AJ, Davies P. Delamination fracture of continuous fibre composites: Mixed-mode fracture. In: European Structural Integrity Society; 2001. p. 335-59.

25. Pullen D. National Composites Network. Materials World. 2006 Apr 1,14(4):4.

26. Scott IG, Scala CM. A review of non-destructive testing of composite materials. NDT International. 1982;15(2):75-86.

27. S.Gholizadeh. A review of non-destructive testing methods of composite materials. Elsevier Inc; 2015.

28. Peter Cawley, Robert D. Adams. A Vibration Technique for
Non-Destructive Testing of
Fibre Composite Structures. Journal of Composite Materials. 1979;13.

29. Shufeng L, Xiaoquan C, Yunyan X, Jianwen B, Xin G. Study on impact performances of scarf-repaired carbon fiber reinforced polymer laminates. Journal of Reinforced Plastics and Composites. 2015 Jan;34(1):60-71.

30. Chong HM, Liu SL, Subramanian AS, Ng SP, Tay SW, Wang SQ, et al. Out-of-autoclave scarf repair of interlayer toughened carbon fibre composites using double vacuum debulking of patch. Composites Part A. 2018 Apr; 107:224-34.

31. Richardson MOW, Wisheart MJ. Review of Low-Velocity Impact Properties of Composite Materials. Composites Part A. 1996;27(12):1123-31.

32. Abrate S. Impact on Composite Structures. Cambridge: Cambridge University Press; 1998.

33. Wong DWY, Zhang H, Bilotti E, Peijs T. Interlaminar toughening of woven fabric carbon/epoxy composite laminates using hybrid aramid/phenoxy interleaves. Composites Part A. 2017 Oct; 101:151-9.

34. Greenhalgh E, Hiley M. The assessment of novel materials and processes for the impact tolerant design of stiffened composite aerospace structures. Composites Part A. 2003;34(2):151-61.

35. Hosur MV, Vaidya UK, Ulven C, Jeelani S. Performance of stitched/unstitched woven carbon/epoxy composites under high velocity impact loading. Composite Structures. 2004;64(3):455-66.

36. Hosur MV, Vaidya UK, Ulven C, Jeelani S. Performance of stitched/unstitched woven carbon/epoxy composites under high velocity impact loading. Composite Structures. 2004;64(3):455-66.

37. Trask RS, Williams HR, Bond IP. Self-healing Polymer Composites: Mimicking Nature to Enhance Performance. Bioinspir Biomim. 2007;2(1): P1.

38. Bascom WD, Cottington RL, Jones RL, Peyser P. The fracture of epoxy- and elastomer-modified epoxy polymers in bulk and as adhesives. Journal of Applied Polymer Science. 1975 Sep;19(9):2545-62.

39. Bascom WD, Cottington RL. Effect of Temperature on the Adhesive Fracture Behavior of an Elastomer-Epoxy Resin. The Journal of Adhesion. 1976 Jan 1,7(4):333-46.

40. Sultan JN, McGarry FJ. Effect of Rubber Particle Size on Deformation Mechanisms in Glassy Epoxy. Polymer Engineering & Science. 1973 Jan;13(1):29-34.

41. Delmonte. Urethane laminates. J. Reinforced Plastics Composites. 1970;14(13):382.

42. Bascom, Ting, Moulton, Riew, Siebert. The Fracture of An Epoxy Polymer Containing Elastomeric Modifiers.

43. Levita G, De Petris S, Marchetti A, Lazzeri A. Crosslink Density and Fracture Toughness of Epoxy Resins. Journal of Materials Science. 1991 May;26(9):2348-52.

44. Huang F, Liu Y, Zhang X, Gao J, Song Z, Tang B, et al. Interface and Properties of Epoxy Resin Modified by Eelastomeric Nano-particles. Sc China Ser B-Chem. 2005 Mar;48(2):148-55.

45. Bruck H, Evans J, Peterson M. The Role of Mechanics in Biological and Biologically Inspired Materials. Experimental Mechanics. 2002 Dec;42(4):361-71.

46. Bar-Cohen Y. Biomimetics—Using Nature to Inspire Human Innovation. Bioinspiration & Biomimetics. 2006 Mar 1,1(1):P1-P12.

47. Curtis, P.T. Multifunctional polymer composites. Advanced Performance Materials. 1996; 3(3-4), pp.279-293.

48. Kassner ME, Nemat-Nasser S, Suo Z, Bao G, Barbour JC, Brinson LC, et al. New Directions in Mechanics. Mechanics of Materials. 2005;37(2):231-59.

49. Wool RP. A Material Fix. Nature. 2001 Feb;409(6822):773-4.

50. Moore JS, Toohey KS, Sottos NR, White SR, Lewis JA. Self-Healing Materials with Microvascular Networks. Nature Materials. 2007 Aug;6(8):581-5.

51. Toohey KS, Sottos NR, White SR. Characterization of Microvascular-Based Self-healing Coatings. Experimental Mechanics. 2009 Oct;49(5):707-17.

52. Cho SH, White SR, Braun PV. Room-Temperature Polydimethylsiloxane-Based Self-Healing Polymers. Chemistry of Materials. 2012 Nov 13,24(21):4209-14.

53. Toohey KS, Hansen CJ, Lewis JA, White SR, Sottos NR. Delivery of Two-Part Self-Healing Chemistry via Microvascular Networks. Advanced Functional Materials. 2009 May 8,19(9):1399-405.

54. Jin H, Mangun CL, Griffin AS, Moore JS, Sottos NR, White SR. Thermally Stable Autonomic Healing in Epoxy using a Dual-Microcapsule System. Advanced Materials. 2014 Jan 15,26(2):282-7.

55. Yuan YC, Rong MZ, Zhang MQ, Chen J, Yang GC, Li XM. Self-Healing Polymeric Materials Using Epoxy/Mercaptan as the Healant. Macromolecules. 2008 Jul 22,41(14):5197-202.

56. E. N. Brown, M. R. Kessler, N. R. Sottos, S. R. White. In situ Poly(urea-formaldehyde) Microencapsulation of Ddicyclopentadiene. Journal of microencapsulation. 2006;20(6):719-30.

57. Naveen V, Raja S, Deshpande AP. A two-step approach for synthesis, characterization and analysis of dicyclopentadiene–urea formaldehyde–siloxane-based double-walled microcapsules used in self-healing composites. International Journal of Plastics Technology. 2019 Nov 26.

58. Yin T, Rong MZ, Zhang MQ, Zhao JQ. Durability of Self-healing Woven Glass Fabric/Epoxy Composites. Smart Mater Struct. 2009;18(7):074001.

59. Kessler MR, Sottos NR, White SR. Self-Healing Structural Composite Materials. Composites Part A: Applied Science and Manufacturing. 2003 August 1, 34(8):743-53.

60. White SR, Sottos NR, Geubelle PH, Moore JS, Kessler MR, Sriram SR, et al. Autonomic Healing of Polymer Composites. Nature. 2001 Feb 15, 409(6822):794-7.

61. Dry C. Procedures developed for self-repair of polymer matrix composite materials. Composite structures. 1996; 35(3), 263-269.

62. Pang JWC, Bond IP. A Hollow Fibre Reinforced Polymer Composite Encompassing Self-Healing and Enhanced Damage Visibility. Composites Science and Technology. 2005 September 1, 65(11):1791-9.

63. Motuku M, Vaidya UK, Janowski GM. Parametric Studies on Self-repairing Approaches for Resin Infused Composites Subjected to Low Velocity Impact. Smart Materials and Structures. 1999 Oct 1, 8(5):623-38.

64. S.M. Bleay, C.B. Loader, V.J. Hawyes, L. Humberstone, P.t. Curtis. A Smart Repair System for Polymer Matrix Composites. 2001; 32:1767-76.

65. Pang JWC, Bond IP. 'Bleeding Composites'—Damage Detection and Self-Repair using a Biomimetic Approach. Composites Part A. 2005;36(2):183-8.

66. Pang JWC, Bond IP. A Hollow Fibre Reinforced Polymer Composite Encompassing Self-Healing and Enhanced Damage Visibility. Composites Science and Technology. 2005;65(11):1791-9.

67. Zhong N, Post W. Self-repair of Structural and Functional Composites with Intrinsically Self-healing Polymer Matrices: A Review. Composites Part A: Applied Science and Manufacturing. 2015 February 1, 69:226-39.

68. Hayes SA, Jones FR, Marshiya K, Zhang W. A self-healing thermosetting composite material. Composites Part A: Applied Science and Manufacturing. 2007 April 1, 38(4):1116-20.

69. Hayes SA, Zhang W, Branthwaite M, Jones FR. Self-healing of damage in fibre-reinforced polymer-matrix composites. Journal of the Royal Society Interface. 2007;4(13):381-7.

70. Luo X, Ou R, Eberly DE, Singhal A, Viratyaporn W, Mather PT. A Thermoplastic/Thermoset Blend Exhibiting Thermal Mending and Reversible Adhesion. ACS Appl Mater Interfaces. 2009 March 25, 1(3):612-20.

71. Zako M, Takano N. Intelligent Material Systems Using Epoxy Particles to Repair Microcracks and Delamination Damage in GFRP. Journal of Intelligent Material Systems and Structures. 1999 October 1, 10(10):836-41.

72. Dry C. Procedures Developed for Self-repair of Polymer Matrix Composite Materials. Composite Structures. 1996 Jul;35(3):263-9.

73. Dry CM, Sottos NR. Passive Smart Self-repair in Polymer Matrix Composite Materials. International Society for Optics and Photonics; 1993/07/23.

74. Dry CM. Smart Materials which Sense, Activate and Repair Damage; Hollow Porous Fibers in Composites Release Chemicals from Fibers for Self-Healing, Damage Prevention, and/or Dynamic Control. International Society for Optics and Photonics; 1992/05/01.

75. Williams G, Trask R, Bond I. A Self-Healing Carbon Fibre Reinforced Polymer for Aerospace Applications. Composites Part A: Applied Science and Manufacturing. 2007 June 1, 38(6):1525-32.

76. Kessler MR, White SR. Self-Activated Healing of Delamination Damage in Woven Composites. Composites Part A: Applied Science and Manufacturing. 2001 May 1, 32(5):683-99.

77. Kessler MR, White SR, Sottos NR. Self-Healing of Composites using Embedded Microcapsules: Repair of Delamination Damage in Woven Composites. Proc. of the 10th Eur. Conf. on Compos. Mater. Brugge, Belgium; 2002.

78. Pang JWC, Bond IP. A hollow fibre reinforced polymer composite encompassing self-healing and enhanced damage visibility. Composites Science and Technology. 2005;65(11):1791-9.

79. Chen X, Dam MA, Ono K, Mal A, Shen H, Nutt SR, et al. A thermally re-mendable cross-linked polymeric material. Science. 2002;295(5560):1698-702.

80. Heo Y, Sodano HA. Self-Healing Polyurethanes with Shape Recovery. Advanced Functional Materials. 2014 Sep 3, 24(33):5261-8.

81. Yoshie N, Saito S, Oya N. A Thermally-stable Self-mending Polymer Networked by Diels–Alder Cycloaddition. Polymer. 2011;52(26):6074-9.

82. Heo Y, Malakooti MH, Sodano HA. Self-healing polymers and composites for extreme environments. J Mater Chem A. 2016 -11-08;4(44):17403-11.

83. Syrett JA, Mantovani G, Barton WRS, Price D, Haddleton DM. Self-Healing Polymers Prepared via Living Radical Polymerisation. Polymer Chemistry. 2010;1(1):102.

84. Chen X, Wudl F, Mal AK, Shen H, Nutt SR. New Thermally Remendable Highly Cross-Linked Polymeric Materials. Macromolecules. 2003 March 1, 36(6):1802-7.

85. Jeffrey R. Jones, Charles L. Liotta, David M. Collard, David A. Schiraldi. Cross-Linking and Modification of Poly(ethylene terephthalate-co-2,6-anthracenedicarboxylate) by Diels-Alder Reactions with Maleimides. 1999.

86. Grigoras M, Colotin G. Copolymerization of a Bisanthracene Compound with Bismaleimides by Diels–Alder Cycloaddition. Polymer International. 2001 Dec;50(12):1375-8.

87. Heo Y, Sodano HA. Thermally Responsive Self-Healing Composites with Continuous Carbon Fiber Reinforcement. Composites Science and Technology. 2015 October 30, 118:244-50.

88. Park JS, Kim HS, Thomas Hahn H. Healing Behavior of a Matrix Crack on a Carbon Fiber/Mendomer Composite. Composites Science and Technology. 2009 June 1, 69(7):1082-7.

89. Cowie, John Mackenzie Grant, and Valeria Arrighi. Polymers: Chemistry and Physics of Modern Materials. CRC press. 2007.

90. Levchik SV, Weil ED. Thermal Decomposition, Combustion and Fire-retardancy of Polyurethanes—A Review of the Recent Literature. Polymer International. 2004 Nov;53(11):1585-610.

91. Amamoto Y, Kamada J, Otsuka H, Takahara A, Matyjaszewski K. Repeatable Photoinduced Self-Healing of Covalently Cross-Linked Polymers through Reshuffling of Trithiocarbonate Units. Angewandte Chemie International Edition. 2011 Feb 11, 50(7):1660-3.

92. Zheng, McCarthy. A Surprise from 1954: Siloxane Equilibration is a Simple, Robust, and Obvious Polymer Self-Healing Mechanism.

93. Ohkawa H, Ligthart, G. B. W. L, Sijbesma RP, Meijer EW. Supramolecular Graft Copolymers Based on 2,7-Diamido-1,8-naphthyridines. Macromolecules. 2007 Mar 6, 40(5):1453-9.

94. Kautz H, van Beek, D. J. M, Sijbesma RP, Meijer EW. Cooperative End-to-End and Lateral Hydrogen-Bonding Motifs in Supramolecular Thermoplastic Elastomers. Macromolecules. 2006 Jun 27, 39(13):4265-7.

95. Ligthart, G. B. W. L, Ohkawa H, Sijbesma RP, Meijer EW. Complementary Quadruple Hydrogen Bonding in Supramolecular Copolymers. Journal of the American Chemical Society. 2005 Jan 26, 127(3):810-1.

96. Scherman OA, Ligthart, G. B. W. L, Sijbesma RP, Meijer EW. A Selectivity-driven Supramolecular Polymerization of an AB Monomer. Angewandte Chemie - International Edition. 2006;45(13):2072-6.

97. Bosman AW, Sijbesma RP, Meijer EW. Supramolecular Polymers at Work. Materials Today. 2004 Apr 1, 7(4):34-9.

98. Binder, Wolfgang H., and Ronald Zirbs. Supramolecular Polymers and Networks with Hydrogen Bonds in the Main- and Side-chain. Berlin: Springer; 2006.

99. Keizer HM, van Kessel R, Sijbesma RP, Meijer EW. Scale-up of the Synthesis of Ureidopyrimidinone Functionalized Telechelic Poly(ethylenebutylene). Polymer. 2003 Sep;44(19):5505-11.

100. Keizer HM, Sijbesma RP, Jansen, Johan F. G. A, Pasternack G, Meijer EW. Polymerization-Induced Phase Separation Using Hydrogen-Bonded Supramolecular Polymers. Macromolecules. 2003 Jul 29, 36(15):5602-6.

101. Schenning, Albertus P. H. J, Jonkheijm P, Peeters E, Meijer EW. Hierarchical Order in Supramolecular Assemblies of Hydrogen-Bonded Oligo(p-phenylene vinylene)s. Journal of the American Chemical Society. 2001 Jan 24, 123(3):409-16.

102. El-ghayoury A, Schenning, Albertus P. H. J, van Hal PA, van Duren, Jeroen K. J, Janssen RAJ, Meijer EW. Supramolecular Hydrogen-Bonded Oligo(p-phenylene

vinylene) Polymers. Angewandte Chemie International Edition. 2001 Oct 1, 40(19):3660.

103. Ramzi A, Meijer EW, Hirschberg, J. H. K. Ky, Vekemans, Jef A. J. M, Brunsveld L, Sijbesma RP. Helical self-assembled polymers from cooperative stacking of hydrogen-bonded pairs. Nature. 2000 Sep 14, 407(6801):167-70.

104. El-Ghayoury A, Peeters E, Schenning, A. P. H. J, Meijer EW. Quadruple Hydrogen Bonded Oligo (p-phenylene vinylene) Dimers. Chemical Communications. 2000;2000(19):1969-70.

105. Berezkin, Y. and Urick, M. Modern polyurethanes: Overview of structure property relationship. In ACS Symp. 2013; 1148: 65-81.

Modern polyurethanes: Overview of structure property relationship.

106. Chattopadhyay DK, Raju, K. V. S. N. Structural Engineering of Polyurethane Coatings for High Performance Applications. Progress in Polymer Science. 2007;32(3):352-418.

107. Thirumal M, Khastgir D, Singha NK, Manjunath BS, Naik YP. Effect of Foam Density on the Properties of Water Brown Rigid Polyurethane Foam. Journal of Applied Polymer Science. 2008 May 5, 108(3):1810-7.

108. Kakeya H, Morishita M, Koshino H, Morita T, Kobayashi K, Osada H. Cytoxazone: A Novel Cytokine Modulator Containing a 2-Oxazolidinone Ring Produced by Streptomyces sp. The Journal of Organic Chemistry. 1999 Feb 5, 64(3):1052-3.

109. Nawata T, Kresta JE, Frisch KC. Comparative Studies of Isocyanurate and Isocyanurate-Urethane Foams. Journal of Cellular Plastics. 1975 Sep;11(5):267-78.

110. John Burkus, Pompton. Plains, N.J., inventor; PROCESS OF TREMERIZNGSOCYANATES Patented. patent A234713965. 2010 Aug 1.

111. Semsarzadeh MA, Navarchian AH. Effects of NCO/OH Ratio and Catalyst Concentration on Structure, Thermal Stability, and Crosslink Density of Poly(urethane-isocyanurate). Journal of Applied Polymer Science. 2003 Oct 24, 90(4):963-72.

112. Sasaki N, Yokoyama T, Tanaka T. Properties of Isocyanurate-type Crosslinked Polyurethanes. Journal of Polymer Science: Polymer Chemistry Edition. 1973 Aug;11(8):1765-79.

113. Ni H, Skaja AD, Sailer RA, Soucek MD. Moisture-curing alkoxysilane-functionalized isocyanurate coatings. Macromolecular Chemistry and Physics. 2000 Mar 1, 201(6):722-32.

114. Krol P. Synthesis Methods, Chemical Structures and Phase Structures of Linear Polyurethanes. Properties and Applications of Linear Polyurethanes in Polyurethane Elastomers, Copolymers and Ionomers. Progress in materials science. 2007;52(6):915-1015.

115. Chattopadhyay DK, Webster DC. Thermal Sability and Flame Retardancy of Polyurethanes. Progress in Polymer Science. 2009;34(10):1068-133.

116. Yeganeh H, Jamshidi S, Talemi PH. Synthesis, Characterization and Properties of Novel Thermally Stable Poly (urethane-oxazolidone) Elastomers. European polymer journal. 2006;42(8):1743-54.

117. Sandler SR, Berg F, Kitazawa G. Poly-2-Oxazolidones. Journal of Applied Polymer Science. 1965 May;9(5):1994-6.

118. R. J. Cotter and M. Matzner. Ring-Forming Polymerizations. New York: Academic Press; 1972.

119. Sandler S. Polymer Synthesis. Elsevier Inc; 2012.

120. Narayan R, Chattopadhyay DK, Sreedhar B, Raju, K. V. S. N, Mallikarjuna NN, Aminabhavi TM. Synthesis and Characterization of Crosslinked Polyurethane Dispersions based on Hydroxylated Polyesters. Journal of Applied Polymer Science. 2006 Jan 5, 99(1):368-80.

121. Younes UE, Boesel DM. Reinforced Isocyanurate/Oxazolidone Polymers for Structural Composites Application. Reinforced isocyanurate/oxazolidone polymers for structural composites application. 1988.

122. Flores M, Fernández-Francos X, Morancho JM, Serra À, Ramis X. Curing and Characterization of Oxazolidone-Isocyanurate-Ether Networks. J Appl Polym Sci. 2012;125(4):2779-89.

123. Culbertson BM, McGrath JE. Advances in Polymer Synthesis. Springer Science & Business Media; 2012.

124. Senger JS, Yilgor I, McGrath JE, Patsiga RA. Isocyanate–epoxy reactions in bulk and solution. Journal of Applied Polymer Science. 1989 Jul 20, 38(2):373-82.

125. Spivey AC, Arseniyadis S. Nucleophilic Catalysis by 4-(Dialkylamino)pyridines Revisited—The Search for Optimal Reactivity and Selectivity. Angewandte Chemie International Edition. 2004 Oct 18, 43(41):5436-41.

126. Kinjo N, Numata S, Koyama T, Narahara T. Synthesis and Viscoelastic Properties of New Thermosetting Resins Having Isocyanurate and Oxazolidone Rings in Their Molecular Structures. J Appl Polym Sci. 1983;28(5):1729-41.

127. Kinjo N, Numata S, Koyama T, Katsuya Y. Synthesis and Viscoelastic Properties of Thermosetting Isocyanurate–Oxazolidone Resins. Polym J. 1982;14(6):505.

128. Caille D, Pascault JP, Tighzert L. Reaction of a Diepoxide with a Diisocyanate in Bulk. Polymer bulletin. 1990;24(1):23-30.

129. Lee YS, Hodd K, Wright WW, Barton JM. A Study in the Formation and Characterisation of Oxazolidone-Isocyanurate Polymers using Differential Scanning Calorimetry and Infrared Spectroscopy. British polymer journal. 1990;22(2):97-105.

130. Uribe M, Hodd KA. The Catalysed Reaction of Isocyanate and Epoxide Groups: A study using Differential Scanning Calorimetry. Thermochimica acta. 1984;77(1-3):367-73.

131. Speranza GP, Peppel WJ. Preparation of Substituted 2-Oxazolidones from 1, 2-Epoxides and Isocyanates. J Org Chem. 1958;23(12):1922-4.

132. Flores M, Fernández-Francos X, Morancho JM, Serra À, Ramis X. Ytterbium Triflate as a New Catalyst on the Curing of Epoxy–Isocyanate based Thermosets. Thermochimica acta. 2012;543: 188-96.

133. Žilić, M., Sendijarević, A., Sendijarević, V., and Frisch, K. C. Studies in the Formation of Poly (oxazolidone)s. III. Catalysis and Kinetics of the Model Oxazolidone Formation from Cyclohexyl Isocyanate and Phenylglycidyl Ether. Journal of Polymer Science Part A: Polymer Chemistry. 1989; 27(6):1843-1851.

134. Ashida K, Frisch KC. Modified Isocyanurate Foams. II: Preparation and Properties of Epoxy-Isocyanurate Foams by Means of a Two-Step Process. Journal of Cellular Plastics. 1972;8(4):194-200.

135. Parodi F. Isocyanate-derived Polymers. In: Comprehensive Polymer Science. Elsevier Ltd; 1989. p. 387-412.

136. Galante MJ, Williams RJ. Polymer Networks based on the Diepoxide–Diisocyanate Reaction Catalyzed by Tertiary Amines. J Appl Polym Sci. 1995;55(1):89-98.

137. Chian KS, Yi S. Synthesis and Characterization of An Isocyanurate–Oxazolidone Polymer: Effect of Stoichiometry. J Appl Polym Sci. 2001;82(4):879-88.

138. Frisch KC, Sendijarevic V, Sendijarevic A, Lekovic H, Kresta JE, Klempner D, et al. New Heat Resistant Isocyanate based Foams for Structural Applications. Journal of cellular plastics. 1992;28(4):316-29.

139. Sendijarevic A, Sendijarevic V, Frisch KC, Vlajic M. Novel Heat-resistant Isocyanate-based Polymers. Journal of Elastomers & Plastics. 1991;23(3):192-217.

140. Fedoseev MS, Derzhavinskaya LF, Borisova IA, Oshchepkova TE, Antipin VE, Tsvetkov RV. Heat-Resistant Polymers and Composites on the Basis of Epoxy–Isocyanate Binding Agents. Polymer Science, Series D. 2018;11(4):407-14.

141. Kordomenos PI, Kresta JE. Thermal Stability of Isocyanate-based Polymers. 1. Kinetics of the Thermal Dissociation of Urethane, Oxazolidone, and Isocyanurate Groups. Macromolecules. 1981;14(5):1434-7.

142. Wong S, Frisch KC. Catalysis in Competing Isocyanate Reactions. I. Effect of Organotin–Tertiary Amine Catalysts on Phenyl Isocyanate and N-butanol Reaction. Journal of Polymer Science Part A: Polymer Chemistry. 1986 Nov;24(11):2867-75.

143. Špírková M, Budinski-Simendic J, Ilavský M, Špaček P, Dušek K. Formation of Poly(urethane-isocyanurate) Networks from Poly(oxypropylene)diols and Diisocyanate. Polymer Bulletin. 1993 Jul;31(1):83-8.

144. HENRY V. KEHIAIAN. A Comparative Study of Thermodynamic Properties and Molecular Interactions in Mono and Polychloroalkane n Alkane or Cyclohexane Mixtures. Fluid Phase Equilibria, 1988;40:23-78.

145. Roberts GCK. NMR Spectroscopy: An Introduction. FEBS Letters. 1981;124(1):130.

146. Kalinowski, Hans-Otto, Stefan Berger, and Siegmar Braun. Carbon-13 NMR Spectroscopy.; 1988.

147. Duff DW, Maciel GE. Carbon-13 and Nitrogen-15 CP/MAS NMR Characterization of MDI-Polyisocyanurate Resin Systems. Macromolecules. 1990;23(12):3069-79.

148. Clark J, Perrin DD. Prediction of the Strengths of Organic Bases. Quarterly Reviews, Chemical Society. 1964;18(3):295-320.

149. Perrin DD, Dempsey B, Serjeant EP. pKa Prediction for Organic Acids and Bases. Springer; 1981.

150. Almdal K, Dyre J, Hvidt S, Kramer O. Towards a Phenomenological Definition of the Term ‘Gel’. Polymer Gels and Networks. 1993;1(1):5-17.

151. Okumoto S, Yamabe S. A Computational Study of Base-catalyzed Reactions between Isocyanates and Epoxides Affording 2-Oxazolidones and Isocyanurates. Journal of Computational Chemistry. 2001;22(3):316-26.

152. Dell'Erba IE, Williams RJJ. Homopolymerization of Epoxy Monomers Initiated by 4-(dimethylamino)pyridine. Polymer Engineering & Science. 2006 Mar;46(3):351-9.

153. Bhattacharjee, D., and R. Engineer. An Improved Technique for the Determination of Isocyanurate and Isocyanate Conversion by Photoacoustic FTIR. Journal of cellular plastics. 1996;32(3):260-73.

154. Neuhaus D. Nuclear Overhauser Effect. eMagRes. 2007.

155. Tortora PG, Johnson I. The Thermal Degradation of Polyacrylonitrile. The Fairchild Books Dictionary of Textiles. 1997; 58:193-202.

156. Cho S, Kim J, Oh S, Chung C. Heat-Induced Crack Healing in a Perfluorocyclobutane-containing Polymer. Macromol Res. 2010 Feb;18(2):212-4.

157. Rieger J. The Glass Transition Temperature Tg of Polymers—Comparison of the Values from Differential Thermal Analysis (DTA, DSC) and Dynamic Mechanical Measurements (torsion pendulum). Polymer Testing. 2001 Oct;20(2):199-204.

158. Earnest C. Assignment of Glass Transition Temperatures Using Thermomechanical Analysis. In: Assignment of the Glass Transition. United States: ; 1994. p. 75-87.

159. Hamerton I, Kratz J. Chapter 9 - The Use of Thermosets in Modern Aerospace Applications. In: Thermosets. Elsevier Ltd; 2018. p. 303-40.

160. Paul C. Hiemenz, Timothy P. Lodge. Polymer Chemistry Second Edition. CRC Press. 2007.

161. Sheng X, Lee JK, Kessler MR. Influence of Cross-link Density on the Properties of ROMP Thermosets. Polymer. 2009;50(5):1264-9.

162. Zhang H, Gao F, Cao X, Li Y, Xu Y, Weng W, et al. Mechanochromism and Mechanical-Force-Triggered Cross-Linking from a Single Reactive Moiety Incorporated into Polymer Chains. Angewandte Chemie International Edition. 2016 Feb 24,55(9):3040-4.

163. Jiaming Zhuang, Mallory R. Gordon, Judy Ventura, Longyu Li and S. Thayumanavan*. Multi-stimuli Responsive Macromolecules and Their Assemblies Chem Soc Rev. 2013; 42:7421.

164. Black AL, Lenhardt JM, Craig SL. From Molecular Mechanochemistry to Stress-Responsive Materials. J. Mater. Chem. 2011 Jan 25, 21(6):1655-63.

165. Dopieralski P, Anjukandi P, Rückert M, Shiga M, Ribas-Arino J, Marx D. On the Role of Polymer Chains in Transducing External Mechanical Forces to Benzocyclobutene Mechanophores. Journal of Materials Chemistry. 2011 May 31, 21(23):839-8316.

166. Chung C, Roh Y, Cho S, Kim J. Crack Healing in Polymeric Materials via Photochemical [2+2] Cycloaddition. Chemistry of Materials. 2004 Oct 19, 16(21):3982-4.

167. Klukovich HM, Kean ZS, Iacono ST, Craig SL. Mechanically Induced Scission and Subsequent Thermal Remending of Perfluorocyclobutane Polymers. Journal of the American Chemical Society. 2011 Nov 9, 133(44):17882-8.

168. Moller J, Barr S, Schultz E, Breitzman T, Berry R. Simulation of Fracture Nucleation in Cross-Linked Polymer Networks. JOM. 2013 Feb;65(2):147-67.

169. S. N. ZHURKOV, V. A. ZAKREVSKYI, V. E. KORSUKOV, V. S. Mechanism of Submicrocrack Generation in
Stressed Polymers. 1972 Jan 1, 2.

170. Josef Jiricny" and Colin B. Reese. The Thermal Decomposition of Isocyanurates.

171. P. I. Kordomenos,* J. E. Kresta, and K. C. Frisch. Thermal Stability of Isocyanate-Based Polymers. 2. Kinetics of
the Thermal Dissociation of Model Urethane, Oxazolidone, and
Isocyanurate Block Copolymers. Macromolecules. 1987(20).

172. Reymore HE, Carleton PS, Kolakowski RA, Sayigh AAR. Isocyanurate Foams: Chemistry, Properties and Processing. Journal of Cellular Plastics. 1975 Nov;11(6):328-44.

173. Merten R. Synthesis of Heterocyclic Ring Systems for Heat-Resistant Plastics from Polyisocyanates. Angewandte Chemie International Edition in English. 1971 May;10(5):294-301.

174. Banea MD, de Sousa, F. S. M, da Silva, L. F. M, Campilho, R. D. S. G, de Pereira, A. M. Bastos. Effects of Temperature and Loading Rate on the Mechanical Properties of a High Temperature Epoxy Adhesive. Journal of Adhesion Science and Technology. 2011 Jan 1, 25(18):2461-74.

175. Jin F, Li X, Park S. Synthesis and application of epoxy resins: A review. Journal of Industrial and Engineering Chemistry. 2015 Sep 25, 29:1-11.

176. Andrews GP, AbuDiak OA, Jones DS. Physicochemical Characterization of Hot Melt Extruded Bicalutamide–Polyvinylpyrrolidone Solid Dispersions. Journal of Pharmaceutical Sciences. 2010 Mar;99(3):1322-35.

177. Zecevic DE, Wagner KG. Rational Development of Solid Dispersions via Hot-Melt Extrusion Using Screening, Material Characterization, and Numeric Simulation Tools. Journal of Pharmaceutical Sciences. 2013 Jul;102(7):2297-310.

178. Vidyasagar A, Sung C, Losensky K, Lutkenhaus JL. pH-Dependent Thermal Transitions in Hydrated Layer-by-Layer Assemblies Containing Weak Polyelectrolytes. Macromolecules. 2012 Nov 27, 45(22):9169-76.

179. Kar KK. Composite Materials. 1st ed. 2016 ed. Berlin, Heidelberg: Springer; 2016.

180. Zhang L, Julé F, Sodano HA. High Service Temperature, Self-mendable Thermosets Networked by Isocyanurate Rings. Polymer. 2017 April 7, 114:249-56.

181. Standard Test Method for Short-Beam Strength of Polymer Matrix Composite Materials and Their Laminates. 2013 Oct 1.

182. Mouritz AP, Gallagher J, Goodwin AA. Flexural Strength and Interlaminar Shear Strength of Stitched GRP Laminates following Repeated Impacts. Composites Science and Technology. 1997;57(5):509-22.

183. Park JS, Darlington T, Starr AF, Takahashi K, Riendeau J, Thomas Hahn H. Multiple healing effect of thermally activated self-healing composites based on Diels–Alder reaction. Composites Science and Technology. 2010 December 15, 70(15):2154-9.

184. Yeung P, Broutman LJ. The Effect of Glass-resin Interface Strength on the Impact Strength of Fiber Reinforced Plastics. Polymer Engineering & Science. 1978 Feb;18(2):62-72.

185. Shen SB, Ishida H. Development and Characterization of High-Performance Polybenzoxazine Composites. Polymer composites. 1996;17(5):710-9.

186. Suzuki M, Nagai A, Suzuki M, Takahashi A. The curing mechanism and properties of bismaleimide–biscyanamide resin. J Appl Polym Sci. 1992 April 5, 44(10):1807-13.

187. Zhao X, Gao H, Zhang G, Ayhan B, Yan F, Kwan C, et al. Active health monitoring of an aircraft wing with embedded piezoelectric sensor/actuator network: I. Defect detection, localization and growth monitoring. Smart Materials and Structures. 2007 Aug 1, 16(4):1208-17.

188. Giurgiutiu V, Zagrai A, Jing Bao J. Piezoelectric Wafer Embedded Active Sensors for Aging Aircraft Structural Health Monitoring. Structural Health Monitoring. 2002 Jul;1(1):41-61.

189. Ian Read, Peter Foote and Stuart Murray. Optical Fibre Acoustic Emission Sensor for Damage Detection in Carbon Fibre Composite Structures. MEASUREMENT SCIENCE AND TECHNOLOGY. 2002;13: N5-9.

190. Groo L, Inman DJ, Sodano HA. In Situ Damage Detection for Fiber-Reinforced Composites Using Integrated Zinc Oxide Nanowires. Advanced Functional Materials. 2018 Aug 29, 28(35): 1802846, n/a.

191. Read I, Foote P, Murray S. Optical fibre acoustic emission sensor for damage detection in carbon fibre composite structures. Measurement Science and Technology. 2002 Jan 1, 13(1): N5-9.